Contents

CHAPTER 1

1 Introduction

1.1 The goals of the thesis and the 'modelling approach'

Recent marine ecosystem studies highlighted the importance of the coupling between biological and physical processes. This coupling might be considered as a continuum of functional responses to changing conditions over a wide range of time scale. This view assumes that biological processes must be embedded in a appropriate physical contest in order to provide a proper description of ecosystem functioning processes (Robinson, 1999; Vichi, 2002). For these reasons the marine ecosystems studies found in numerical models a refined and useful analysis tool. If the experimental models (i.s batch colture, mesocosms) can provide useful informations in terms of physiological processes (nutrients starvation, adjustment to pollution stress etc), the numerical model allow to insert this processes in a multidisciplinary and multidimensional framework.

Even if the non linear interactions between biogeochemical components of an ecosystem and its connections with the physical forcing, makes the concept of predicibility not appropriate for a natural ecosystem, the analysis of mathematical simulations can be, on the other hand, an useful instrument for the interpretation of the observations.

Experimental analysis and numerical simulations would have to be linked by means of a feed back mechanism: observational data and laboratory experiments provide information about models parameters setting and model initialization, and the numerical simulation, based on known assumptions, offer a way to data interpretation.

The aim of this work is to understand the processes governing the Adriatic sea ecosystem, with particular reference to the dissolved organic matter, by means of a comparison between numerical simulations and observational data.

The work is divided in three main parts. After a general overview of the biogeochemical model used (chapter 2), in the chapter 3 we describe the development of a new conceptual model describing the interactions between organic carbon and bacteria. This conceptual model is tested in a zero dimensional system. In the chapter 4 the new bacterial sub model is inserted in a three dimensional physical–biogeochemical coupled ecosystem model, implemented on the Adriatic sea domain, in order to test the general capacity of the model to reproduce the main ecosystem feature of the Adriatic Sea. Finally, in the last chapter (5), we use the three dimensional Adriatic ecosystem model to describe the dynamics of the dissolved organic matter in the Adriatic sea and for testing some hypotheses about DOC accumulation and consumption.

1.2 The dissolved organic carbon (DOC)

Dissolved Organic Carbon (DOC) is defined as all the organic carbon present in seawater that passes a 0.2 μm filter and is a term used to describe the dissolved compounds in water that derive from organic materials.

DOC is organic materials from plants and animals broken down into such a small size that it is 'dissolved' into water. It can be present as truly dissolved molecules, or as colloids or viruses. Some DOC molecule have a recognizable chemical structure that can easily be defined (fats, carbohydrates, and proteins) however most have non readily identifiable structure and are lumped under the term humic substance. The plant material is slowly broken down by organisms into very small particles that are dissolved into water. Because they are not quickly fed on, they have more time to hang out in the water and react with other molecules to form complex structure that are difficult to define as any one type of compound. The most part of dissolved marine organic matter is therefore undefined in terms of chemical structure and composition, and is composed by humic substance

1.3 The Adriatic Sea

The Adriatic sea is an elongated basin located between Italian peninsula and the Balkans. The Northern part is very shallow water and has gently sloping batimetry with an average bottom depth of about 35 meters. The meddle part of the basin is 140m deep on the average, while the southern part is characterized by e wide depression deeper than 1200m (Zavaterelli *et al*, 1998).

The Adriatic basin is subject to strong forcing functions, producing a clear seasonal variability in both the circulation (Artegiani *et al*., 1997a) and the ecosystem (Zavatarelli *et al*., 1997). Atmospheric forcing at the surface determines an annual average heat loss of about 20 Wm^{-2} inducing a deep water formation process (Artegiani *et al*.,1989). River runoff is particularly strong in the northern basin and affects the circulation through buoyancy input and the ecosystem by introducing large amount of nutrients.

Levantine Intermediate Water (LIW) penetrates the Adriatic through the Otranto Channel compensating the heat loss, assuming the basin to be in steady state. LIW also represent the main nutrients input for the Southern part of the basin. From climatological studies (Artegiani *et al*., 1997) we can identify three main water types in the Adriatic sea : Surface water, Deep Water and the Modified Levantine Intermedieate Water, that is LIW partially mixed with local waters.

The baroclinic circulation exhibits an evident seasonality mainly in the Northern and meddle part of the basin. The circulation is generally cyclonic, with two main cyclonic gyres in the middle and southern Adriatic, observed in all seasons except for winter, and an autumn cyclonic gyre also in the northern basin (Zavatarelli *et al*.,1997). Coastal currents develop during most of the year along both the western and eastern coastlines, with seasonal changes in strength and extension. The western side of the Adriatic basin is a site of an intense coastal current, which is observed only in the northern basin in winter, while in the other seasons it extends along the entire coastline. The shallow Northern part of the basin is strongly affected by rivers discharge and is characterized by a high primary production while in the middle and southern part of the Adriatic sea there is a quite low primary with the exception of the coastal area of Albania where a consistent

riverine input is present.

CHAPTER 2

2 The Biogeochemical model

2.1 The ERSEM philosophy and assumptions

The ecosystem model used in this work is based on the pelagic part of the European Sea Regional Ecosystem Model (ERSEM), Baretta *et al* (1995). ERSEM considers the ecosystem to be a series of interacting chemical and biological processes that together exhibit coherent system behavior. The dynamics of biological functional groups are described by population process (growth, migration and mortality) and physiological (ingestion, respiration, excretion and egesting). The ecosystem is subdivided into three functional types: producers (phytoplankton), decomposers (bacteria) and consumers (zooplankton).

The phytoplankton uptake of nutrients (NO3, NH4, and PO4) have been decoupled from the carbon assimilation processes by including dynamic nutrients kinetics according to Droop (1973) and Nyholm (1977), whereby, nutrient uptake is dependent on both the level of intracellular storage and external nutrient concentrations. The microbial food web contains bacteria, heterotrophic flagellates and microzooplankton, each with dynamically varying C:N:P ratios (Baretta-Bekker *et al*., 1995; 1998). Bacteria act to consume dissolved organic carbon, decompose detritus and can compete for inorganic nutrients with phytoplankton.

The ERSEM state variables can be of two types: functional grups and ordinary state variables. Each functional group state variables is formally written as a four dimensional vector varying in time and space $C_i(\vec{x},t)$, $i=1,2,3,4$. The ordinary state variables can be a scalar or vector, while a functional group state variable can only be a vector whose components are the projection of the functional group into the major biochemical elements considered in the model, carbon, nitrogen, phosphorus and silica, as shown in Tab. 2.1. A schematic

description of ERSEM structure and functionality is given in Fig.2.1.

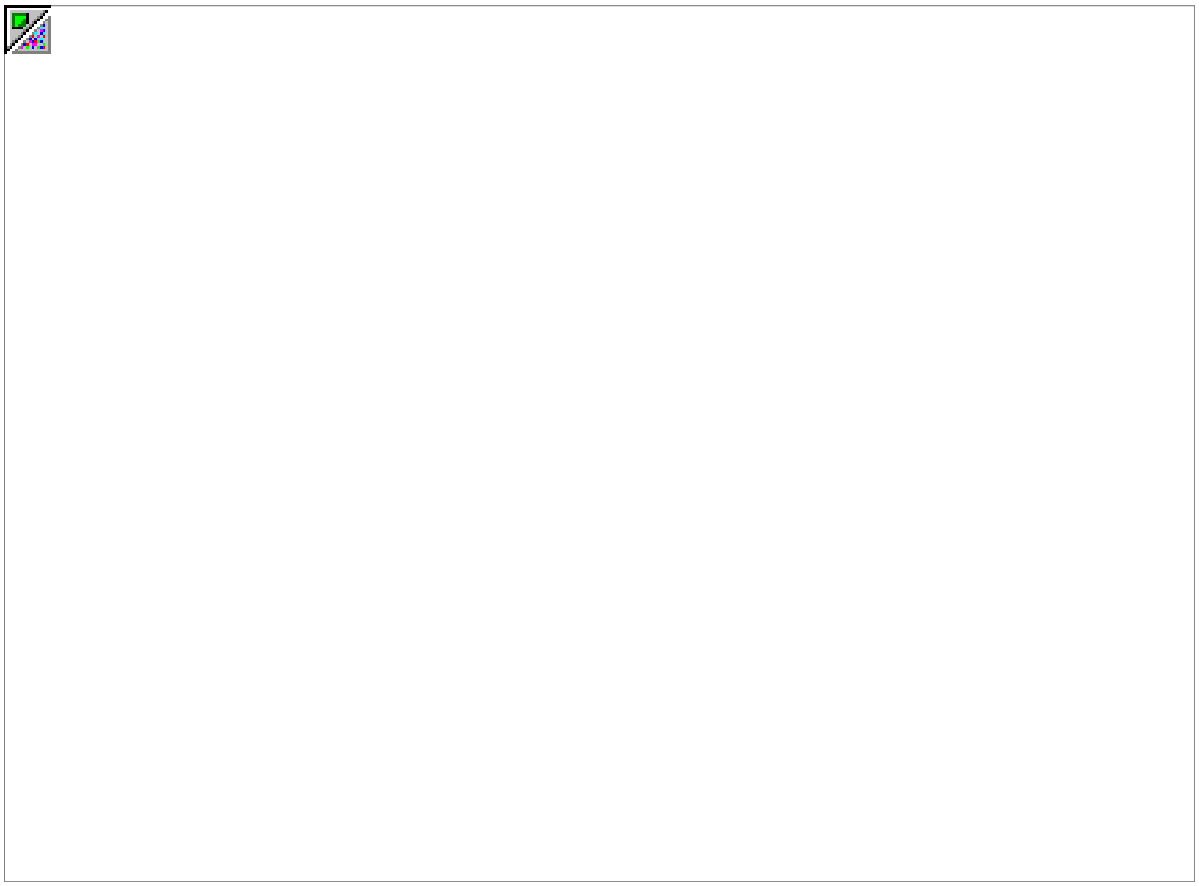

Figure 2.1. General overview of the biogeochemical state variables and matter fluxes implemented in the ERSEM pelagic module. Squere boxes represent functional groups defined in the model. Continuous arrows indicate fluxes of carbon and inorganic nutrients, dashed arrows fluxes of inorganic nutrients alone, and dotted arrows the gas exchange. From Vichi *et al*., (2003).

Variable	*type*	*Constituent*	*Description*	*References*
N(1)	OSV	P	Phosphate(mmolP m^{-3})	Baretta *et al,.* 1995
N(3)	OSV	N	Nitrate (mmol N $m^{-3)}$	"
N(4)	OSV	N	Ammonium (mmol N m^{-3})	"
N(5)	OSV	Si	Silicate (mmol Si m^{-3})	"
O(2)	OSV	O	Dissolved oxygen (mmolO2 m^{-3})	Baretta *et al.*, 1995
O(3)	OSV	C	Carbon Dioxide (mg C m_{-3})	"
$P_j(1)$	FG	C,N,P,Si	Diatoms (mg C m^{-3}) and mmol N,P,Si m^{-3})	Varela *et al*., 1995 Ebenhoeh *et al*.,1997 Baretta-Bekker *et al.* 1998
$P_j(2)$	FG	C,N,P	Flagellates (mg C $m^{-3)}$ and mmol N,P m-3)	"
$P_j(3)$	FG	C,N,P	Picophytoplankton (mg C m^{-3} and mmol N,P m-3)	"
$P_j(4)$	FG	C,N,P	Large phytoplankton (mg C m^{-3}) and mmol N,P m^{-3})	"
$B_j(1)$	FG	C,N,P	Pelagic bacteria(")	"
$Z_j(3)$	FG	C,N,P	Carnivorous Mesozooplankton (")	Broekhuizen *et al*.,1995
$Z_j(4)$	FG	C,N,P	Omnivorous Mesozooplankton(")	"
$Z_j(5)$	FG	C,N,P	Microzooplankton (")	Baretta-Bekker *et al.*, 1997
$Z^j(6)$	FG	C,N,P	Heterotrophic Flagellates (")	"
$R_j(6)$	FG	C,N,P	Dissolved organic matter (")	Baretta *et al*., 1995
$R_j(6)$	FG	C,N,P	Particulate organic matter (")	"
I^{opt}	OSV	-	Optimal Irradiance	Ebenhoe *et al.*.1997

Table 2.1. The ERSEM pelagic state variables.

The biochemical model equation for a generic variable C can be written in the following way:

$$\left.\frac{\partial C}{\partial t}\right|_{bio} = \left.\frac{\partial C}{\partial t}\right|_{V1}^{e1} + \left.\frac{C}{\partial t}\right|_{V2}^{e1} - \left.\frac{\partial C}{\partial t}\right|_{V3}^{e3} \ldots + \left.\frac{\partial C}{\partial t}\right|_{Vn}^{en} \qquad \text{(eq.1)}$$

where the right hand side contains the series of source and sink terms. The superscript *'e'* indicate the processes which determine the rate of change of C. All the processes considered in the model are listed in Table. 2.2. The subscripts V indicate the state variable(s) or functional group vector component(s) involved. If V=C, we refer to intra-group fluxes such as cannibalism. In equation 1 the sign of each flux terms is algebraically written and the following identity, which is actually an expression of the mass conservation law, is always verified:

$$\left.\frac{\partial C}{\partial t}\right|_{V}^{e} = \left.\frac{\partial V}{\partial t}\right|_{C}^{e} \qquad \text{(eq.2)}$$

All the organisms considered to be in a particular group (e.g. diatoms, picophytoplankton etc) share the same functional properties in the ecosystem and have the same trophic interactions. This approach has been shown to be a good choice for the description of unicellular organism, population and community dynamics, and the nutrients cycles. This kind of approach on the other hand fails, generally when dealing with size structured populations as mesozooplankton, where experimental data are derived from individuals (Vichi *et al*., Baretta *et al*., 1995). For a complete description of all ERSEM equations see Vichi (2002) and Vichi *et al*., (2004). Here we give e general conceptual description of the phytoplankton and zooplankton model parameterization, limiting the full mathematical description to the bacterial parameterization and their interactions with detritus that is the focus of the present study.

Abbreviation	*Ecological Processes*
gpp	Gross primary production
rsp	Respiration
prd	Predation
out	Excrection/release
exudation	Exudation
upt	Uptake

Table 2.2. Ecological processes symbolic abbreviations.

2.1.1 Phytoplankton

Primary producers in ERSEM are divided in four functional group by means of which is possible, on a first approximation, reproduce the functionality of phytoplankton in marine ecosystem.

The operational model definition of the phytoplankton functional types are:

1) diatoms (state variable vector P1), dimension (20-200μm), unicellular eukaryotes enclosed by silica frustule eaten by micro and mesozooplankton;
2) autotrophic nanoflagellates (state variable vector P2), dimension 2-20μm, motile unicellular eukaryotes comprising smaller dinoflagellates and oyher autotrophic nanoplankton flagellates eaten by heterotrophic nanoflagellates, micro- and mesozooplankton;
3) picophytoplankton (state variable vector P3), dimension 0.2 -2 μm, smallest autotrophic unicellular organism grazed by heterotrophyc nanoflagellates, with an almost total preferential use of ammonium nitrogen instead of other nitrogen species;
4) inedible or partially inedible phytoplankton (state variable vector P4), dimension 20-200 μm, that represent a wide group of phytoplanktonic species also comprising larger species belonging to the previous groups but also those that during some period of the year develop a form of (chemo) defense to predator attack. This group generally has low growth rates and small or zero food matrix elements with respect to micro and mesozooplankton groups.

Because a lacking of data and informations for a correct parameterization, the P4 functional group is not considered in the present study.

2.1.2 Phytoplankton Environmental regulating factors

The physiological regulating factors for the phytoplankton groups contain the functional response of the organism to environmental conditions such temperature, light, inorganic nutrients or local food availability. The net growth rate of phytoplankton depends mainly on light, temperature, nutrient availability and, according to Droop (1973), and Nyholm (1977), on the internal nutrient storage. In order to account for the environmental and intracellular conditions in the parameterized functional response of phytoplankton, a set of a non dimensional regulating factor are also included in the mathematical formulation. As a general rule, the value of a regulating factor is 1, under optimum conditions, and tends to 0 when organisms are limited by one of the environmental limiting factor

Temperature

The dependence of the physiological regulating factor from environmental water temperature T is common to all the parameterizations of the functional groups and of many other biogeochemical processes It is written in an exponential forms as

$$f^t = Q_{10}^{T-T_0/T_0}$$

Where Q_{10} is the characteristic temperature coefficient specific to the involved functional group or chemical reaction and $T_0 = 10^{\circ}C$. In the case of phytoplankton, Q_{10} is set to 2 for all the group, indicating that the potential growth rate doubles every 10°C This is the only regulationg factor that can give a value larger than 1.

Light regulating factor

We here summarize the main aspects of the light parameterization in

phytoplankton that lead to the following light regulation factor. For a more detailed description of the parameterization of light utilization by phytoplankton see Ebenhoh *et al*. (1997).

$$f_P^I = \frac{1}{(P_{opt} D)} \int_{-D}^{0} P(P_{opt}, \frac{I_{PAR}}{I_p^{opt}}) dz$$

It is assumed that the Photosynthetic Available Radiation (PAR) I_{par} is derived from the shortwave irradiance term given by the physical model (see next chapter) taking in to account the extinction due to suspended living particles. The irradiance used as forcing function for the calculation of production rates is written as:

$$I_{PAR} = \epsilon_{PAR} Q_s \mathrm{e}^{(\lambda_v + \lambda_{bio}) z}$$

Where ε_{par} is the coefficient determining the portion of PAR (usually 0.5), λ_v is the background extinction coefficient of the water and

$$\lambda_{bio} = \sum_j C_{P^{(j)}} Pc^{(j)} + C_{R6} R6c + C_{ISM} ISM$$

This is the extinction coefficient due to phytoplankton groups, particulate detritus and suspended inorganic matter, respectively. The different C factor represent the specific fraction to the total extinction coefficient of each suspended substance.

Nutrient s regulating factor

The nutrients uptake processes in phytoplankton are decoupled from the photosynthetic carbon assimilation process. This kind of approach has been chosen on the basis of several observations indicating a decoupled interactions

between the uptake of inorganic carbon and nutrients (Sambrotto *et al*., 1993; Copin-Montegut, 2000; Thomas *et al*., 1999; Osterroht and Thomas, 2000). The basic idea of the decoupling is that the Redfield ratio (Redfield *et al*., 1963) is considered as the threshold value between a nutrient-limiting and non-limiting situation, and that the intracellular varying nutrient/carbon quota in phytoplankton always vary within a fixed range around a fixed threshold. The Redfield ratio ($R_{(r_c^{p,n})}$) values are introduced in the model equations as a constant parameters.

According to the value given by Sommer (1994), it is assumed that the minimum quota for nitrogen and phosphorus correspond to the nutrient content of the structural parts of the cell and are taken to be half the Redfield ratio as follows:

$$P_p^{min} = \frac{R_{(r_c^p)}}{2}, N_n^{min} = \frac{R_{(r_c^n)}}{2}$$

The maximum value are the maximum storage capacity of phosphorus and nitrogen with respect to carbon, taken to be twice the Redfield ratio:

$$P_p^{max} = 2\,R_{(r_c^p)}, N_n^{max} = 2\,R_{(r_c^n)}$$

The minimum quota are used in conjunction with Redfield ratio for determining the internal nutrient status of cells. The regulating factor for the nutrient limitation depends on the difference between the minimum reference value and the actual dynamical internal quota as:

$$f_p^P = min\left(1, max\left(0, \frac{(P_p / P_c - p_p^{min})}{(R_r^n - p_p^{min})}\right)\right)$$

$$f_p^n = min\left(1, max\left(0, \frac{(P_p/P_c - n_p^{min})}{(R_r^p - p_p^{min})}\right)\right)$$

In order to make the decoupling effective, these non dimensional parameters are only applied to the carbon loss terms and not to the assimilation of CO_2 trough the photosynthesis.

Concerning the silica dynamics it remains coupled to the uptake of inorganic carbon. This difference with respect to the others nutrients is due to the lack of internal storage capacity for silica in diatoms. A Michaelis-Menten function controls the regulating factor for silica:

$$f^s_{(P^{(1)})} = \frac{N^{(5)}}{(N^{(5)} + h_{(p)})}$$

This is function of the external silica concentration, where h_p is the half saturation constant of silicate concentration in the water.

The combined effect of the regulating factors for nutrient limitation is parameterized applying the Liebig principle of the most limiting nutrient, in the following form:

$$f_p^{n,p} = min(f_p^p, f_p^n); f_{(p^{(1)})}^{n,p,s} = min(f_{(p^{(1)})}^{n,p}, f_{(p^{(1)})}^s)$$

2.1.3 Zooplankton

Four different zooplankton groups are present in the model, with different position in the food web and parameter values:

1) microzooplankton (state variable Z5), representing the biomass concentration of heterotrophic microzooplankton with dimensions ranging from 20 to 200 μm, exluding flagellates and naupliar/larval stage of multicellular zooplankton or meroplankton larvae of benthic organism;
2) heterotrophic nanoflagellates, state variable Z6, protozoa with dimensions

between 2 and 20 μm, mainly grazing upon picophytoplankton and bacteria;

3) carnivorous mesozooplankton Z3, including copopods, anellids chetognaths and cnidarians
4) omnivourus mesozooplankton Z4, mainly composed of calanoid copepods

2.1.4 Pelagic bacteria

Pelagic bacteria (state variable B1) in the model are a large group comprising free-living heterotrophic bacteria that utilize non-living organic substrate, both in dissolved and particulate detritus form. The complete mathematical model formulation of the bacteria sub model is given in the box equation1 and 2 (from Vichi, 2002).

The formulation of the carbon uptake process (equation 5) suppose that it is regulate either by the environmental factors and by the availability of the substrate itself if limiting. The environmental control defines the carbon uptake in case of non limiting substrate, and it is a function of the bacterioplankton physiological state and the environmental temperature and oxygen availability. Several non dimensional factors controls the health status of bacterioplankton as a function of intracellular ratios with respect to the internal nutrient content:

$$f_B^{n,p} = min(q^n, q^p)$$

where

$$q^p = min\left(1, \frac{B_p / B_c}{p^{opt}}\right) \quad \text{and} \quad q^n = min\left(1, \frac{B_n / B_c}{n^{opt}}\right)$$

where p^{opt} and n^{opt} are the Goldman *et al*., (1987) P/C and N/C intracellular reference ratios in the model unit (mmol (N,P)/mg C)

The terms G^{sub} in the carbon uptake equation (5) is the carbon demand dependent on the dissolved and particulate substrate "quality" and size-defined time scale for the uptake processes ($\nu_R^{(1)}$ and $\nu_R^{(6)}$). The quality of the substrate is

defined on the basis of the N/C and P/C ratios in $R_j^{(1)}$ and $R_j^{(6)}$ through a non dimensional factor computed according to a Liebig limiting factor formulation:

$$f_{R^{(j)}}^{n,p} = min\left(1, \frac{R_p^{(j)}/R_c^{(j)}}{P^{opt}}, \frac{R_n^{(j)}/R_c^{(j)}}{n^{opt}}\right)$$

this term tends toward zero when the available substrate is nutrient-depleted, and to 1 in case of optimal N and P content with respect to the reference intracellular ratio p^{opt} and $n^{opt.}$

Bacterial Flux equation	
$\left.\frac{\partial B_C}{\partial t}\right\|_{bio} = \left.\frac{\partial B_C}{\partial t}\right\|_{R_C^{(1)}}^{bcd} + \left.\frac{\partial B_C}{\partial t}\right\|_{R_n^{(6)}}^{bcd} - \left.\frac{\partial B_C}{\partial t}\right\|_{O^{(3)}}^{rsp} - \left.\frac{\partial B_C}{\partial t}\right\|_{R_C^{(1)}}^{out} - \sum_j \left.\frac{\partial B_C}{\partial t}\right\|_{Z_C^{(j)}}^{prd}$	(1)
$\left.\frac{\partial B_n}{\partial t}\right\|_{bio} = \frac{R_n^{(1)}}{R_C^{(1)}} \left.\frac{\partial B_C}{\partial t}\right\|_{R_C^{(1)}}^{bcd} + \frac{R_n^{(6)}}{R_C^{(6)}} \left.\frac{\partial B_C}{\partial t}\right\|_{R_n^{(6)}}^{bcd} + f_B^n \left.\frac{\partial B_n}{\partial t}\right\|_{N^{(4)}}^{upt,rel} - \frac{B_n}{B_C} \left.\frac{\partial B_C}{\partial t}\right\|_{R_C^{(1)}}^{out} - \frac{B_n}{B_C} \sum_j \left.\frac{\partial B_C}{\partial t}\right\|_{Z_C^{(j)}}^{prd}$	(2)
$\left.\frac{\partial B_p}{\partial t}\right\|_{bio} = \frac{R_p^{(1)}}{R_C^{(1)}} \left.\frac{\partial B_C}{\partial t}\right\|_{R_p^{(1)}}^{bcd} + \frac{R_p^{(6)}}{R_C^{(6)}} \left.\frac{\partial B_C}{\partial t}\right\|_{R_p^{(6)}}^{bcd} + f_B^p \left.\frac{\partial B_p}{\partial t}\right\|_{N^{(1)}}^{upt,rel} - \frac{B_p}{B_C} \left.\frac{\partial B_C}{\partial t}\right\|_{R_C^{(1)}}^{out} - \frac{B_p}{B_C} \sum_j \left.\frac{\partial B_C}{\partial t}\right\|_{Z_C^{(j)}}^{prd}$	(3)
$\left.\frac{\partial B_S}{\partial t}\right\|_{bio} = 0$	(4)

Box equation 1.

Bacterial functional processes equations	
$\left.\frac{\partial B_C}{\partial t}\right\|_{R_C^{(1)}, R_C^{(6)}}^{bcd} = \min\left(G^{env}, G^{sub}\right)$ (5)	
$G^{env} = f_B^{n,p} f^T r_{0_B} B_C$	(6)
$G^{sub} = v_{R^{(6)}} f_{R(6)}^{n,p} R_C^{(6)} + v_{R^{(1)}} f_{R^{(1)}}^{n,p} R_C^{(1)}$	(7)
$\left.\frac{\partial B_C}{\partial t}\right\|_{O^{(3)}}^{rsp} = b_B f_B^T B_C + [1 - \eta_B - \eta_B^o (1 - f_B^o)] \left.\frac{\partial B_C}{\partial t}\right\|_{R_C^{(1)}, R_C^{(6)}}^{bcd}$	(8)
$\left.\frac{\partial B_C}{\partial t}\right\|_{R_C^{(1)}}^{out} = f_B^T d_{0_B} B_C$	(9)
$\left.\frac{\partial B_p}{\partial t}\right\|_{N^{(1)}}^{upt,rel} = v_B^p \left(\frac{B_p}{B_C} - p_B^{max}\right) B_C$	(10)
$\left.\frac{\partial B_p}{\partial t}\right\|_{N^{(4)}}^{upt,rel} = v_B^n \left(\frac{B_n}{B_C} - n_B^{max}\right) B_C$	(11)

Box equation 2.

The respiration terms is divided in basal and activity respiration as shown in (8). The basal respiration is parameterized as for phytoplankton with a constant specific respiration rate b_B and the regulating factor for temperature given in the previous section. The parameter η_b in the activity respiration term, represents the bacterial growth efficiency (BGE) under oxic situation, and η_b^o is the efficiency decrease under low oxygen conditions. This parameterization has been chosen in order to consider the differences in the energetic of the metabolic pathways in relation to the oxygen availability, since anaerobic bacteria have a lower actual BGE because they need to respire more carbon in order to produce the same amount of energy. The oxygen regulating factor is parameterized with a Michaelis-Menten formulation as:

$$f_b^o = \frac{(O_2)}{(O_2 + h_B^o)}$$

where O_2 is the dissolved oxygen concentration and h_B^o is the oxygen concentration at which the metabolic functionality are halved.

Concerning the remaining loss term (equation 9), it has been assumed that bacteria in the model have no carbon losses except for respiration and a first order background mortality meant to mimic viral density dependent lysis. The mortality term is composed by a constant specific mortality rate d_0 and is modulate by the temperature regulating factor. Note that all bacterial lysis products go to the DOM pool.

The heterotrophic flagellates are the major predators of bacteria, but the predation terms is extended to other groups. Bacteria can also be preyed by microzooplankton.

Nutrient Dynamics

Nutrient dynamics are mostly connected to carbon dynamics, except for the direct nutrients uptake and remineralization processes as shown in the dynamical equations for nitrogen and phosphorus components. The rate of change of the P-component of bacteria is related to the phosphorus content into particulate and dissolved organic matter via the bacterial uptake rates written in equation 10. the uptake/remineralization term from or to the dissolved nutrient pool is given in the equation 10, where ν_B^p is the constant specific maximum uptake rate (in d^{-1}). Depending on the internal nutrient-to carbon ratios bacteria can behave as remineralizer or as competitors with the phytoplankton, taking up inorganic nutrients directly from the water. In the model this is achieved using the non dimensional parameter f_B^p that gets different value according to the following equations:

$$f_B^p = -1 \quad \text{if} \quad \frac{B_p}{B_c} - p^{opt} > 0$$

and

$$f_B^p = \frac{N^1}{(N^1 + h_B^p)} \qquad \text{if} \qquad \frac{B_p}{B_c} - p^{opt} < 0$$

If the nutrients ratio is higher than the maximum one allowed in the cell, there is excretion and the f_B^p becomes equal to -1. In the opposite case, when bacteria have lower the internal optimal ratio, they can take inorganic phosphorus from the water column as a function of the nutrient concentration in a Michaelis-Menten form competing for nutrients with phytoplankton. h_B^p is the concentration of nutrients at which the uptake velocity is halved (half saturation constant).
The nitrogen dynamics in Bacteria involves only ammonium and the uptake release term is equal to the one for phosphate substituting the ammonium concentration and the relative half saturation constant.

2.1.5 Dissolved organic matter

The source/sink terms in functional process form for dissolved organic matter (ordinary state variable R1) are the consequence of the production/consumption rates of phytoplankton, zooplankton and bacterioplankton. Dissolved organic matter (DOM) is produced by phytoplankton, bacteria and microzooplankton and used as organic substrate by bacteria.
In the basic model that we have used only one kind of DOM was present. This thesis developed new state variables for DOM (R2 and R7) which consider the more or less labile state of the organic matter depending on its production process due to phytoplankton, zooplankton and bacteria.

CHAPTER 3

3 DOM-Bacteria interactions in marine oligotrophic systems: a theoretical modelling study

3.1 Introduction

Dissolved organic carbon (DOC) in the ocean is one of the largest carbon pools of the Earth. Consequently, understanding the processes governing DOC production, accumulation and consumption is a very important goal for the quantitative assessment of the global carbon cycle. The extracellular release of recently fixed photosynthate is the major DOC production process in the marine ecosystem (Maranon *et al*., 2004). This DOC flux is particularly important in defining the structure of the marine planktonic trophic web, since the released carbon can be taken up by heterotrophic bacteria establishing a direct link between primary and bacterial production that is essential for the cycling of matter through the food web (Ducklow and Carson 1992; Legendre and Rassoulzadegan 1996). DOC cycling in marine ecosystem is almost completely governed by bacteria but the process occurs over different time scales: about 20% of the DOM pool constitutes the labile fraction and turns over rapidly, on a time scale of hours to days; this labile fraction almost entirely supports bacterial production. The remainder (refractory pool) is cycled by bacteria on a time scale ranging from week to months (Ogura, 1976; Moran and Hodson, 1990). Bacterioplankton actively contribute to the refractory DOC pool through the release of extracellular mucopolisaccharides to form mucilaginous protective capsules around the cell and/or slimes and fibrils (Stoderegger and Herndl, 1998; Azam *et al*., 1999; el Giorgio and Cole, 1998). The release rate of capsular material has been estimated to be about 25% of the bacterial respiration rate and this suggest that a considerable portion of the oceanic DOC pool should consist of ‘semi labile’

bacterial derived DOC (Stoderegger and Herndl, 1998). This release of metabolites could be a pathway of energy dissipation that may contribute to the maintenance of intracellular stoichiometry (del Giorgio and Cole, 1998).

Bacterially driven Dissolved Organic Matter (DOM) cycling is particularly important in the oligotrophic system where heterotrophic bacteria constitute the major living carbon pool in the euphotic zone (Jurgens *et al*, 2000) and the prokaryotes are the dominant primary and secondary producers of organic matter (Whitman *et al*., 1998). In such systems there is a significant competition between bacteria and phytoplankton for inorganic nutrients (Hagstrom *et al*., 2001) and heterotrophic nanoflagellate excretion products (DOC and inorganic nutrients) are a significant source of substrate for both bacteria and picophytoplankton (Hagstrom *et al*., 2001). This ecosystem structure characterizing oligotrophic systems is often referred to as the "microbial loop" (Azam *et al*., 1983).

The mean DOC concentration in the open ocean appears remarkably constant (Fajon et. al, 1999) suggesting that most of the marine DOC is made of very slowly degradable substances, however, in coastal areas, DOC accumulation may occur on a seasonal scale. DOC accumulation was found to be caused by both to sustained phytoplankton DOC excretion occurring during the spring bloom and to a weakened bacterial efficiency in organic carbon cycling. (Carlson *et al*., 1994, Williams, 1995). On the other hand Azam *et al*. (1999) stressed the bacterial role in DOM accumulation suggesting that bacterial processing of organic matter and bacterial exopolysaccharides production are the pivotal control on polysaccharides accumulation.

An increase in DOC concentration during the high primary productivity period, means that the flux of energy and organic carbon through the chain DOC-bacteria-protozoa-metazoa could vary in terms of efficiency. Low bacterial growth efficiency (BGE) boosts the bacterial respiration and hence causes a decrease in biomass. BGE tends to be high in eutrophic environments and decrease with increasing oligotrophy (Eiler *et al*., 2003); this is supposed to be the consequence of a decoupling between anabolism and catabolism observed when bacteria growth is constrained by organic substrate or inorganic nutrients (Del Giorgio and Cole, 1998). Despite the fact that it is well known that the carbon flux into

bacteria (and BGE) may be limited by dissolved organic matter quality, inorganic nutrients and temperature (Church *et al*., 2000), it is not yet clearly understood how external nutrients concentration and the C/(N,P) ratio of organic substrate affect the BGE and the degradability of DOC .

We propose a theoretical model to describe DOC-bacterial interactions, in particular describing the variation of bacterial growth efficiency and the bacteria DOM 'processing' mechanisms leading to the DOC accumulation. We also use numerical simulations to test the following hypothesis: can a simplified microbial loop-like system to sustain itself by recycling nitrogen and phosphorus without invoking external sources?

3.2 The Model

The model used is a recent version of the European Regional See Ecosystem Model (ERSEM), (Baretta *et al*., 1995) which is described in full in Blackford *et al* (2004). ERSEM is a modelling framework in which the ecosystem is represented as a network of physical, chemical and biological processes. A 'functional group' approach is used to describe the biota. The ecosystem is subdivided into three functional types: primary producers, consumers and decomposers, and subdivided on the basis of trophic links and/or size. It should be noted that individual species may straddle more that one functional group, and that the functional groups describe particular types of behaviour rather than species lists. Physiological (ingestion, respiration, excretion and egestion) and population (growth, and mortality) processes are included in the descriptions of functional group dynamics. These dynamics are described by fluxes of carbon and nutrients between functional groups. Each functional group is defined by a number of components, namely carbon, nitrogen, and phosphorus and, in the case of diatoms silicon, each of which is explicitly modelled. The model is generic and has been demonstrated to function in a wide range of ecosystems from temperate eutrophic coastal waters, to upwelling areas and the ultra oligotrophic eastern Mediterranean without making parameter changes (Blackford *et al* 2004).

In its standard configuration the bacterial and DOC dynamics is described

according to Allen *et al*. (2002). However the capacity of bacteria to actively produce DOC is not well described in the model and the role of bacteria in terms of their capacity to 'transform' organic matter is under estimated. For this work we have used a zero D version of ERSEM2004 (Blackford *et al* 2004) to which we added a new bacterial submodel.

3.2.1 The bacterial sub-model

The labile characteristics of DOM are thought to be dependent on two factors: its "quality", defined in terms of its C:N and C:P ratios and the structure of organic molecules constituting the DOM matrix. In order to account for these factors, the bacterial and DOM dynamics proposed here is based on the partition of the DOM (differently from previous ERSEM configurations Baretta Bekker *et al.,* 1998, Allen *et al.,* 2002, Vichi *et al.,* 2003) into three distinct classes/state variables, each having different production pathways, different structure and composition and corresponding to different degrees of lability.

A schematic representation of our proposed DOM-Bacteria interactions is given in Fig. 3.1. The most labile fraction of the total DOM pool (R1 in Fig. 3.1) is produced by phytoplankton, zooplankton and bacteria via lysis, mortality and sloppy feeding processes and is characterized by high N:C and P:C values. A semi-labile DOM faction is excreted by phytoplankton and bacteria in order to achieve/maintain their internal 'optimal' stoichiometry (R2 in Fig. 3.1). This part of DOM production can be thought of as a release of excess of carbon and, therefore, is constituted only by DOC. Finally DOM release by bacteria as capsular material (R7 in Fig. 3.1) is, in our system, the most refractory fraction of the DOM. This component of the DOM pool is also assumed to be only DOC and formed by high molecular weight substances which are assumed to be quite resistant to enzymatic attack (Stoderegger and Herndl, 1998). Each DOM variable is linked to a different time scale of degradation, R1 being the most rapidly degraded and R7 the most refractory.

A schematic description of DOM classification and production is given in tab 3.1.

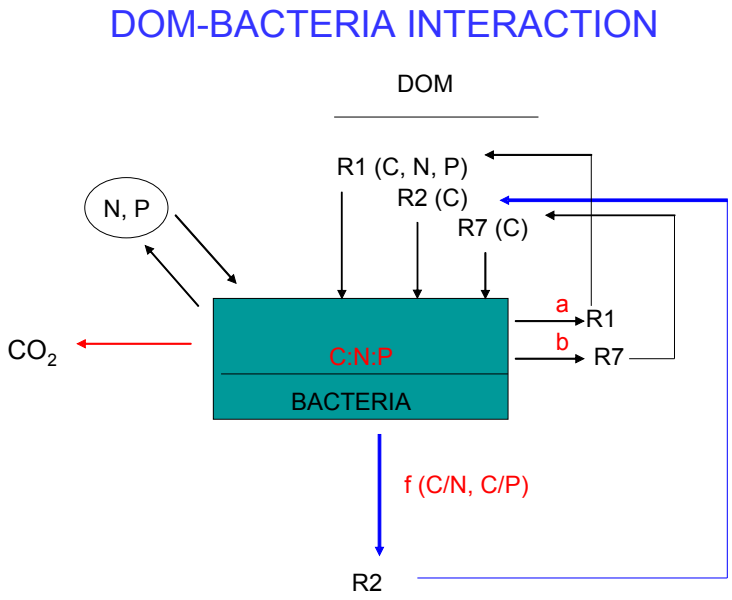

Figure 3.1. DOM Bacteria interactions. R1=labile organic matter; R2=semilabile organic matter R7=refractory organic carbon, a=excrection due to the mortality, b=fraction of DOM uptake released as capsular material; f=carbon release flux as function of the total C/N and C/P ratio.

.

	Variable	***Producers***	***Process***	***Composition***
DOM	R1 (labile)	Phytoplankton Zooplankton Bacteria	Mortality Sloppy feeding	C,N,P
	R2 (semilabile)	Phytoplankton Bacteria	Exudation Release	C
	R7 (refractory)	Bacteria	Capsular material release	C

Table 3.1. Dissolved organic carbon components, producers and composition

The bacterial carbon uptake was, therefore, formulated as follows (modified from Vichi *et al*. 2003).

All the following formulation are written in the form $\left.\frac{\partial A}{\partial t}\right|_{Y}^{X}$ where A is the state variable, X is the process described and Y the other variables involved.

The carbon uptake on each DOM class is given by

$$\left.\frac{\partial B1c}{\partial t}\right|_{R1c,R2,R7}^{uptake} = \min\left(Genv, Gsub\right)$$

Where *Genv* is the maximum potential uptake of DOC given by

$$Genv = f^{t}\ r_{o} B1c$$

And *Gsub* is the substrate availability given by

$$Gsub = n_1 R1 + n_2 R2 + n_7 R7$$

B1c is the bacterial carbon biomass, f^t is a temperature dependant growth function (Blackford *et al* 2004), r_o is the potential uptake and n_1, n_2 and n_7 are the daily fraction of each substrate available for uptake.

The dissolved organic phosphorus and nitrogen uptake is based on the uptake of the R1 following the formulation:

$$\left.\frac{\partial B1n,p}{\partial t}\right|_{R1n}^{uptake} = \left.\frac{\partial B1c}{\partial t}\right|_{R1c}^{uptake} \frac{R1n,p}{R1c}$$

Where B1(n,p) is the content of nitrogen and phosphorus inside bacteria and R1n,p is the dissolved organic nitrogen and phosphorus concentration.

It should be stressed that the DOC available for uptake is not constrained by nitrogen and phosphorus availability in the DOM. The bacteria can balance their

'optimal' internal nutrients carbon ratio level by assimilating inorganic dissolved nitrogen and/or phosphorus, if available or, conversely, by releasing the excess DOC into the R2 pool.

The carbon release and the inorganic N and P uptake are regulated by the reference C/N and C/P optimal value for the bacteria proposed by Goldman *et al*. (1987) in the following way: (for the uptake/remineralization process we show only the case of phosphorus).

$$\left.\frac{\partial B1_c}{\partial t}\right|_{R2}^{release} = \max\left[0, \max\left(1-\frac{qpb}{p^{opt}}\right)\left(1-\frac{qnb}{n^{opt}}\right)\right] B1_c \nu$$

$$\left.\frac{\partial B1_p}{\partial t}\right|_{N1p}^{uptake,remineralization} = \nu\left(\frac{B1_p}{B1_c} - p^{opt}\right) B1_c f_n$$

Where:

$$f_n = -1 \qquad \text{if} \qquad \frac{B1_p}{B1_c} - p^{opt} > 0$$

$$f_n = \frac{N1_p}{N1_p + h_b} \qquad \text{if} \qquad \frac{B_p}{B_c} - p^{opt} < 0$$

Where p^{opt} and n^{opt} are the optimal internal nutrient quota (C:N:P=45:9:1, Goldman *et al*.,1987), qpb and qnb are the actual N:C and P:C cellular ratio, ν is the characteristic time scale of the process (d^{-1}) and h_b is the half saturation constant.

Consequently bacteria work as a 'biological filter' of organic matter whose capacity to keep organic carbon (and therefore convert it in biomass) is dependent on the availability of nutrients (both organic and inorganic). This allows bacteria to modify the C/N and C/P ratio inside the DOM and then reproduce the 'enzymatic fractionation', due to a selective utilization of dissolved nitrogen and

phosphorus rather than carbon, described by Azam *et al*. (1999).

The carbon flux from bacteria to the semi labile DOC pool (R2) represents the carbon taken up but not assimilated, allowing the model to reproduce the uncoupling between cellular catabolism and anabolism (and therefore a decrease in bacterial growth efficiency) observed when bacterial growth is constrained by nutrient depleted conditions (Del Giorgio and Cole, 1998).

A fixed quota of bacteria production is directed to the R7 variable in order to describe the capsular material release observed by Stoderegger and Herndl (1998).

$$\left.\frac{\partial B1_C}{\partial t}\right|_{R7}^{release} = \left(\left.\frac{\partial B1_C}{\partial t}\right|_{R1c,R2,R7}^{uptake} - \left.\frac{\partial B1_C}{\partial t}\right|_{O2}^{respiration} \right)\alpha$$

Where α is the daily fraction of bacterial production released as capsular mucopolisaccharides material. The respiration term is broken down in rest respiration and activity respiration in this way:

$$\left.\frac{\partial B1_C}{\partial t}\right|_{O2}^{respiration} = \left.\frac{\partial B1_C}{\partial t}\right|_{O2}^{activitiresp} + \left.\frac{\partial B1_C}{\partial t}\right|_{O2}^{restresp}$$

where the activity respiration term is given by:

$$\left.\frac{\partial B1_C}{\partial t}\right|_{O2}^{activityresp} = \left[1-\eta_b-\eta_b^0\left(1-f_0\right)\right]\left.\frac{\partial B1_C}{\partial t}\right|_{R1c,R2,R7}^{uptake}$$

where η_b is the maxima theoretical assimilation efficiency and η_b^o is the efficiency decrease under the low oxygen condition. f_o is the oxygen regulating factor parameterized with a Michaelis-Menten formulation as

$$f_0 = \frac{(O_2)}{(O_2 + h_o)}$$

where O_2 is the oxygen concentration and h_b is the oxygen concentration at which the metabolic functionalities are halved.
The rest respiration term is given by:

$$\left.\frac{\partial B1_C}{\partial t}\right|_{O2}^{restresp.} = b_o f^t B1_c$$

where b_o is the daily rest respiration activity
The background mortality is described by a simple first order equation in order to mimic viral lysis:

$$\left.\frac{\partial B1_C}{\partial t}\right|_{R1c}^{mortality} = f^t d_0 B_c$$

where f^t is the temperature regulation factor and d_0 is the specific mortality rate.

The major change in the phytoplankton dynamics, with respect to ERSEM 2004, is that the cellular exudation regulated by nutrients stress is directed to the R2 variable instead R1.

3.2.2 Bacterial growth efficiency

The BGE is calculated as the ratio between the particulate bacterial production (BSP) and the total carbon uptake:

$$BGE = BSP / \left.\frac{\partial B1_C}{\partial t}\right|_{R1c,R2,R7}^{uptake}$$

where BSP is given by:

$$BSP = \left.\frac{\partial B1_C}{\partial t}\right|_{R1c,R2,R7}^{uptake} - \left.\frac{\partial B1_C}{\partial t}\right|_{CO2}^{respiration} - \left.\frac{\partial B1_C}{\partial t}\right|_{R2}^{release} - \left.\frac{\partial B1_C}{\partial t}\right|_{R7}^{release} - \left.\frac{\partial B1_C}{\partial t}\right|_{R1c}^{mortality}$$

In this way BGE can vary for C-limitation when the rest respiration is significant

with respect to the carbon uptake and in a nutrient limitation condition when the carbon-release flux is high.

3.3 Simulations setup

In order to investigate the behaviour of our model we performed three sets of experiments.

A simple degradation experiments with only bacteria and organic matter. This system was run with 2 different initial conditions for nutrients in order to simulate contrasting environmental conditions (eutrophic and oligotrophic).
A bacteria-primary producer (diatoms) system in order to investigate the competition between phyto and bacterioplankton for dissolved nutrients.
A simplified microbial loop consisting of bacteria, picophytoplankton and heterotrophic nanoflagellates, to investigate if the microbial loop can sustain it self with out invoking external source of N and P.

All the simulations are run in batch mode with a dark/light cycle of 12 hours and a constant temperature of 20°C.

The initial conditions for each experiment carried out are shown in Tab. 3. The list of the bacterial parameters used is referred in Tab. 2. All the other parameters concerning the zooplankton and phytoplankton sub model are taken from Blackford *et al* 2004.

System	*Functional groups*	*Sub system*	*SiO2*	*NO3*	*NH4*	*PO4*	*DOC (R2)*
1	Bacteria	1a	-	-	0,5	0,15	5000
		1b	-	-	10	1	5000
2	Bacteria Diatoms	2a	1,25	1,25	0,25	0,07	0
		2b	3	2,5	0,5	0,15	0
		2c	6	5	1	0,3	0
		2d	1,25	1,25	0,25	0,07	5000
3	Bacteria Picophyto. Eteroflag.	3a	1,25	1,25	0,25	0,15	0
		3b	3	2,5	0,25	0,07	0
		3d	6	5	1	0,3	0

Table 3.2. Initial conditions and experiments configuration.

3.4 Results

3.4.1 The degradation experiment

This experiment is designed to demonstrate the interactions between, bacteria, DOC and nutrients. Figure 3.2.A shows the distribution of DOC in the two sub-experiments 1a and 1b which are characterized by with different initial nutrient concentrations. The simulation with the larger amount of nutrients as initial conditions (1b) degrades the organic carbon faster (Fig. 3.2A). The bacteria biomass distribution (Fig. 3.2.B) shows that, even though the rates of DOC degradation are similar in magnitude, the biomass is significantly larger in the higher nutrient simulation. This indicates that when inorganic nutrients are available bacterial growth is enhanced.

Analysis of bacterial C/P ratio (Fig. 3.2C) shows that bacteria in the system 1b are nutrient limited for the first 10 days while in system 1a the C/P ratio reach its equilibrium value (45, the transition between nutrient and carbon limitation), after 19 days (the point at which it reaches the Goldman limit). This trend is confirmed by the bacterial carbon release flux whose maximum is 120 mg C m^{-3} d^{-1} in the

system 1a and 60 mg C m^{-3} d^{-1} in the system 1b (data not shown). The bacterial respiration is scaled by the biomass and is therefore much higher in the low nutrient simulation (Fig. 3.3D). Bacterial growth efficiency (Fig.3.2E) calculated during the growth phase of bacteria (the first ten days) is higher in the simulation 1b resulting in a larger transformation of DOC in bacteria biomass. When the carbon supply is exhausted the bacteria die.

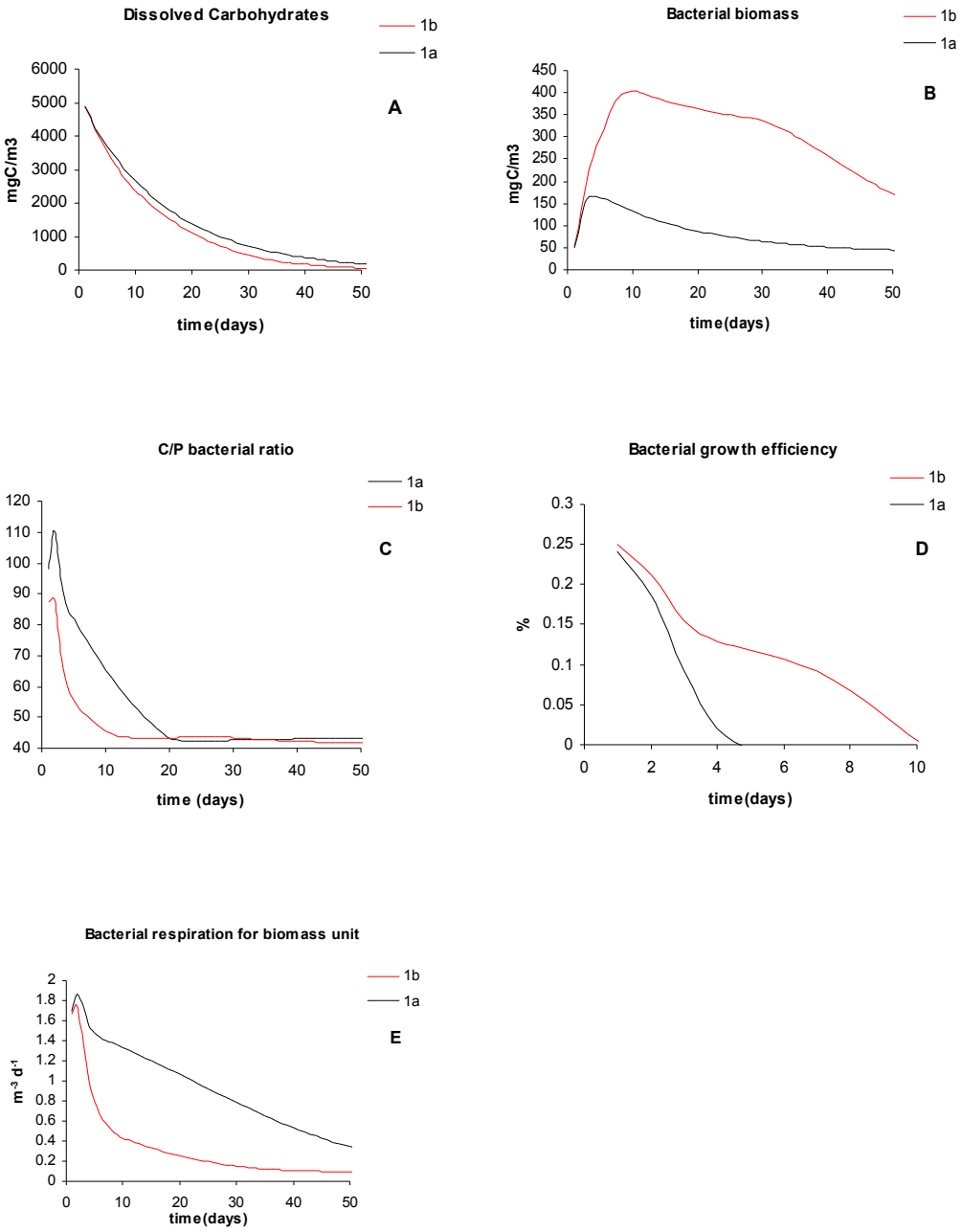

Figure 3.2. Results description of the system 1 experiments (sub system 1A and 1B): Dissolved Carbohydrates (A), Bacterial biomass (B), C/P bacterial ratio (C), Bacterial growth efficiency (BGE) (D) and Bacterial respiration for biomass unit (E).

3.4.2 Diatoms-bacteria system

This experiment investigates the competition between phytoplankton and bacteria for dissolved nutrients and the accumulation of DOC in relation to nutrient availability. The 300-day simulations (Fig. 3.3 and Fig. 3.4) show an oscillatory behavior for all the variables. In particular the oscillation of the internal bacterial carbon-to-nutrient ratios (Fig. 3.4B) around the reference values (45 for P, and 5 for N) denotes that bacterial dynamics is constrained between carbon and nutrient limitation. The oscillation of the release of carbohydrates (Fig. 3.3C) and the remineralization flux of nutrients (Fig. 3.4A) are not in phase indicating that the carbohydrate release occurs in nutrient limitation conditions and nutrient release in C-limited conditions. The period of the oscillations is larger in the system with low nutrients as initial conditions. The trend of the BGE (Fig. 3.3A) shows two kinds of periodicity: after the first 40 days it reaches a minimum value corresponding to the minimum nutrients level and the maximum C-release flux. This minimum value is 0.15 for the system 2a and 0.11 for the system 2b and 2c where the presence of a larger DOC pool, due to the higher primary production, keeps the system in a more strongly N-limited condition avoiding the onset of carbon limitation. Between two minima there are two maxima between which is a relative minimum which corresponds to a minimum concentration of carbohydrates (Fig. 3.3B) indicating carbon limitation as confirmed by the absence of bacterial carbon release (Fig.3.1B). During this phase nutrient remineralization occurs (Fig. 3.3C) The periodic accumulation of DOC occurs with different frequency and intensity in the different systems. The amount of C released by bacteria is related to the DOC produced by diatoms and it is, on the average, 20% of the DOC produced by diatoms through lysis and excretion (data not shown) This percentage is quite similar in the system 2a, 2b and 2c and became higher only in the system with high carbohydrates as initial conditions. In this last experiment during the first 50 days the BGE decreases dramatically and bacteria release a large amount of carbohydrates (Fig. 3.5.A and 3.5.C). Bacterial inorganic nutrient uptake increases causing resource competition with phytoplankton (Fig. 3.5.B). The flux of phosphate uptake by bacteria reaches 0.03 mmol P m^{-3} d^{-1} and the bacterial carbon release 120 mg C m^{-3} d^{-1} .

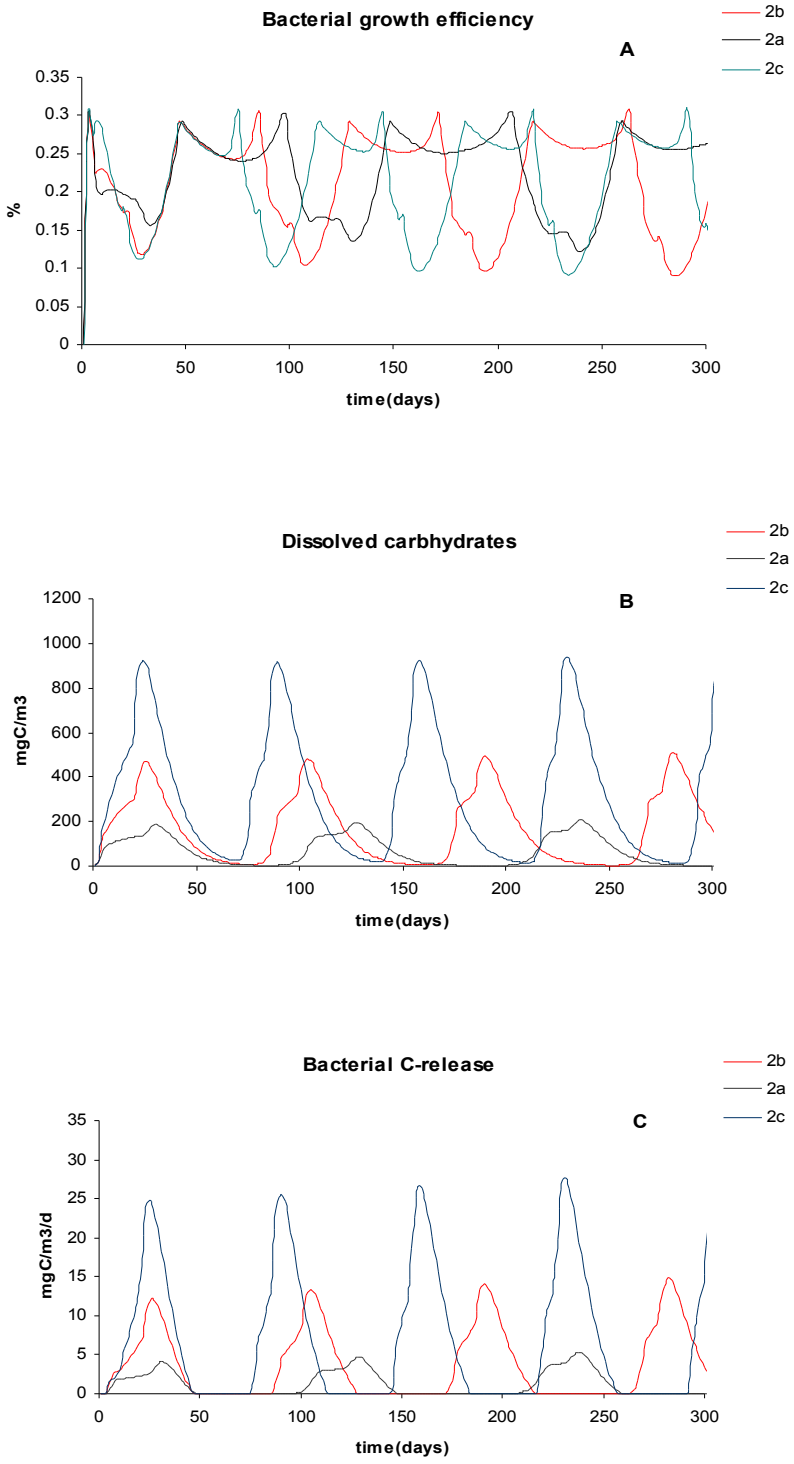

Figure 3.3. Bacterial growth efficiency (A), Bacterial carbon release (B) and dissolved carbohydrates concentration (C) in the system experiments 2. 2a, 2b and 2c are the sub systems described in Table 3.2.

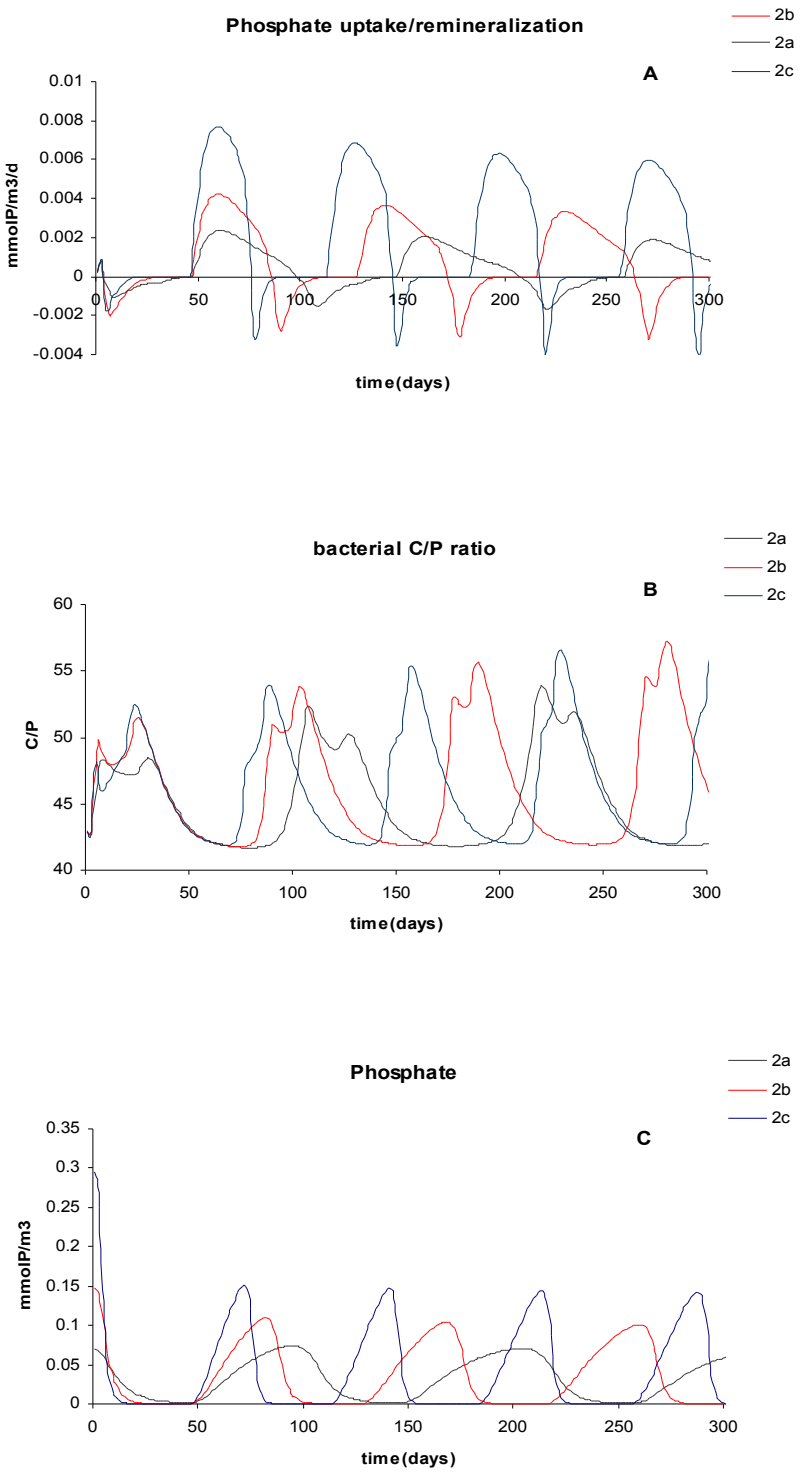

Figure 3.4. Phosphate uptake/remineralization flux (A), bacterial C/P ratio(B) and phosphate concentration (C) in the system2 experiments. 2A, 2b and 2c are the sub system described in Table 3.2.

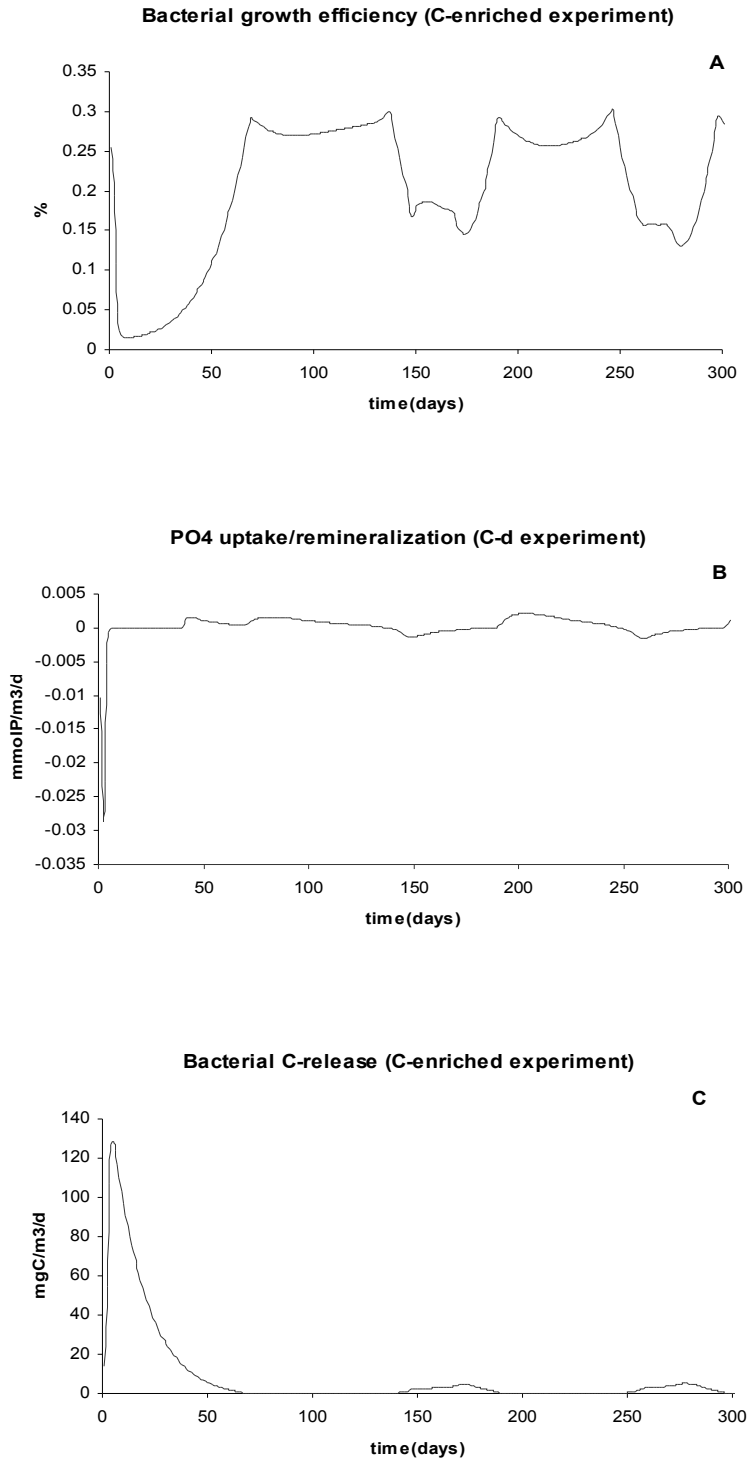

Figure 3.5. Bacterial growth efficiency(A), phosphate uptake remineralization flux(B) and bacterial carbon release (C) in the 2d subsystem experiment (carbon enriched experiment).

3.4.3 Microbial loop simulation

Figure 3.6A shows the BGE in the three simulations. After a 100 day adjustment period (production of DOC by phytoplankton and zooplankton) the BGE reaches a steady state value of 0.22 for the system 3c, 0.17 for the system 3b and 0.11 for system 3a. The phytoplankton biomass (Fig. 3.6B) reaches a steady state after 80 days. In the first 20 days there is a bloom whose magnitude is related to the amount of nutrients available in the initial conditions. Bacterial release of carbohydrates (Fig. 3.6C) reaches its maximum value during the first 20 days of the run when the phytoplankton production is higher. The highest value is reached in the more eutrophic system (58 mg C d^{-1}) where a quite high value is still present after the 20^{th} day. This flux reach a steady state after 100 days. The remineralization/uptake flux of PO4 by bacteria (Fig. 3.7A) is always negative meaning that bacteria are only taking up dissolved nutrients and are competing with phytoplankton. System 3c is characterized by the highest primary productivity rates and shows the maximum uptake of PO4. The flux reaches a stationary value after 100 days. Zooplankton biomass (Fig. 3.7B) achieves the maximum value in the first 20 days as for phytoplankton and bacteria. The excrection of PO4 (Fig. 3.7C) reaches a steady state after 100 days and is more pronounced in system 3c. In Fig. 3.8 is shown the distribution of gross primary production and total (autotrophic and eterotrophic) respiration in the most oligotrophic system (3a): after the first 100 days the gross primary production just compensates the carbon loss due to community respiration and the system reaches a steady state.

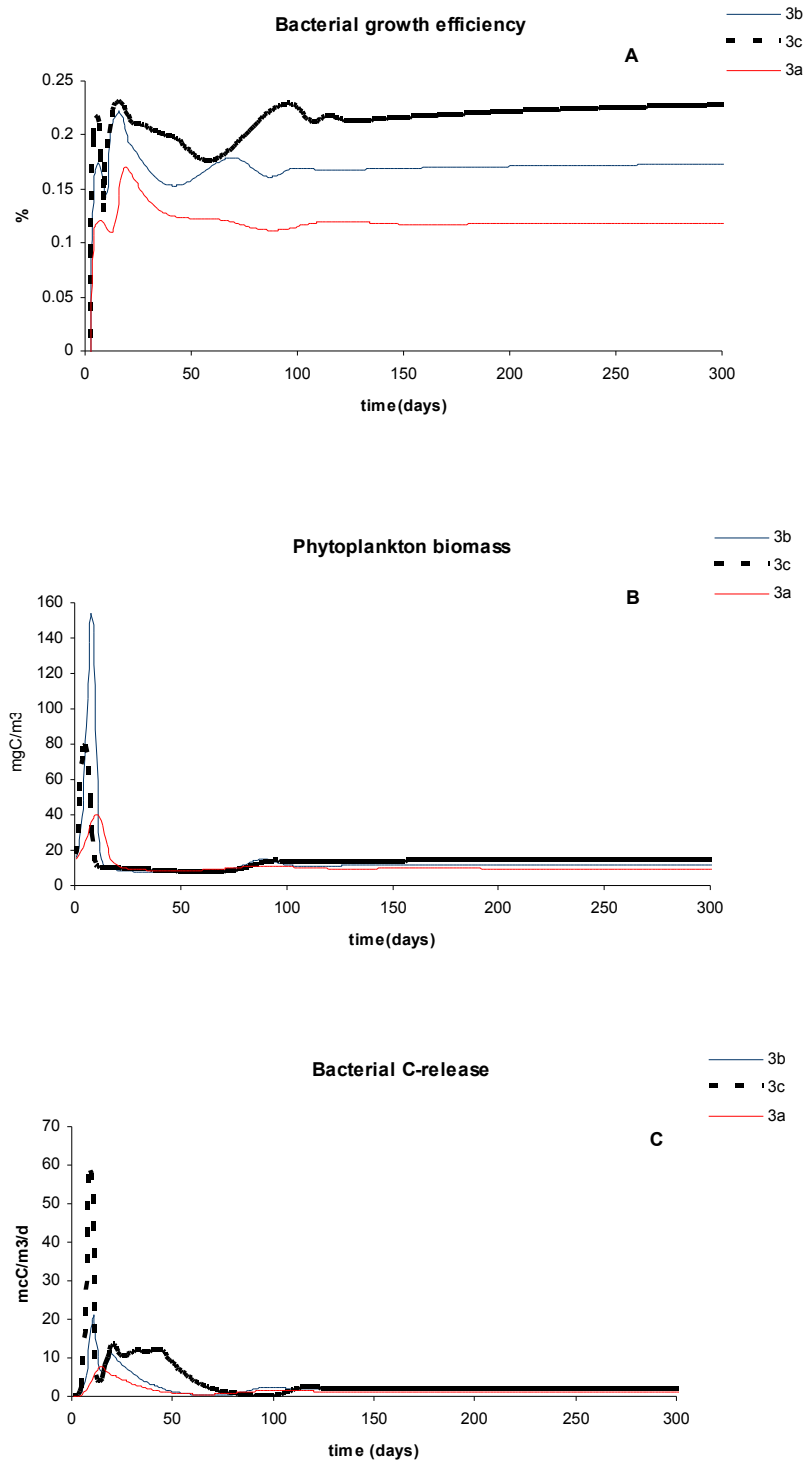

Figure 3.6. Bacterial growth efficiency(A), Phytoplankton biomass(B) and bacterial carbon release(C) in the system 3 experiment; 3a, 3b and 3c represent the different sub system described in Table 3.2.

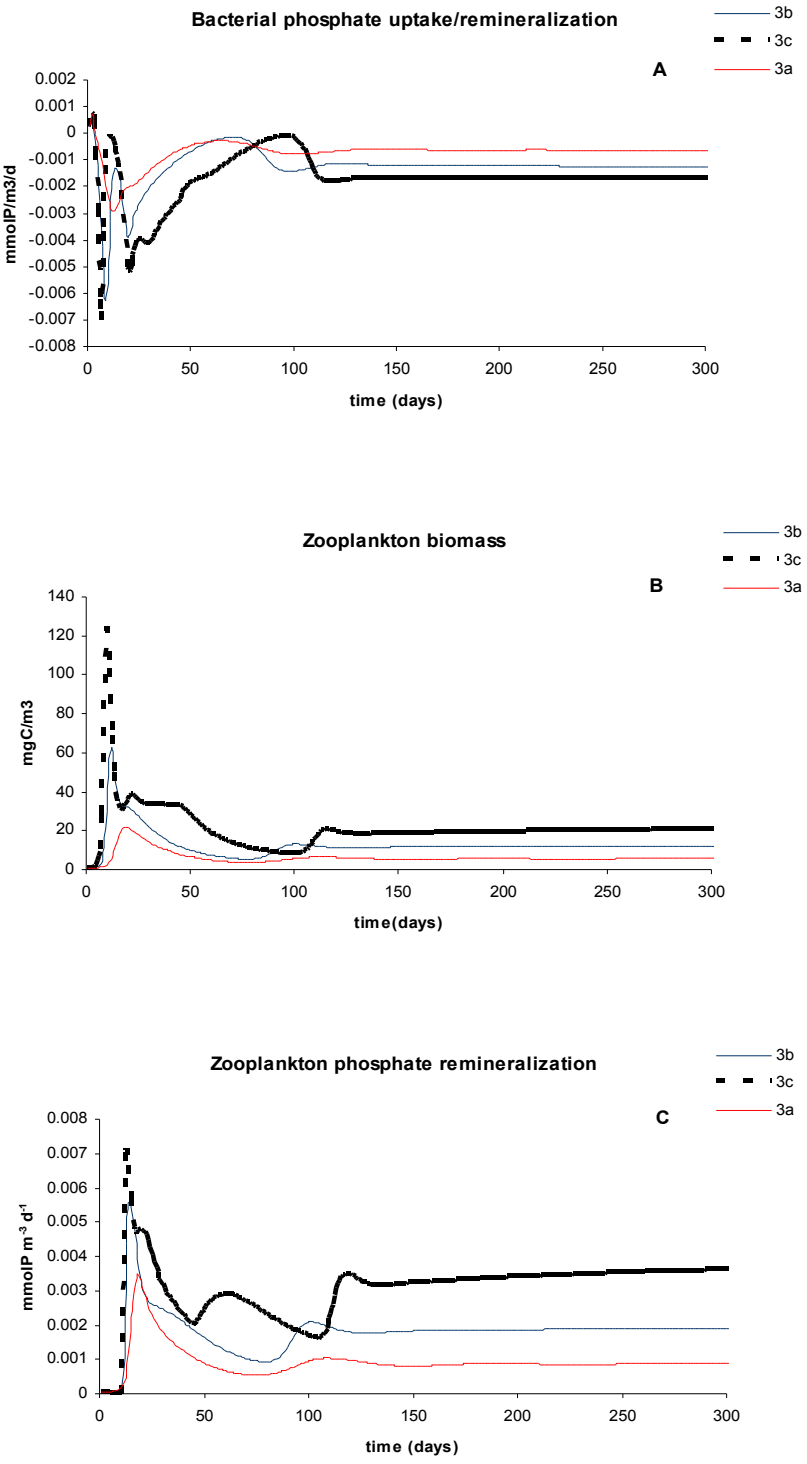

Figure 3.7. Bacterial uptake/remineralization flux (A), zooplankton biomass (B) and zooplankton phosphate remineralization (C) in the system experiment3; 3a, 3b and 3c represent the different sub system described in Table.3.2.

3.5 Discussion

The main difference between this work and the classical Monod approach, based on a fixed BGE value and on a fixed internal carbon/nutrients ratio, is that we based our model on the variability of BGE and the possibility that bacteria modify their cellular stoichiometry. The BGE is regulated by respiration and by the release of surplus carbon. Its variation can be thought of as an adaptation mechanism to different trophic conditions. We also use the concept of 'optimal' carbon/nutrient ratios that bacteria try to achieve but we allow the possibility of adaptation to different intracellular nutrient ratios.

The degradation experiment demonstrates a strong link between the presence of external nutrients and degradation activity. The BGE is higher in the nutrient rich system allowing bacteria to convert detritus into biomass more efficiently. The diatoms-bacteria system shows how bacteria can compete with phytoplankton for external nutrients. This occurs when the primary production is high and the ratio of DOC to nutrients (organic and inorganic) tend to be higher with respect the carbon/nutrient reference ratios of bacteria. When primary production is low bacteria reduce their BGE consequently their biomass becomes carbon limited and starts to remineralize nutrients allowing diatoms to grow again. This mechanism allows the system to sustain itself but not in a stationary mode.

In the microbial loop simulations the presence of a top down control (the heterotrophic nanoflagellates) constrains the oscillations of the system and after an initial unstable phase it reaches a steady- state condition.

During the steady-state, bacteria are nutrient limited as the C/P cellular ratio is higher then the reference ratio. In this case BGE is related to the availability of nutrients. Bacteria can survive in a permanent nutrient limitation condition while the carbon limitation can be just a transitory condition. This is because of the decoupling of nutrients assimilation and carbon metabolism in the bacteria enabling the uptake of DOC without convert it to biomass but just to compensate for the loss due to respiration. The regeneration of nutrients is due to the heteroflagellate activity.

DOC accumulation is described by the flux of carbohydrates from bacteria to the

R2 variable which also indicates the transition between a carbon limitation condition and a nutrients limitation condition. Low nutrient concentrations are a necessary condition for DOC accumulation, but this must be preceded (in time or space) by a period of high primary productivity as suggested by the carbohydrate enriched experiments. The presence of a large amount of DOC with low organic and inorganic N and P concentrations induces a strong competition between bacteria and phytoplankton for PO_4 and NH_4.

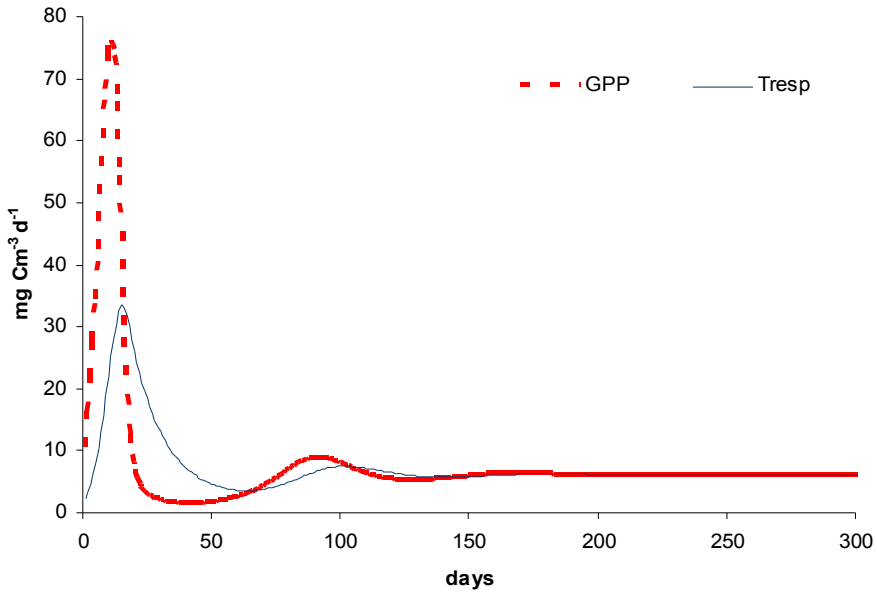

Figure 3.8. Gross primary production (GPP) and community respiration (Tresp) in the 3a subsystem.

3.6 Conclusions

The model proposed appears to be able to describe the bacterial behavior in the oligotrophic systems. The simulations reproduce the variation of BGE with the variation of external nutrients concentration and the simulated values of BGE are consistent with the values reported in literature (Del Giorgio and Cole, 1998). Bacteria contribute to the DOC accumulation in two ways: by decreasing their BGE (and hence the degradation activity) and actively producing semi-labile organic carbon.

Model simulations suggest that bacteria try to maximize the uptake of carbon rather than BGE as suggested by Cole and del Giorgio (1998). They aim to reach their internal 'optimal' stoichiometery taking up both organic and inorganic N and P, and any excess of carbon is released as carbohydrates. When the C/N and C/P ratios are higher than the optimal bacterial level (Goldman value) BGE decreases and DOC accumulation may occur. Bacteria contribute to the refractory carbon pool producing, as a constant part of the bacterial carbon uptake, high molecular weigh polysaccharides.

The model can reproduce a quasi steady state system with a simplified microbial loop situation without invoking external source of N and P. This could explain how a microbial food chain can sustain it self in a natural ultra-oligothrofic systems such as the eastern Mediterranean and the sub tropical gyres.

Bacterial parameters		
	Symbol	***B1***
Environmental effect		
Characteristic Q_{10} (day^{-1})	Q_{10}	2
Half O_2 saturation (day^{-1})	h_o	7,81
Uptake		
Max.spec.uptake rate10°C (day^{-1})	ro	0,5
Availability of R1c (day^{-1})	n_1	1
Availability of R2c (day^{-1})	n_2	0,1
Availability of R7c (day^{-1})	n_7	0,01
Loss terms		
Max assimilation efficiency	η	0,6
Fraction of C-uptake released as capsular material	α	(1-η)0.25
Mortality	d_0	0,01
Rest respiration at 10°C(day^{-1})	b_o	0,05
Nutrients dynamics		
Optimal N/C ratio (mol g C^{-1})	N^{opt}	0,02
Optimal P/C ratio (mol g C^{-1})	P^{opt}	0.0019
Half saturation constant for N uptake (mmol m^{-3})	h_n	0.5
Half saturation constant for P uptake (mmol m^{-3})	h_p	0.1

Table 3.3 Parameters list of the bacteria sub model

CHAPTER 4

4 The Adriatic Sea primary production seasonal cycle: calibration and validation of a numerical ecosystem model

4.1 Introduction

The physical and biological oceanographic characteristics of the Adriatic Sea have been extensively studied in the past. Biological oceanography studies dealt mainly with factors controlling dissolved nutrient concentrations, and primary production processes in the northern basin (Franco, 1984; Degobbis *et al*., 1986, Smodlaka, 1986; Gilmartin *et al*., 1990; Degobbis and Gilmartin, 1990; Revelante and Gilmartin, 1992). Despite the large research effort in this area, many open questions remains about the evolution of the Adriatic Sea trophic state (Zoppini *et al*., 1995). Therefore Adriatic Sea trophic dynamics is still a challenge for biological oceanography.

Conventionally the Adriatic Sea (Fig. 4.1.a) is divided (on the basis of its morphological characteristics) in three sub regions: the northern the middle and the southern Adriatic Sea (Fig. 4.1.b) This partition also identifies distinct physical (Artegiani *et al*. 1997 a, b) and biological (Zavatarelli *et al*., 1998) oceanographic characteristics. From an ecological point of view the northern basin has meso to eutrophic characteristics, while the middle and the southern basins show distinct oligotrophic features. The Northern coastal areas primary production cycle is strongly influenced by the riverine discharge of land-derived nutrients (Degobbis and Gilmartin, 1990; Zavatarelli *et al.*, 2000). The most important riverine source is the Po river, but the whole northern Adriatic is bordered by many smaller rivers providing a significant flow of both fresh water and nutrients. In this area the strong, fresh water related, buoyancy input coupled with the nutrients discharge in the coastal water and the higher dissolved and particulate

organic carbon production, can give rise to extreme ecological phenomena such as dystrophic events and, consequently, anoxia in the bottom layers of the water column. Phenomena of strong organic matter aggregation (mucilage) are also periodically observed. The middle and southern regions of the Adriatic Sea are characterized by lower primary production, with the continental input and the benthic pelagic interactions being of minor importance in comparison to the northern area (Zavatarelli *et al*., 2000). Exceptions are the south-eastern coastal areas where Albanian rivers discharge are certainly an important (albeit almost unquantified) nutrient source. The offshore middle and southern Adriatic, however, have clearly oligotrophic characteristics (Vilibic *et al*., 1989) and the primary production cycle is regulated by the nutrient supply to the euphotic zone depending by the vertical stratification-mixing processes *(*Zavatarelli *et al*., 2000*)*. Another supply of nutrients in the southern sub basin is the Mediterranean Levantine Intermediate Water (LIW) entering the Adriatic from the Ionian Sea through the Otranto Channel (Zavatarelli *et al*., 1998).

The close coexistence of coastal-eutrophic and open ocean-oligotrophic conditions implies a north-to-south and west-to-east trophic gradient, which is one of the most interesting ecological characteristics of the Adriatic sea.

In this section we show the preliminary results concerning the simulations of the main biogeochemical state variables and their comparison with the available observations.

4.2 The numerical model

The numerical model used in the present study derived from the coupling of a biogeochemical model with a hydrodynamic model. The biogeochemical pelagic model is a development of the European Sea Ecosystem Model (ERSEM), described in the chapter 2 with the new bacteria-DOM sub model described in the chapter 3. The circulation model is the Adriatic Sea implementation (Zavatarelli and Pinardi, 2003) of the Princeton Ocean Model (POM).

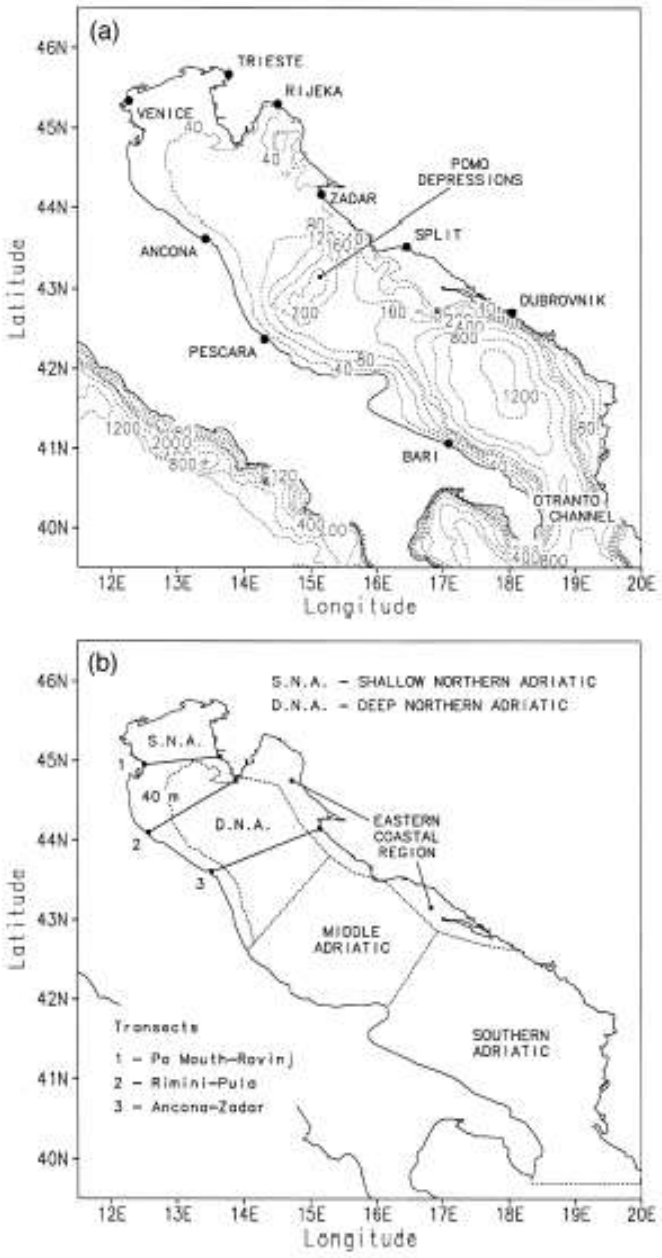

Figure 4.1. The Adriatic Sea morphology (a) and the Adriatic Sea sub-basin (b) (from Zavaterelli et., al 1998).

4.2.1 2.1The Princeton Ocean Model and the coupling with ERSEM

The Princeton Ocean Model (Blumberg and Mellor, 1987) is a free surface primitive equation, finite difference model containing a second order turbulence closure scheme (Mellor and Yamada, 1982) which provides vertical diffusion coefficients. It integrates the Navier Stokes equations in the rotating earth frame, under the Boussinesq, incompressible and hydrostatic approximations.

The governing equations are:

$$\frac{D\vec{U}}{Dt} + fX\,\vec{U}_h = -\frac{1}{\rho_0}\vec{\nabla}_h p + \vec{F}_{\vec{U}_h}$$

$$\frac{\partial p}{\partial z} = -\rho g$$

$$\vec{\nabla}\cdot\vec{U} = 0$$

$$\rho = \rho(\theta, S, p)$$

$$\frac{D\Theta}{Dt} = F_\theta - \frac{\partial I}{\partial z}$$

$$\frac{DS}{Dt} = F_s$$

Where $\vec{U} = (u, v, w)$; $\vec{U}_h = (u, v)$; $\vec{f} = 2\Omega\sin(\phi)\vec{k}$, where ϕ is the latitude, $\vec{k}$ is the unit vector in z direction and the symbol "X" in the first equation indicates the a vector product; ρ is the constant density, $D/Dt = \partial/\partial t + U\cdot\nabla$ p is the pressure, g the gravity, θ and S are the potential temperature and salinity fields , and I is the solar radiation penetring the water column, supposed to be of the form

$$I = Q_s(\rho_o C_p)^{-1} T_r e^{-\lambda z}$$

Here C_p is the water specific heat , T_r is the trasmission coefficient for heat (taken to be 0.71); Q_s is the incaming solar radiation (in Wm^{-2}) at the surface, and l is the

short wave extinction considered from Jerlov (1976) to correspond to clear water (l=0.042 m.1). The F terms in the previous equations represent the turbulent flux divergences, and are written as

$$F_u = \frac{\partial \tau_{xx}}{\partial x} + \frac{\partial \tau_{yx}}{\partial y} + \frac{\partial \tau_{xz}}{\partial z}$$

$$F_v = \frac{\partial \tau_{xy}}{\partial x} + \frac{\partial \tau_{yy}}{\partial y} + \frac{\partial \tau_{zy}}{\partial z}$$

$$F_t = \frac{\partial \tau_{\theta_x}}{\partial x} + \frac{\partial \tau_{\theta_y}}{\partial y} + \frac{\partial \tau_{\theta_z}}{\partial z}$$

$$F_s = \frac{\partial \tau_{sx}}{\partial x} + \frac{\partial \tau_{sy}}{\partial y} + \frac{\partial \tau_{sz}}{\partial z}$$

where τ_{ij} is the simmetric tensor representing the Reynolds stresses. As usual for the ocean, the horizontal turbulent stresses are treated differently from the verticals ones. The orizontal turbulent stresses are parameterized with the Smagorinsky scheme (Smagorinsky, 1993) and the vertical one with the Mellor and Yamada scheme (Mellor and Yamada, 1993), which solves two equations, one for the turbulent kinetic energy and the second one for mixing length, and provides the vertical diffusion coefficients for the momentum and the scalar propertis K_m and K_h, to which a constant background diffusivity K_{mol}= 10-5 m^2 s^{-1} is added.

The coupling between the two models is schematically represented in Fig. 4.2. At every time step (900 second) POM provides ERSEM with information about the physical environment. ERSEM receives information about temperature to calculate the metabolic response of biota and salinity to calculate oxygen saturation. The advective and diffusive rate of change of each pelagic state variable is determined from the velocity fields, horizontal and vertical viscosity coefficients generated by POM.

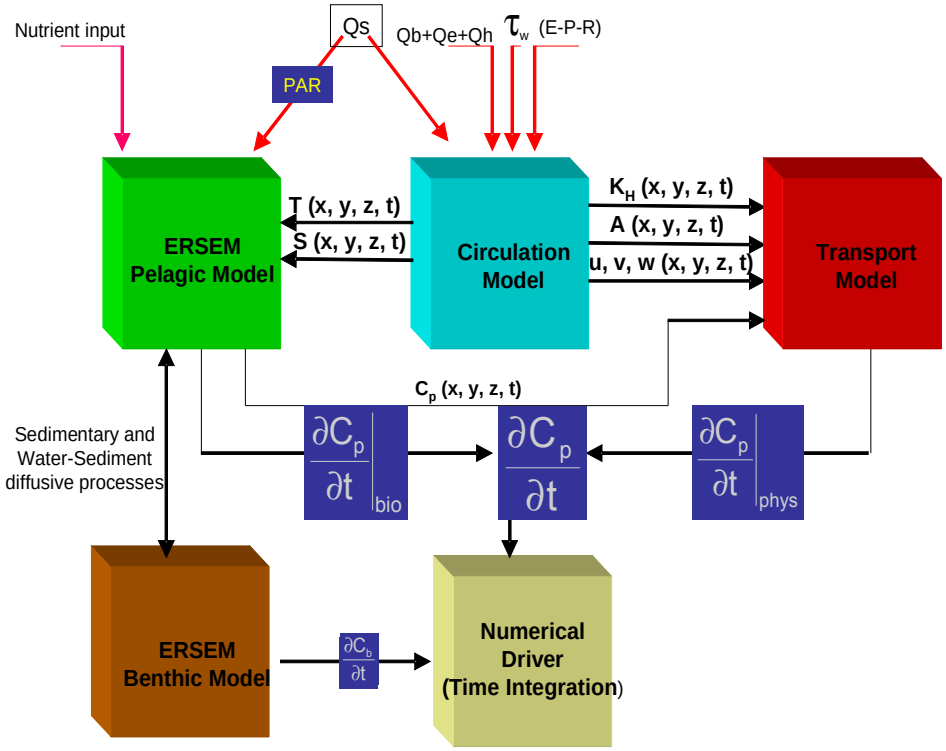

Figure 4.2. POM ERSEM coupling scheme. $\frac{\partial C_p}{\partial t}$ is the total rate of change of a generical biochemical variable C_p. $\left.\frac{\partial C_p}{\partial t}\right|_{phys}$ is the rate of chance due to physical processes, and $\left.\frac{\partial C_p}{\partial t}\right|_{bio}$ is the rate of change due to the biogeochemical processes. Q_s is the solar radiation flux, Q_h, Q_e, Q_b are the sensible, latent and long-wave radiation fluxes emitted at the surface (in W m^{-2}). K_h is the vertical diffusion coefficient for scalar properties, and A is the orizontal diffusion coefficient; τ_w is the wind stress. E-P-R is the salt/fresh water flux (evaporation-precipitation-runoff).

The coupling between POM and ERSEM is done at the level of the internal mode time step, where for the pelagic ERSEM variables (C) is a 'physical' rate of change is calculate a

$$\left.\frac{\partial C}{\partial t}\right|_{phys} = \frac{\partial C}{\partial t} + \vec{U}\nabla\cdot C - F_c$$

Where F_c is the divergence of the turbulent eddy fluxes, mixing and dispersing the tracers with turbulent stresses of the same form used for salinity.
The total rate of change for the pelagic state variables is defined by:

$$\left.\frac{\partial C}{\partial t}\right|_{tot} = \left.\frac{\partial C}{\partial t}\right|_{phys} + \left.\frac{\partial C}{\partial t}\right|_{bio}$$

where $\left.\frac{\partial C}{\partial t}\right|_{bio}$ represent the set of biogeochemical interactions described by ERSEM. The solution is found with an Euler forward time integration scheme.

4.3 Model design

4.3.1 Grid and bathymetry

The model domain (Fig. 4.3) encompasses the whole Adriatic basin and extends south of the Otranto channel into the northern Ionian Sea, where the only open boundary is located.

The model grid has a horizontal resolution of approximately 5 km. In the vertical the model uses a 21 σ coordinate system with 21 levels, where σ=(z-η)/(H+η), H (x, y) is the bottom topography and η(x, y, t) is the free surface elevation. The sigma layers have a logarithmic distribution near the surface and the bottom.

The model bathymetry was obtained from the U.S. Navy 1/60° bathymetric database DBDB1, by bilinear interpolation of the depth data into the model grid.

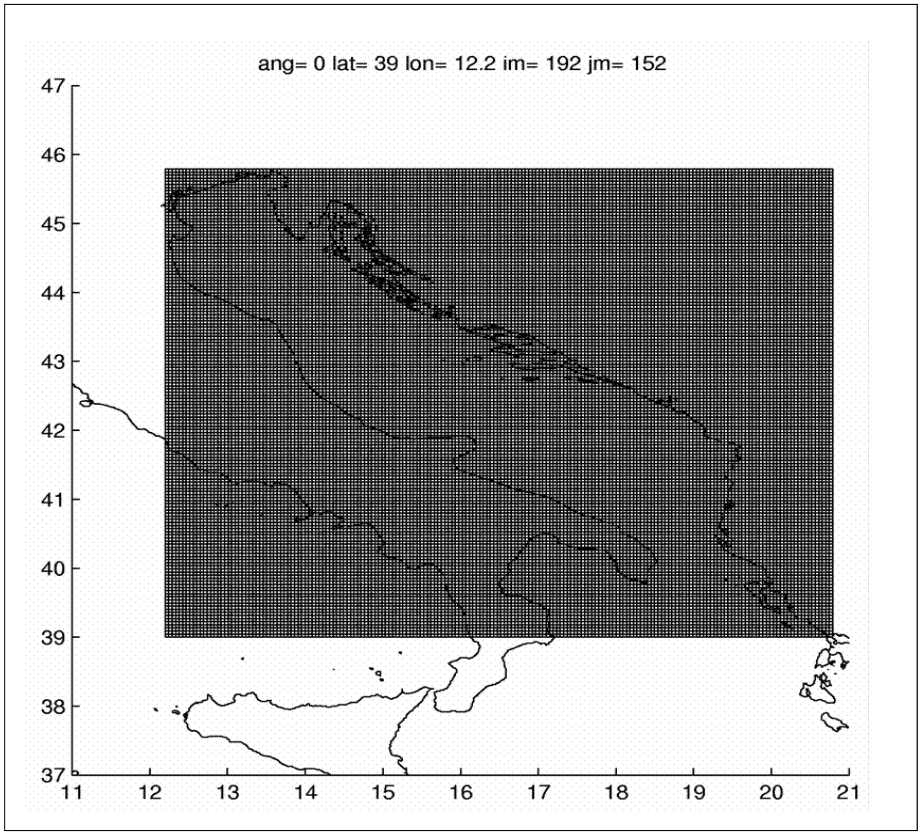

Figure 4.3. The model domain.

4.3.2 Initial Conditions for the physical model

The initial temperature and salinity fields where obtained from the ATOS II (Adriatic Temperature, Salinity and Oxygen, version 2) hydrological data set (Artegiani *et al*., 1997) through an objective analysis procedure (Carter and Robinson, 1987) carried out directly on the model grid. Since this dataset has no information south of the Otranto channel, in order to cover the Ionian sector of the model domain, the ATOS dataset was merged with the temperature and salinity gridded (0.25°) monthly data available from the MED6 (Brankart and Pinardi, 2001) dataset. The initial hydrological fields refer to the winter season, where winter is defined, according to Artegiani *et al*, (1997), as the four-month period from January to April.

4.3.3 Initial condition for the biogeochemical model

The initial conditions for the nutrients and phytoplankton have been estimated from the ABCD (Zavatarelli *et al*., 1998) climatological winter averages and are assumed to be horizontally homogeneous but vertically variable. The initial conditions for pelagic biomass were reduced by 2 orders of magnitude below the euphotic zone.

4.3.4 Surface and bottom boundary conditions for the physical model

The model is forced with climatological monthly varying fields of surface heat, water, momentum (wind stress) and river runoff. For the computation of the heat flux and wind stress monthly fields, the 6-hrs, 1.125°, 1982-1993 ECMWF surface re-analysis data (Gibson *et al*., 1997) and the COADS (da Silva *et al*., 1995) monthly cloud cover data were used. The sea surface temperature data needed for the surface flux computation were obtained from the Reynolds and Smith (1994) data set.

The computation of the total heat fluxes (Q) at the air sea interface is given by:

$$Q=Qs-Qb-Qh-Qe.$$

The solar radiation (Qs) has been computed according to the Reed (1975) formula and the Reed (1977) parameterization. Clear sky radiation has been computed according to Rosati and Miyakoda (1988). The sea surface albedo was computed according to Payne (1972). The long wave radiation flux (Q_b) was computed according to Bignami *et al*., (1995). The sensible (Q_h) and latent (Q_e) heat fluxes were computed according to classical formula, with the turbulent exchange coefficients computed according to Kondo (1975).

Following Zavatarelli *et al*., (2002), the heat flux was forced to produce sea surface temperatures consistent with the seasonal climatology (and avoiding excessive winter cooling resulting from the use of the uncorrected surface forcing), by adding a heat correction term to the surface boundary condition for temperature. For a detailed description of the heat flux formulation see Zavatarelli *et al*., (2002 and 2003).

The surface salinity flux:

$$W_s = (E - P - R)S_{z=\eta}$$

is composed by the balance between Evaporation (E), Precipitation (P) and River-runoff (R≠0 at the "estuary" grid points only), while $S_{z=\eta}$ is the model predicted surface salinity field. In our simulations we do not consider a real water flux condition for both E-P and R, since climatological fields force the model. Monthly varying evaporation was computed from the Q_e fields and monthly precipitation data were obtained by interpolation of the Legates and Wilmott (1990) global, 0.5°, monthly precipitation dataset.

The monthly river runoff data were obtained from the Raicich (1994; 1996) monthly climatology. The approximate location of the river mouth considered in the present study is shown in Fig. 4.4. Raicich 's(1994) estimate for the non-point runoff partitioned for the pertinent segments of the Adriatic coastline has been considered as a distributed source function. On the contrary, the major Adriatic rivers listed in Fig. 4.4 were considered as point sources. Only the Po River runoff was distributed along more grid points, in order to represent the freshwater discharge of the various mouths of the delta. Mouths partitioning of the Po total runoff was defined according to the estimates reported in Provini *et al.* (1992). Particular care was taken to ensure that the maximum rivers discharge (R_{max}) was never exceeding the "estuary" grid cell volume, i.e.:

$$R_{max} \leq \frac{\Delta x \Delta y \Delta \sigma_1 H}{\Delta t_{int}}$$

Where $\Delta\sigma_1 H$ is the thickness of the surface "estuary" grid cell.

Also the salinity flux required a flux correction term in order to impose a forcing producing sea surface salinities consistent with the seasonal climatology and to avoid the excessive freshening of the basin resulting by the use of the climatological river forcing.

The wind stress (τ) is computed using the Hellerman and Rosenstein (1983)

formula. Following Zavatarelli *et al*., (2002) the components of the wind stress (obtained through scalar averaging) were multiplied by a factorof 1.5 following the indications of Cavaleri and Bertotti (1997).

All the monthly forcing fields (Q, W_s, τ) applied to the model were linearly interpolated between adjacent months, assuming that the monthly mean average is applied to day 15 of the month. However, Killworth (1996) pointed out that this procedure does not conserve the monthly average value. To overcome this, Killworth (1996) proposed a simple procedure based on the computation of the so-called "pseudo values" whose linear interpolation preserve the correct average value. His technique was adopted in the present study. Seasonal $T^*_{z=0}$ and $S^*_{z=0}$ fields were instead kept seasonally constant and changed suddenly at the end of each season. At the bottom, adiabatic boundary conditions are applied for temperature and salinity. For velocity, a quadratic bottom drag law is used utilizing the drag coefficient from the logarithmic 'law of the wall' profile as described in Zavatarelli and Pinardi (2003)

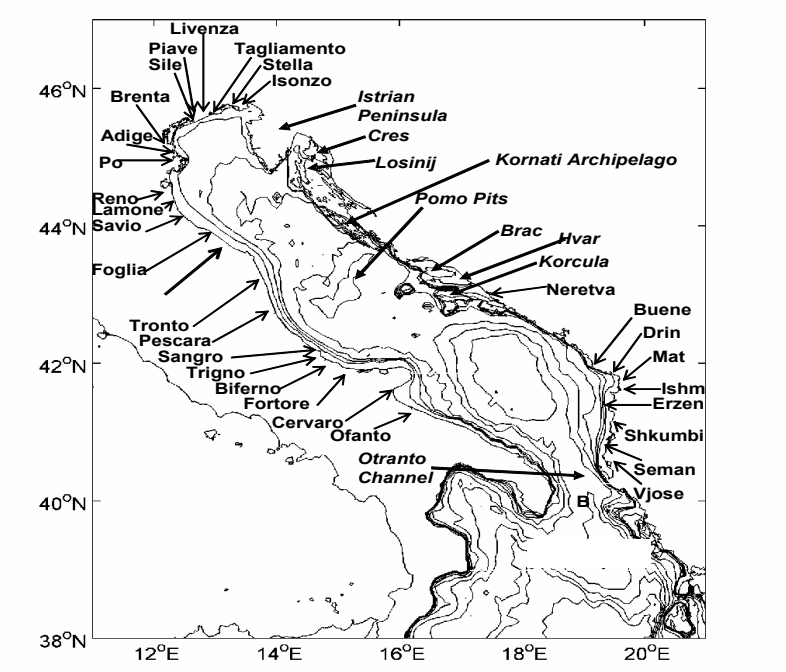

Figure 4.4. Rivers mouth location in the model.

4.3.5 Lateral open Boundary conditions for the physical model

For the computation of the lateral open boundary conditions in the nirthern Ionian, a simple off line, one way nesting technique is used (Zavatarelli and Pinardi 2002). Salinity, temperature and velocity fields along the open boundary are obtained from a Modular Ocean Model (MOM) simulation of the Mediterranean Sea general circulation (Demirov and Pinardi 2003). The MOM-POM nesting was designed in a way to ensure that the volume transport across the open boundary of the "nested" model (Adriatic Sea POM) matches the volume transport across the corresponding sections of the "nesting" model (Mediterranean Sea MOM), model in the following way:

$$\int_{x_2}^{x_1}\int_{-H_{nested}}^{\eta_{nested}} V_{nested}\,dzdx = \int_{x_2}^{x_1}\int_{-H_{nesting}}^{\eta_{nesting}} V_{orig}\,dzdx$$

Where x_1, x_2 are the extreme of the open boundary section, η_{nested}, H_{nested} are the surface elevation and the bathimetry of the "nested" model at the boundary respectively; $\eta_{nesting}$, $H_{nesting}$ are the surface elevation and the bathymetry of the "nesting" model at the boundary respectively; $V_{orig}=V_{orig}(x, y, z, t)$ is the "nesting" model velocity normal to the boundary and V_{nested} is the normal velocity field at the "nested" model open boundary.

In the case of the of our nesting, the rigid lid characteristics of the Mediterranean Sea model and the location of the Adriatic model open boundary, cutting across two coastlines, ensures that the right hand side of the previous equation is identically zero. Therefore, in this special case, reduces to:

$$\int_{x_2}^{x_1}\int_{-H_{nested}}^{\eta_{nested}} V_{nested}\,dzdx = 0$$

Let define V_{int} as the V_{orig} interpolated on the nested open boundary. V_{nested} will then contain V_{int} and a correction to preserve the volume transport across the open boundary. Let us define also $M_{int} = \int_{x_2}^{x_1}\int_{-H_{nested}}^{\eta_{nested}} V_{int}\,dzdx$, $M_{orig} = \int_{x_2}^{x_1}\int_{-H_{nesting}}^{\eta_{nesting}} V_{orig}\,dzdx$,

$\Delta M = M_{int} - M_{orig}$ and $S = \int_{x_2}^{x_1} \int_{-H_{nested}}^{\eta_{nested}} dzdx$.

Therefore the corrected velocity component normal to the boundary (V_{nested}) is given by:

$$V_{nested}(x, y, z, t) = V_{int} - \frac{\Delta M}{S}$$

The open boundary conditions used are therefore:

1) For the total velocity,

$$U_{O.B.} = U_{int}$$

where $V_{O.B.}$ and $U_{O.B.}$ are the normal and tangential velocity components on the open boundary respectively, U_{int} is the "nesting" model tangential velocity component ηinterpolated on the "nested" model.

2) For the barotropic velocity component, defined as:

$$\overline{V} = \frac{1}{H + \eta} \int_{-H}^{\eta} V dz$$

we impose (Zavatarelli *et al.*, 2002),

$$\overline{V}_{O.B.} = \overline{V}_{nested} \frac{H_{nesting}}{H_{nested} + \eta_{nested}} \; ; \; \overline{U}_{O.B.} = \overline{U}_{int}$$

Where $\overline{V}_{O.B.}$, $\overline{U}_{O.B.}$ are the normal and tangential barotropic velocity components on the open boundary respectively and $\overline{U}_{int}$ is the OGCM model tangential velocity component normal to the boundary interpolated on the AIM. The fractional term involving H and the η's guarantees volume continuity.

This procedure ensures that the interpolation does not modify the net transport across the "nested" model open boundary.

Temperature and salinity on the open boundary outflow are locally upwinded:

$$\frac{\partial T_{O.B.}}{\partial t} + V_{O.B}\frac{\partial T_{O.B.}}{\partial y} = 0 \; ; \frac{\partial S_{O.B.}}{\partial t} + V_{O.B}\frac{\partial S_{O.B.}}{\partial y} = 0$$

while, on the inflow, they are prescribed from the "nesting" model data interpolated on the "nested model open boundary ($T_{nesting}$ and $S_{nesting}$):

$T_{O.B.} = T_{nesting}$; $S_{O.B.} = S_{nesting}$

4.3.6 Vertical and lateral biogeochemical boundary conditions

Nutrients river discharge was introduced into the model by defining a river water nutrient concentration multiplied by the monthly varying runoff (R). to obtain a surface nutrient flux in a following way

$$K_v \frac{\partial N}{\partial z}\bigg| = \frac{R(t)N_0}{\int_1^{12} R(t)dt}(\Delta x \Delta y)^{-1}$$

where K_v is the vertical eddy diffusivity, the integral is done on the twelve monthly mean values and R is different from 0 only that at the "estuary" grid points (Fig. 4.4). The river water nutrient concentrations for Po river were computed from the Degobbis and Gilmartin (1990), estimate of the annual mean Po river nutrient loads into the northern Adriatic Sea (corresponding to a nitrate, phosphate, ammonium and silicate of 7347, 230, 1056 and 5990 10^6 mol/yr respectively), and the Raicich (1994) annual Po river runoff.

For all the other rivers the estimated mean nutrient concentration was supposed to be 50% of the Po river concentration.

Concerning the open boundary we used the same open boundary scheme condition implemented for temperature and salinity, but for the pelagic state variables of the model values from the nested model are lacking. Therefore we imposed a constant value for each biogeochemical variable estimated from the ABCD data set.

A simple benthic return model has been used for the benhtic closure. In order to parameterize the benhtic re-mineralization, a fixed quota (1 %) of each detritus component (C,N,P,Si) reaching the bottom is re-injected to the water column as

dissolved nutrients and carbon dioxide.

4.4 Results and discussion

In this section we discuss the simulation results and we intercompare them with climatological observations from the ABCD data set. Following Zavatarelli *et al*., (1998) and Artegiani *et al* (1997) we partitioned the Adriatic Sea into different regions (see Fig. 4.1.B) distinguishing between northern, middle and southern Adriatic. The northern Adriatic is further subdivided into a shallower region and a deeper region, separated by the 40-m isobath. Seasons are defined as follow: winter is from January to March, spring from April to June, summer from July to September and autumn from October to December.

4.4.1 The biochemical spin up problem

POM was run alone (without the biogeochemical model coupling) in a perpetual year mode for three years. At the end of the three years the resulting hydrodynamic and hydrological fields were used as initial conditions for the ecosystem simulations: this means that the physical components of the ecosystem had already reached a repetitive annual cycle. Coupled simulation progressed forward in time for an additional four years period. Results shown in the following sections are extracted from the fourth integration year of the coupled model. To check whether the biogeochemical state variables reached a stable repetitive cycle, a check on the volume averaged time series of selected state variables (phosphate, nitrate and the dissolved organic carbon in its 'labile', 'semilabile' and 'refractory' components) was computed. Phosphate (Fig. 4.5A) reach a stable seasonal cycle after the first year of simulation. As expected, maximum concentrations are reached in winter in and autumn in correspondence of the maximum rivers runoff. On the contrary Nitrate (Fig. 4.5B) and ammonium (Fig. 4.6A) do not reach a stable cycle, but they respectively exhibits a decreasing and increasing temporal trend. However, the total inorganic dissolved nitrogen (sum of the Nitrate and Ammonium basin averaged concentration) shows (Fig. 4.6B) a more stable cycle. The reason for this could be traced to the new implementation of the bacterial dynamics that,

increasing bacterial activity, determines the increase of the Ammonium pool, however leaving almost constant the dissolved inorganic nitrogen pool.

In Fig. 4.7 are shown the time series of the basin averaged components of the dissolved organic carbon pool. The 'labile' DOC fraction cycle (Fig. 4.7A) stabilizes in about 1 year. As expected, given the description of the DOM bacteria interactions implemented in the model, the 'labile' DOC cycle stabilises on very low concentrations (less than 0.4 μm/l). The 'semilabile' DOC (Fig. 4.7B) exhibits a clear seasonal cycle with large amplitude characterised by summer maximum and winter minimum. 'semilabile' DOC concentrations maxima are clearly related with nutrient (phosphate in particular). Zero dimensional experiments (see chapter 3) demonstrated that under low inorganic nutrients concentration the bacterial release of carbohydrates is enhanced leading to the increase of the 'semilabile' carbon pool. We find this kind of dynamics reproduced also in the bulk characteristics of the three dimensional model. The "refractory" DOC cycle (Fig. 4.7C) stabilises in about one year and it is characterised by a small amplitude seasonal variability.

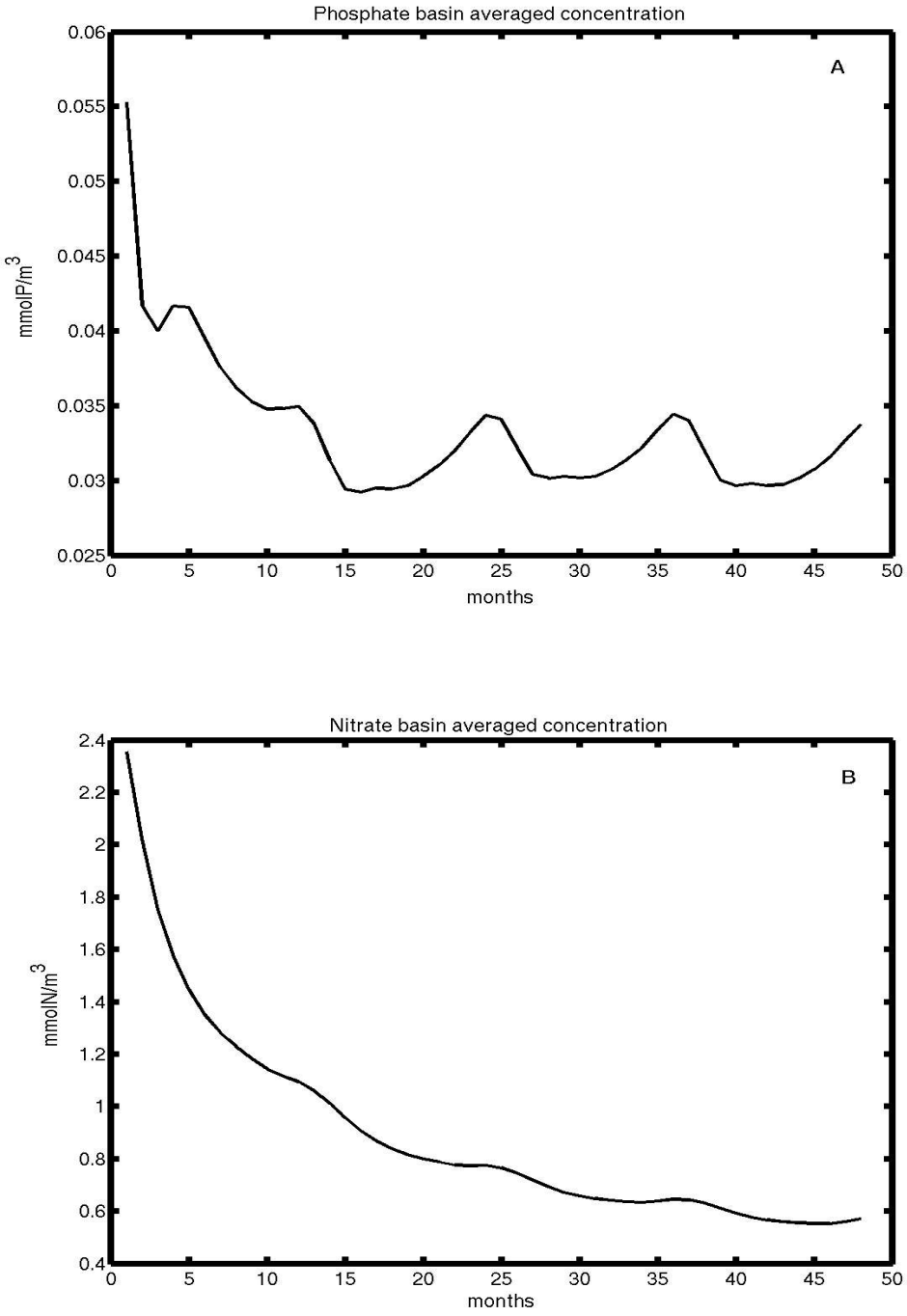

Figure 4.5. Phosphate (mmol P m^{-3}) (A) and nitrate (mmol N m^{-3}) (B) basin mean in the four years coupled model run.

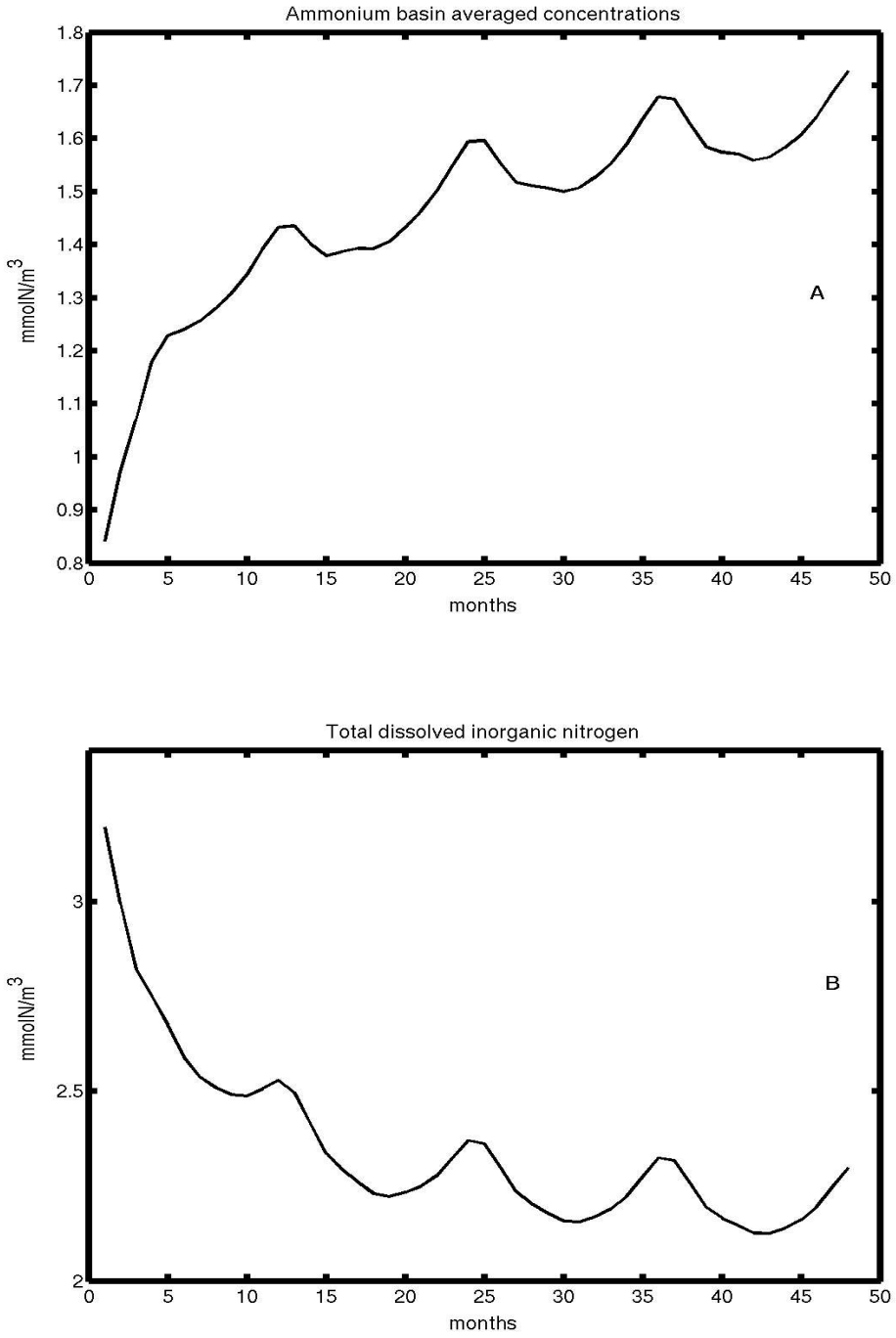

Figure 4.6. Ammonium (A) and total inorganic dissolved nitrogen (B) (mmol N m^{-3}) basin mean concentration in the four years coupled run.

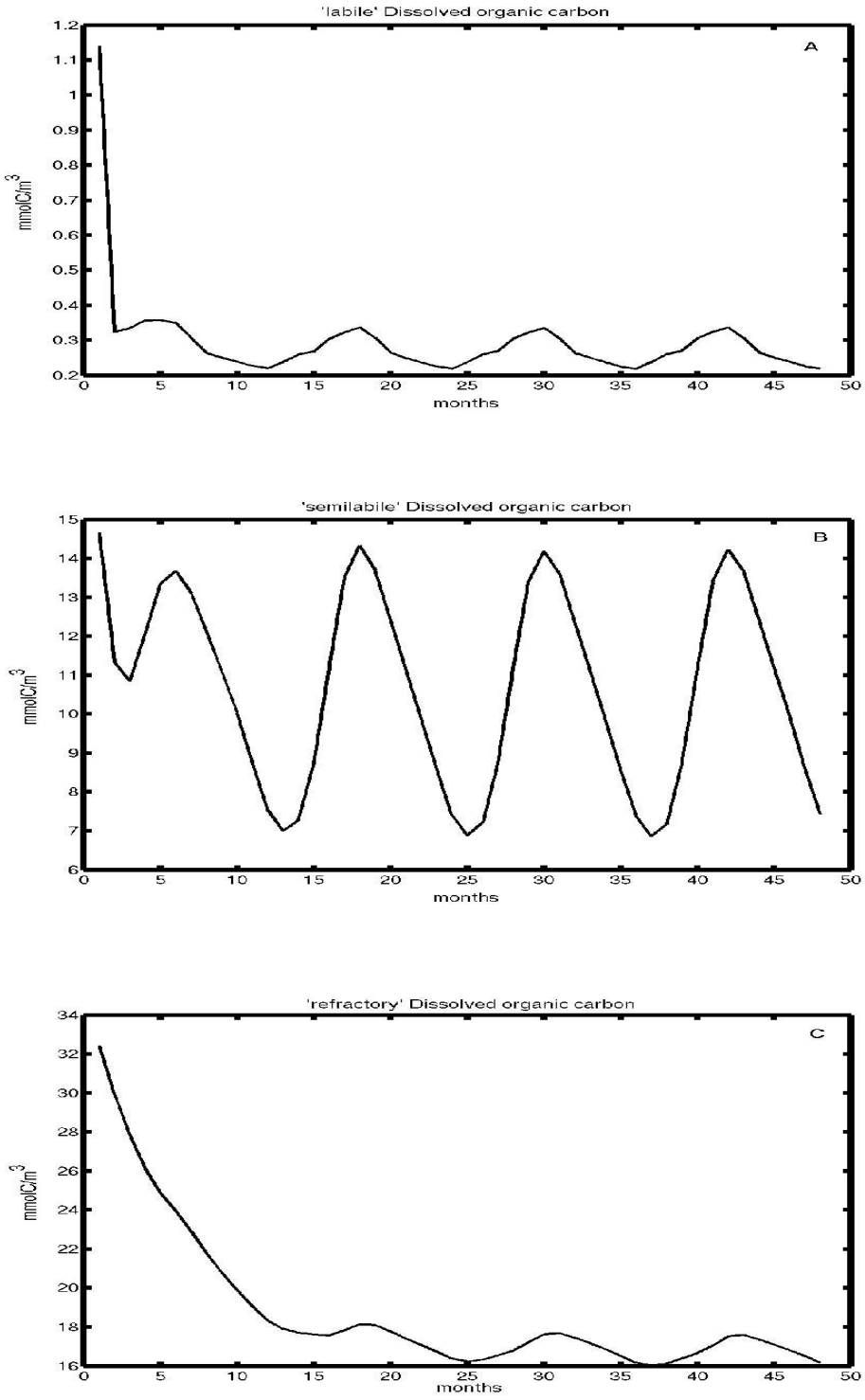

Figure 4.7. 'Labile' (A), 'semilabile' (B) and 'refractory' (C) DOC (mmol m^{-3}) basin mean in the four years coupled run.

4.4.2 Chlorophyll

The surface simulated Chlorophyll distribution monthly cycle is shown in Fig. 4.8. The northern Adriatic basin and the western coastal areas are characterized in all months by higher surface concentration values with respect to the offshore areas. This distribution structure confirms that the model is able to maintain at least qualitatively the trophic gradient in a way that is consistent with the CZCS (Fig. 4.9) satellite (remote observations) (Barale *et al*., 2004). In general, higher concentrations appear in the late winter-early spring period while in summer the offshore areas show very low surface biomass concentrations marking (surface) oligotrophic conditions. The distribution of the high chlorophyll values along the western coast is clearly governed by the nutrient input from the Po river and the circulation features of the area that is affected by the southward flowing Western Adriatic Coastal Current (Artegiani *et al*., 1997; Zavatarelli *et al*. 2002, Zavatarelli and Pinardi, 2003) causing southward advection of the phytoplankton (Zavatarelli *et al*., 2002). The Po river nutrient discharge causes a permanent bloom condition, in the area proximal to the delta, with chlorophyll concentration values higher than 10 mg/m^3,a value consistent with the CZCS observations even if the model in general overestimate the chlorophyll budget.

The chlorophyll overestimation in winter-spring seems to be a general feature of the model. In the middle Adriatic Sea the distribution and monthly variability of the surface chlorophyll is in qualitative agreement with the CZCS observation, but again the simulated values are higher than CZCS observations. Winter-spring values range from 4 to 6 mg/m^3 along the Italian coast and are about 1 mg/m^3 in the central part, while the CZCS data are sensibly lower (0.3 – 0.8 mg/m^3). In summer the model results for the northern Adriatic are in agreement with satellite observations only in the coastal areas, while in the offshore the model values are slightly lower with respect to CZCS.

It is argued that the winter overestimation may be due to a non accurate definition of the river nutrients discharge. In fact the river nutrients input was defined by estimating the mean river water concentration, without considering removal and transformation processes possibly occurring trough the rivers mouth, which might cause a significant reduction of the nutrient loading. An

overestimation of the nutrient upwelling processes related to the cyclonic circulation in the southern Adriatic could be also involved in determining the discrepancy between remotely sensed observations and simulations. The underestimation of the surface chlorophyll concentration in the middle Adriatic can be due to the strong bacteria phytoplankton competition for nutrients due to the high DOC concentration during summer when nutrients level are low.

Insight on the seasonal and vertical variability of the biogeochemical state variables in the Adriatic sub basins defined above, is offered by the comparison of seasonally averaged vertical profiles with the corresponding profiles from the ABCD dataset (Zavatarelli et. al., 1998). The analysis of the seasonally averaged chlorophyll vertical profiles for the Adriatic Sea sub basins (Fig. 4.20, A,B,C,D) confirms the strong North-South trophic gradient both in the model and the data. This negative north-south gradient is correctly reproduced by the model. In the Northern Shallow basin the simulated chlorophyll surface concentration is about 4 mg/m^3 in winter and is constantly above 3 mg/m^3 throughout the year. Below the surface concentrations progressively decrease with depth in all seasons and a chlorophyll subsurface maximum is not developing in summer. Comparison with the ABCD data indicates overestimation at surface and underestimation at depth, as the observed seasonal profiles indicate a roughly constant concentration with depth, contrasting with the depth concentration decrease of the simulated profiles. The chlorophyll overestimation in the surface layer is evident also in the deep northern and the middle Adriatic. However, the vertical structure of the profiles and their seasonality shows elements of qualitative agreement with the ABCD observations, notably the development of a summer subsurface chlorophyll maximum at about 70-80 m depth in the middle Adriatic. In any case the general overestimation suggests that the chlorophyll parameterization in the model still needs further improvements.

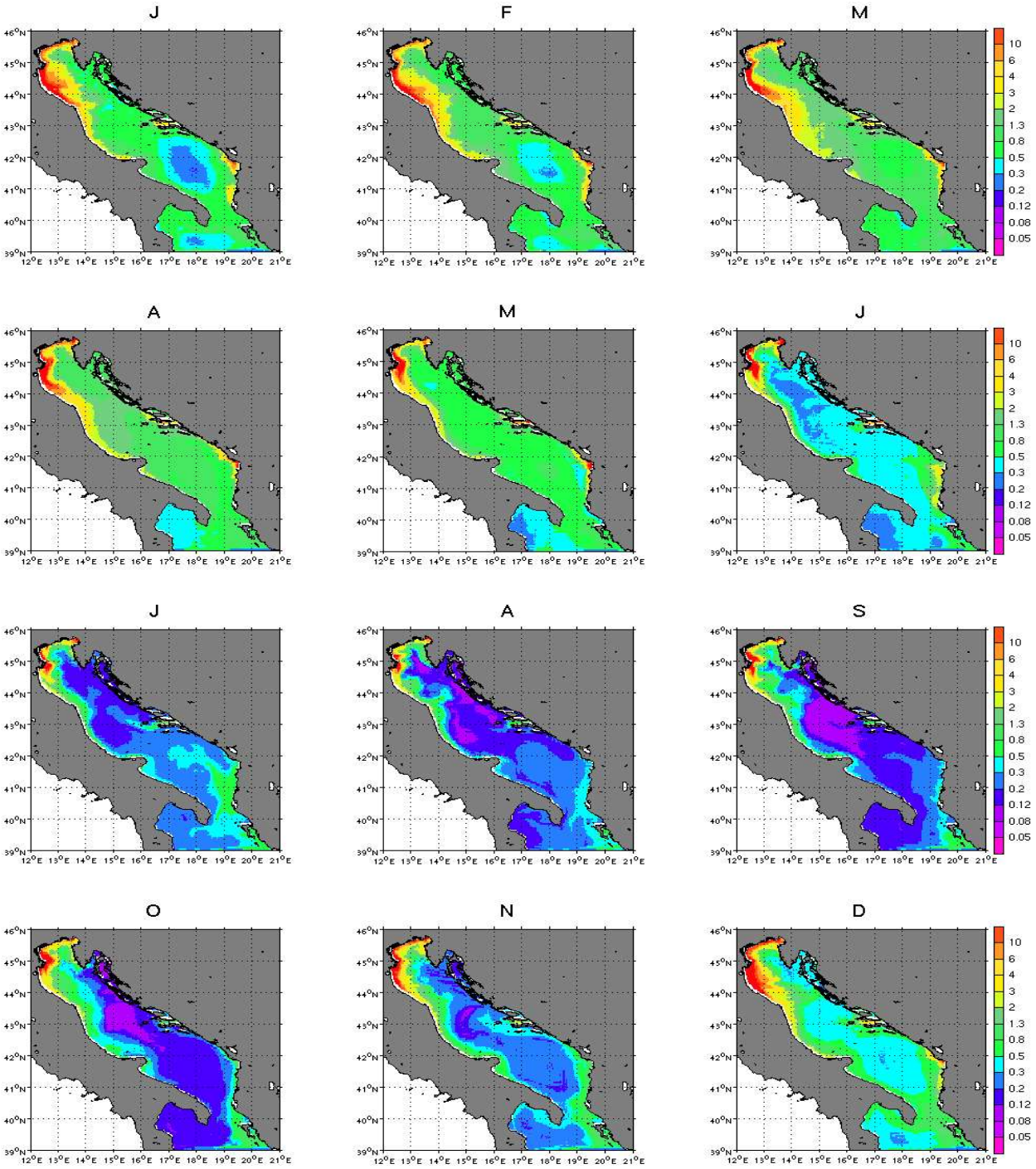

Figure 4.8. Chlorophyll (mg m^{-3}) surface monthly mean distribution.

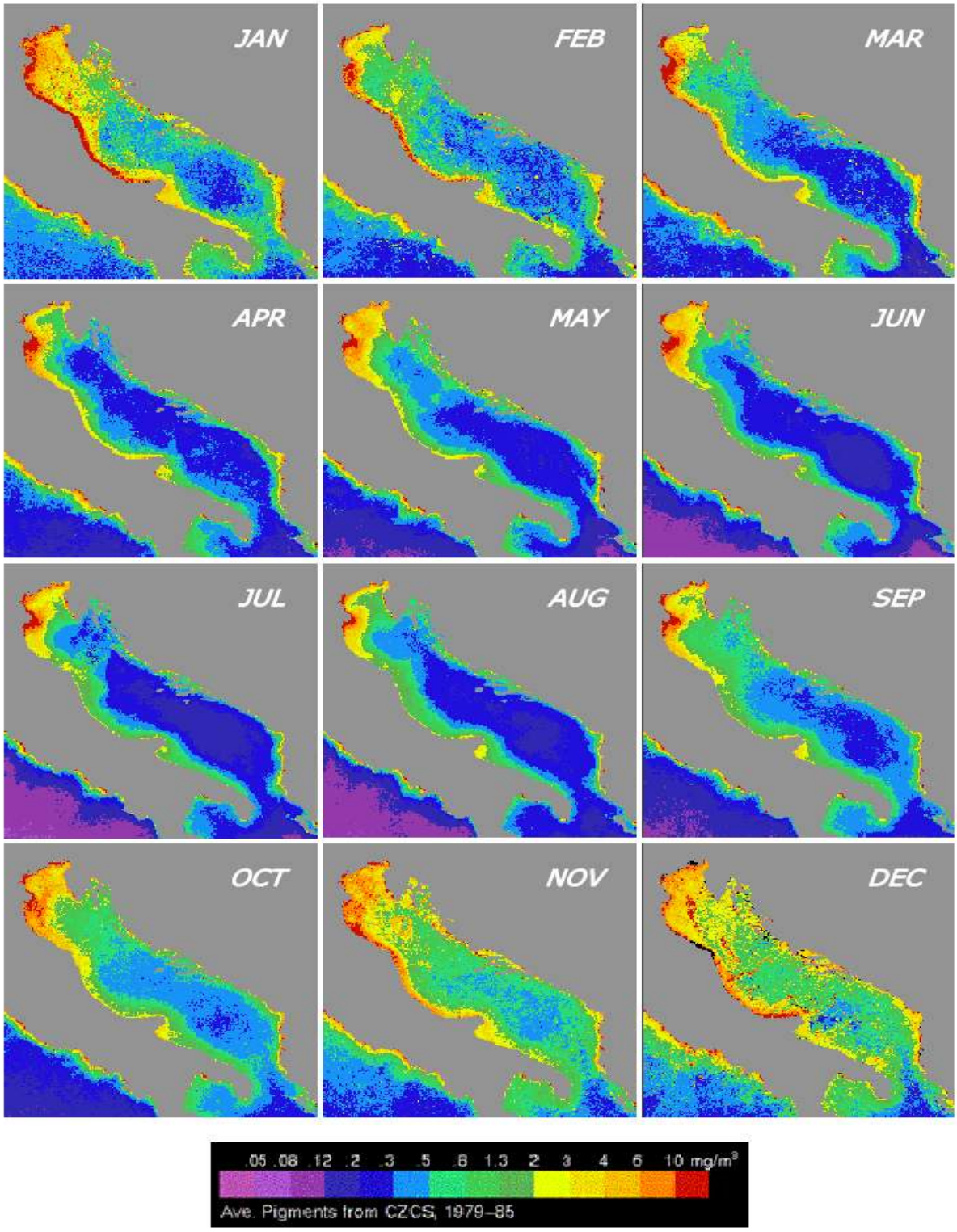

Figure 4.9. Chlorophyll (mg m^{-3}) monthly mean distribution from CZCS. (from Barale *et al*., 2004).

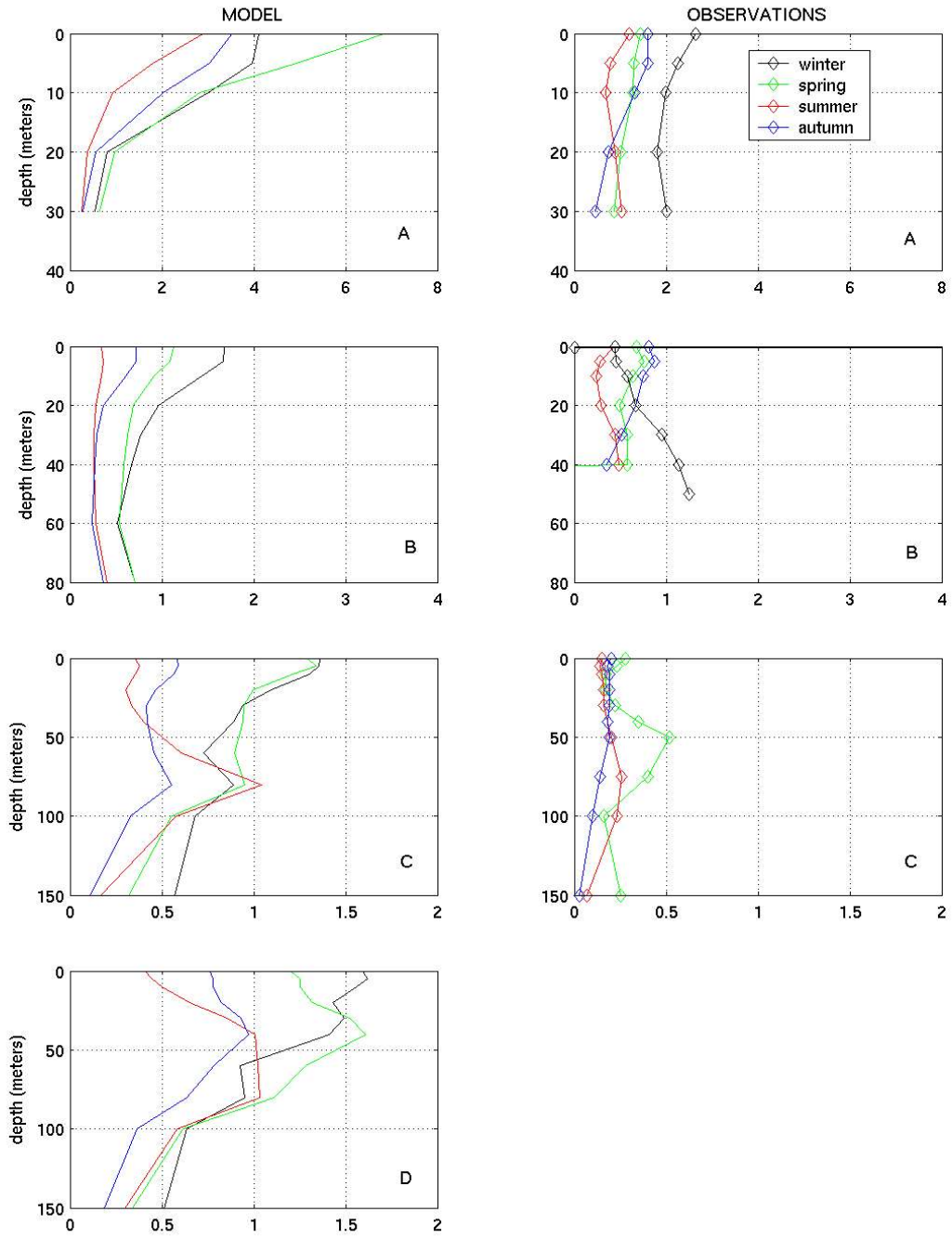

Figure 4.10. Seasonal chlorophyll (mg Chl m^{-3}) averaged profiles for model (left side) and observations (right side). A=shallow north,B=deep north,C=middle, D=South.

4.4.3 Nutrients and oxygen

Seasonally averaged vertical nutrient profiles and their comparison with the ABCD data are shown in Fig. 4.11. In the shallow northern basin (Fig.4.11.A) the surface phosphate distribution is clearly influenced by the Po river discharge: the maximum surface concentrations (0.1 mmol/m^3) are reached in autumn, in correspondence with the maximum Po river discharge. The comparison with the observations shows a general underestimation particularly evident below the surface. The major discrepancy between model results and observations is the lack of concentration increase with depth. The low nutrient concentrations are clearly related to the overestimation of the phytoplankton biomass described above that causes strong phosphate uptake. In addition, out benthic closure parameterization could impose low re-mineralization rate from pore waters so that benthic-pelagic exchange of nutrients could be heavily underestimated. This process was found to be important in previous one dimensional simulation (Vichi *et al*., 1999).

In the deep north (Fig. 4.11.B) the simulated values indicate a strong phosphate depletion all along the water column in all seasons, suggesting a strong uptake due to both phytoplankton and bacteria. In this sub basin the difference with the observations is evident in terms of amount and shape of the simulated average profile: the observational data show a clear seasonality and a presence of a nutricline particularly, strong in winter. This features are not captured by the model.

In the middle basin (Fig. 4.11.C) the model underestimation of the observation is still present but the shape of the profile is closer to the observations profile. The simulated values are very close to 0.01 mmol/m^3 in the upper 50 m. Below such depth the summer, spring and autumn observed profiles depict a nutricline that is also weakly appears in the simulated data.

The simulated seasonal profiles for the southern Adriatic Sea (Fig. 4.11.D) have characteristics similar to those computed for the middle basin but with lower surface values in all seasons and with a more evident and deep nutricline. The agreement with observation seems to be good in this sub basin.

The nitrate mean seasonal profiles (simulated and observed) for the four different sub basin are shown in Fig.4.12 (A,B,C,D) The general distribution and

simulated profile shape are very close to those of phosphate, but the values are more consistent with the observations. In the shallow northern basin (Fig. 4.12.A) the nitrate concentration reach the maximum values in the upper ten meters of the water column. The values progressively decrease with depth and become very close to zero starting below 20 meters. The simulated values are below the observations everywhere in the water column except than in summer, when the surface simulated values are slightly higher than the observations. As for the phosphate the deep north basin is the region with the minimum concentration of nitrate. This could be due to the fact that this is a region in which the model simulates high primary production (as highlighted by the chlorophyll results) and then a strong uptake, but, at the same time, is not strongly affected by Po river nutrients input like the shallow northern basin. The main discrepancy between observations and simulation in terms of shape of profile is the constancy of the simulated concentrations below 20 meters depth while the observations show a spring-autumn nutricline at 20-25 meters depth. Model simulations are in qualitative good agreement with the observations in the middle basin (Fig. 4.12.C) : the amount of nitrate still appears underestimated but the shape of the vertical profile with a nutricline, starting from 100 meters depth, is well reproduced. The minimum values in the simulations appear, in summer, in the first 100 meters of the water column, while, in winter, in the deepest part of the water column (below 100 m depth). The seasonal variability is consistent with the observations in the upper 100 meters, with winter maximum and summer minima In the southern basin (Fig. 4.12.D) simulated nitrate profile reproduce quite well the general trend of the observations. The agreement with the observations in terms of both shape of the profile and total amount of nutrient, is better in summer and spring. However, the simulated values do not show the pronounced seasonal variability of the observations.

Silicate mean profiles Fig. 4.13 (A, B, C, D) show a behavior similar to the other nutrients with higher values in the surface layer in the northern shallow basin decreasing with depth, an almost constant concentration through the water column in the deep northern basin and with a presence of a nutricline in the middle and southern basin. In these regions there is a minimum of correspondence with a

maximum subsurface of chlorophyll. In general the value of silicate are in good agreement with the observed data. As the silicate are not affected by the bacteria dynamics, this behavior could confirm the hypothesis that the phosphate and nitrate underestimation could be due to the bacteria utilization of phosphate and a selective ammonium remineralization made by zooplankton and bacteria rather than nitrate.

Oxygen mean profiles are shown in Fig. 4.14 (A, B, C, D). The value seems to be consistent with the observations in terms of magnitude but the seasonality is not well reproduced. The maximum simulated value is in winter in the northern shallow basin and in autumn in the others three sub basins. In the middle and south basins the maximum values are, as expected, in correspondence with a subsurface chlorophyll maximum.

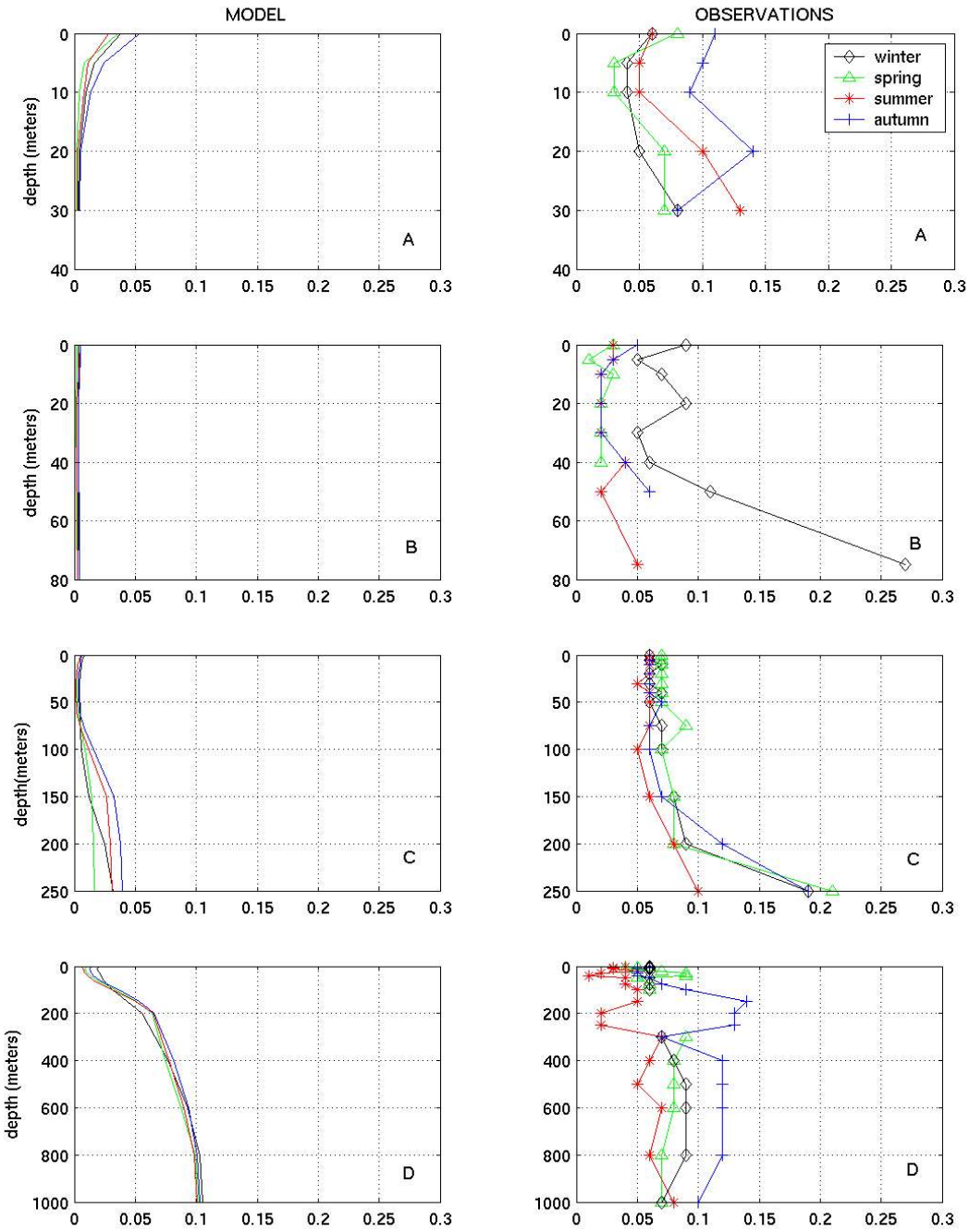

Figure 4.11. Seasonal phosphate (mmol P m^{-3}) averaged profile for model (left side) and observations (right side) in the four Adriatic sub basin. A=shallow north, B=deep north, C=middle, D=south.

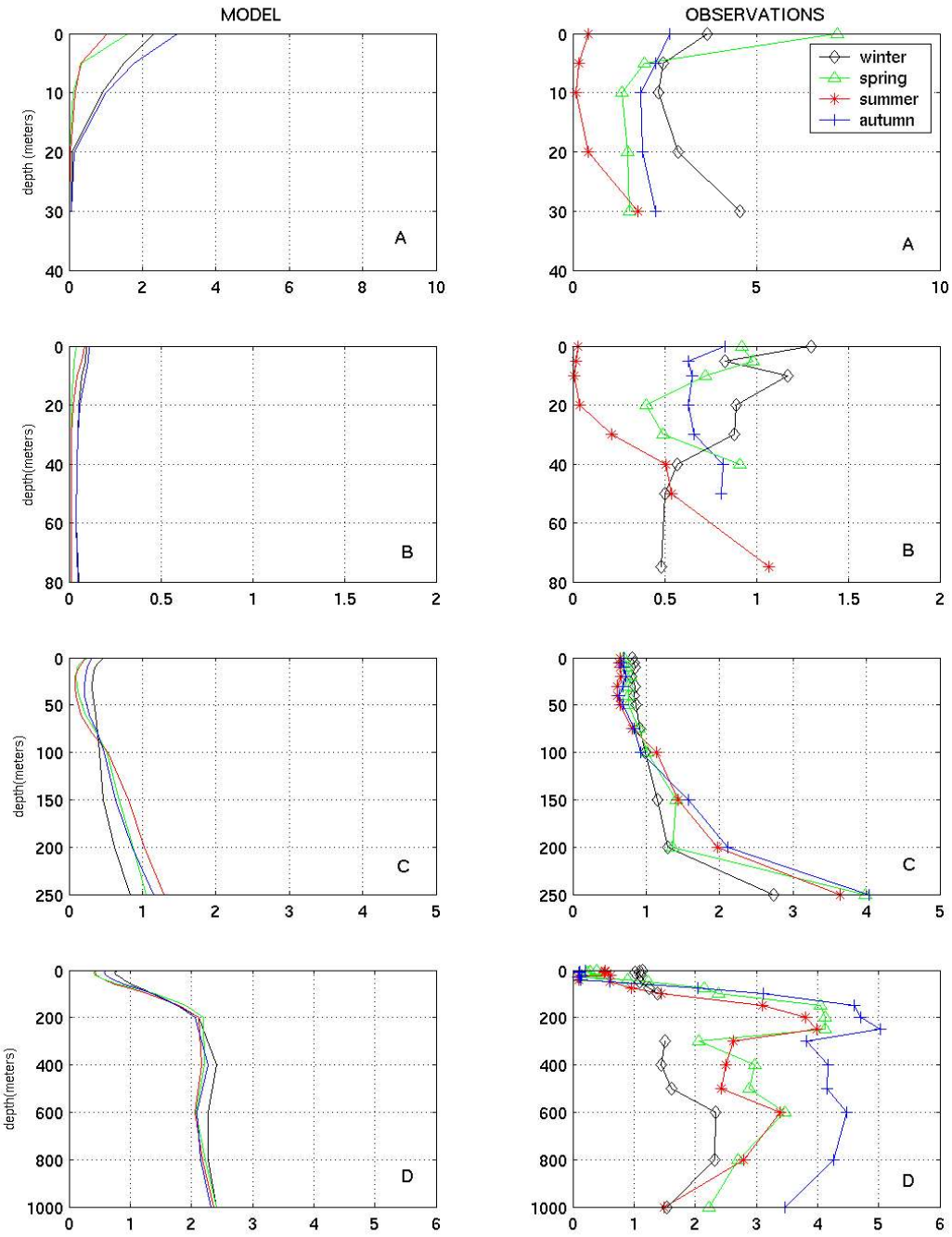

Figure 4.12. Seasonal nitrate (mmol N m^{-3}) averaged profile for model (left side) and observations (right side) in the four Adriatic sub basin. A= shallow north, B=deep north, C= middle, D= south.

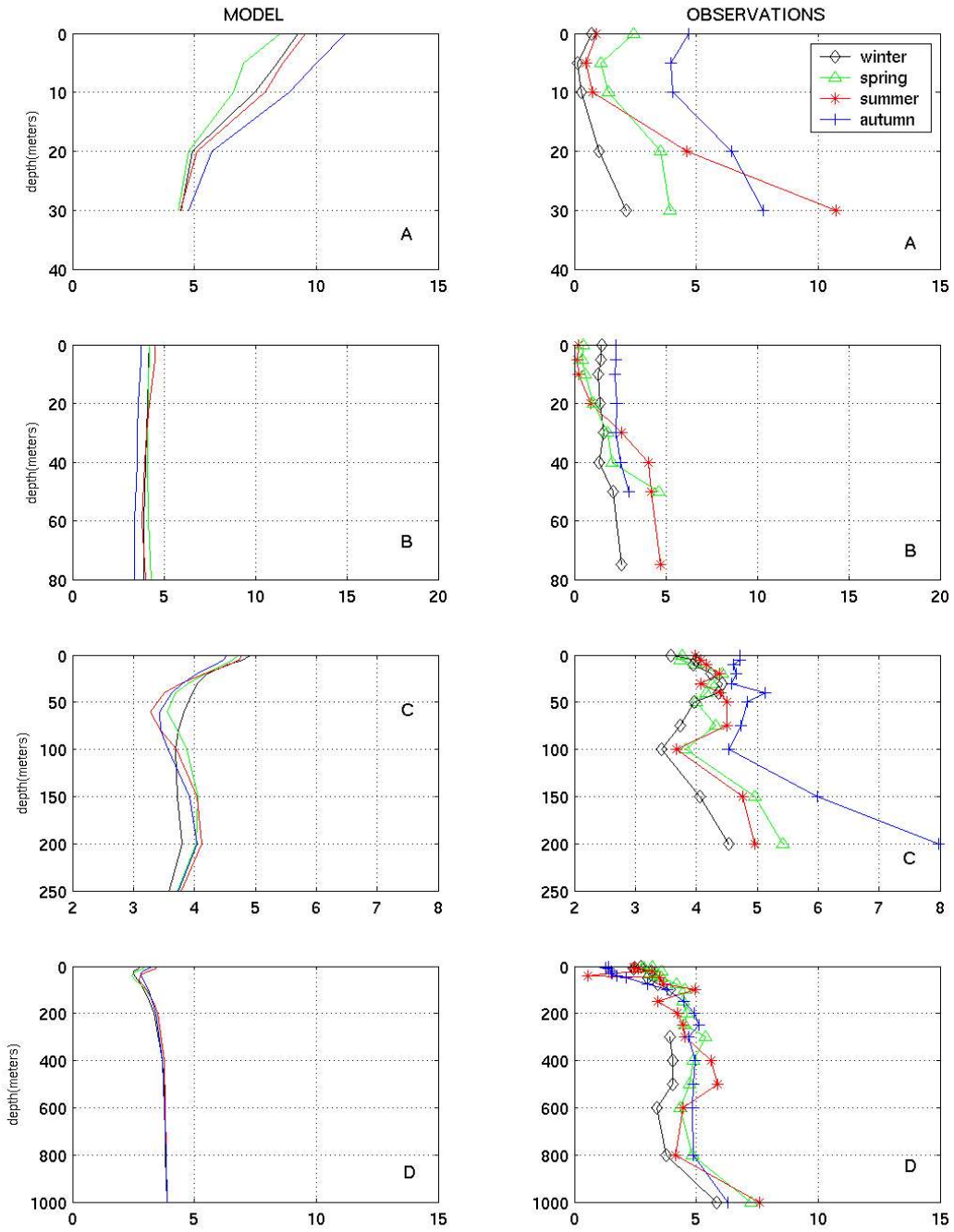

Figure 4.13. Seasonal silicate (mmol Si m^{-3}) profile for model (left side) and observations (right side) in the four Adriatic sub basin. A=shallow north, B=deep north, C=middle, D=south.

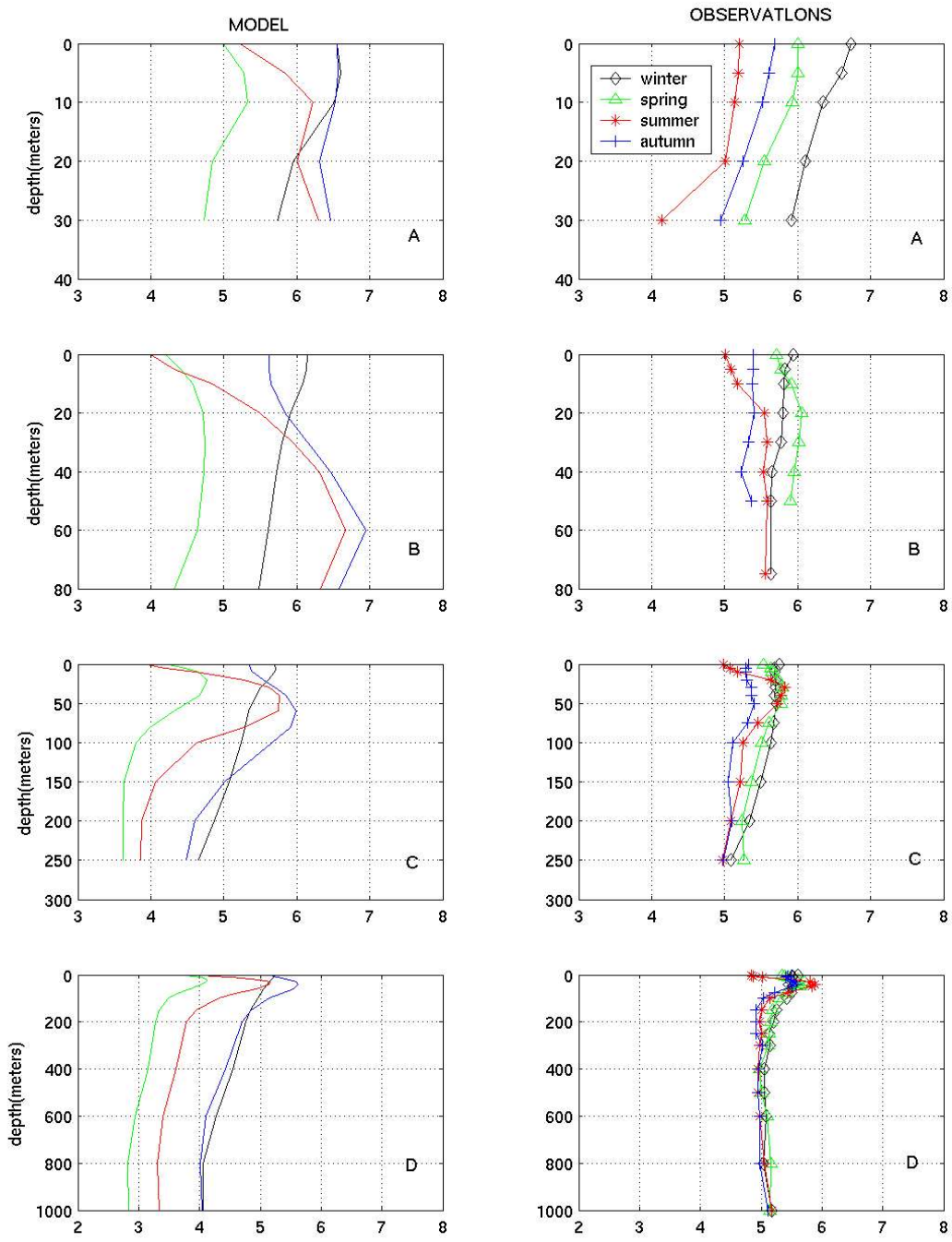

Figure 4.14 Seasonal oxygen (ml O_2/l) averaged profile for model (left side) and observation (right side) in the four Adriatic sub basin A=shallow north, B=deep north, C=middle, D=south.

4.4.4 Phytoplankton community structure

In Fig. 4.15, 4.16 and 4.17 are shown the annual phytoplanktonic averaged annual cycle of biomass vertical distribution (in form of Hovmoller diagrams) averaged in the four Adriatic sub basins for the three phytoplanktonic functional groups (carbon content) present in our model implementation. The Shallow northern basin is characterized by a high peak of diatoms during spring reaching a value of 150 mg C m^{-3}. During autumn we recorded high concentration of diatoms (100 mg C m^{-3}). During summer the simulated diatoms distribution show a minimum value but diatoms concentration is still high (between 100 and 50 mg C m^{-3}) The nanoflagellates distributions shows a peak during the spring period three time lower, in terms of biomass, with respect to that of diatoms. The simulated nanoflagellates biomass concentrations during summer and autumn appear to be quite constant and does not show any increase during autumn. The picophytoplankton concentration distribution shows two weak peacks in spring and autumn with a biomass level one order of magnitude less then diatoms. Therefore, in this sub basin, the development of large size phytoplanktonic cells is favored. In the deep northern basin diatoms biomass distribution shows two peaks in spring and late autumn and minimum values during the summer. The decrease of diatoms biomass with respect to the shallow northern basin is quite evident during winter and spring (maximum values in the deep North basin 100 mg C m^{-3}) and, (even more) during summer, where diatoms biomass is less then 20 mg C $m^{-3.}$ The nanoflagellates and the picophytoplankton biomass distribution in the deep northern basin does not show remarkable difference with respect to the shallow northern basin. In the middle basin the phytoplanktonic community structure seems to shift toward a more oligotrophic system (according to the chlorophyll concentration described above). The maximum diatoms biomass, recorded in spring, is, in this sub basin, very close to that of nanoflagellate that are the dominant phytoplanktonic groups during the summer. The simulations also show an increase of picophytoplankton whose biomass, during the summer, is comparable with that of diatoms. According to the Chlorophyll, simulated value we recorded a subsurface maximum of phytoplankton biomass around 70-80 meters deep. The south basin phytoplanktonic biomass distribution did not show a

significant difference with respect to the middle basin and the simulation results are not shown.

4.5 Conclusions and future work

This first simulation of the Adriatic Sea ecosystem seasonal variability with a full three-dimensional approach and with a realistic model set up appear to reproduce some of the main characteristics of the Adriatic Sea biogeochemistry in a reasonable way. In particular the seasonal primary producers variability is qualitatively captured by the model as well as the north-south trophic gradient. The comparison with the ABCD data shows that the basic assumptions of the model are reasonable. Despite the correct simulation of some features, the model still has many weak points. The overestimation of chlorophyll concentration suggests the need for an improvement of the the nutrients discharge parameterizations. We can argue that nutrients depletion condition generated by the model could be due to the high bacterial activity that needs phosphate for more efficiently utilization of the 'refractory' and 'semilabile' dissolved organic carbon. The underestimation of the nitrification processes could be the reason for e nitrate depletion. In addition, the simple benthic return model used in this study is certainly not able to reproduce the complexity of the water column-sediments interactions, therefore the introduction of a full benthic model would enhance the processes occurring on the bottom layer improving the simulation of the deep water column nutrients. Finally a more realistic phytoplanktonic community composition with the inclusion of dinoflagellates, conveniently parameterized, could improve the capacity of the model to capture the Adriatic Sea ecosystem features.

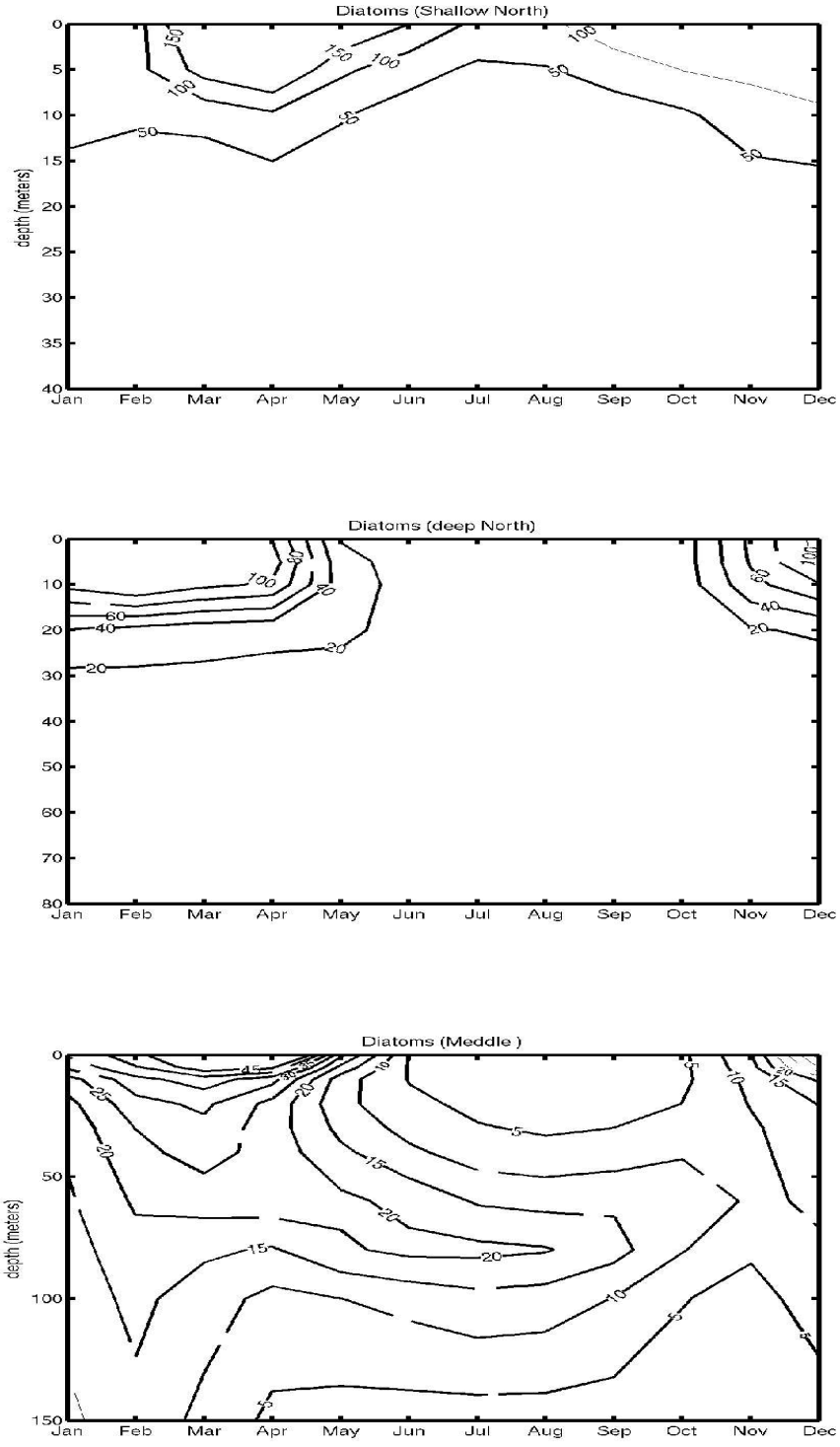

Figure 4.15. Hovmoller diagrams for diatoms functional group annual distribution (mg C/m^3) in the shallow northern, deep northern and middle basin.

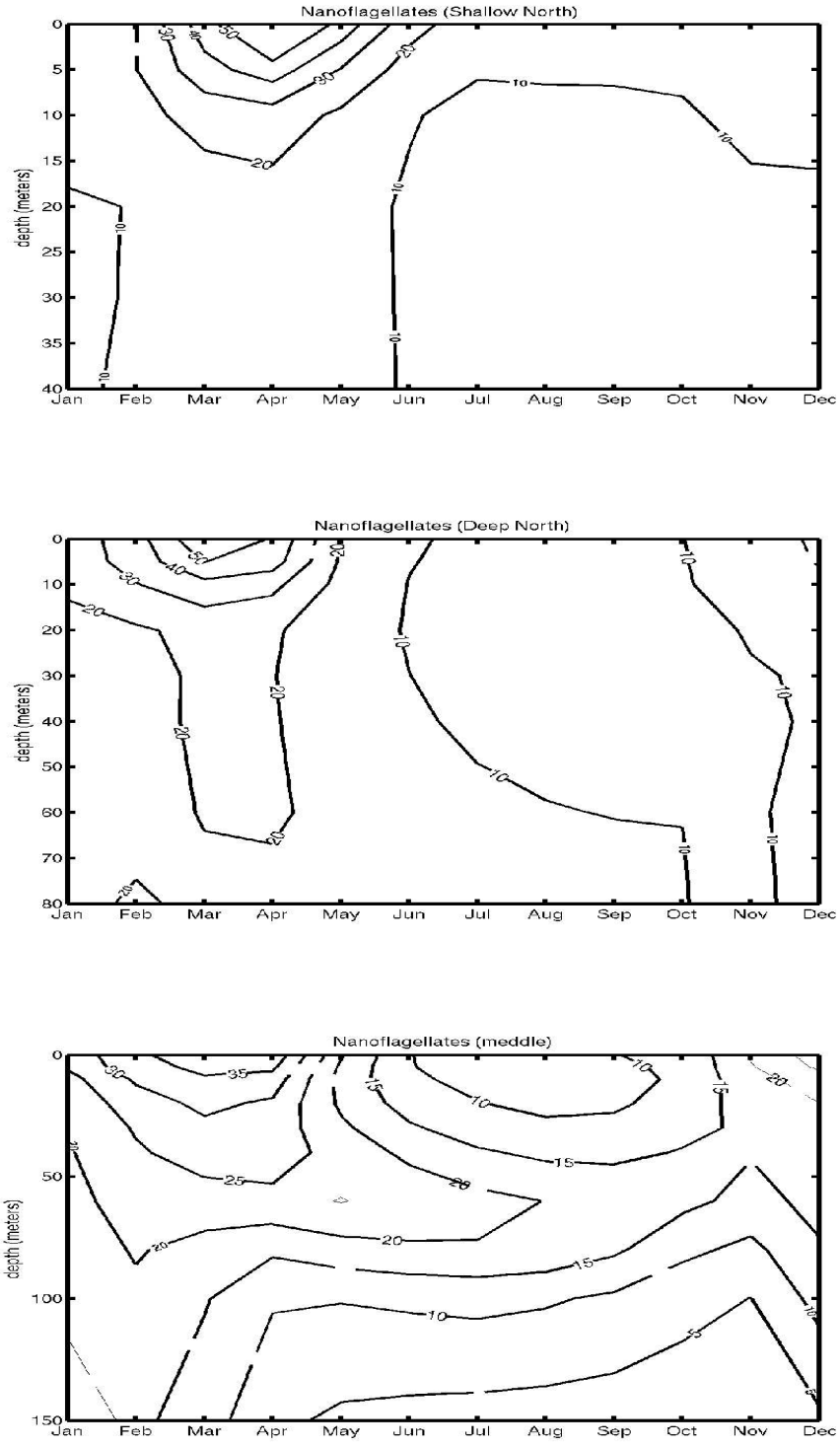

Figure 4.16. Hovmoller diagrams for nanoflagellates functional group annual distribution (mg C/m^3) in the shallow northern, deep northern and middle sub basin.

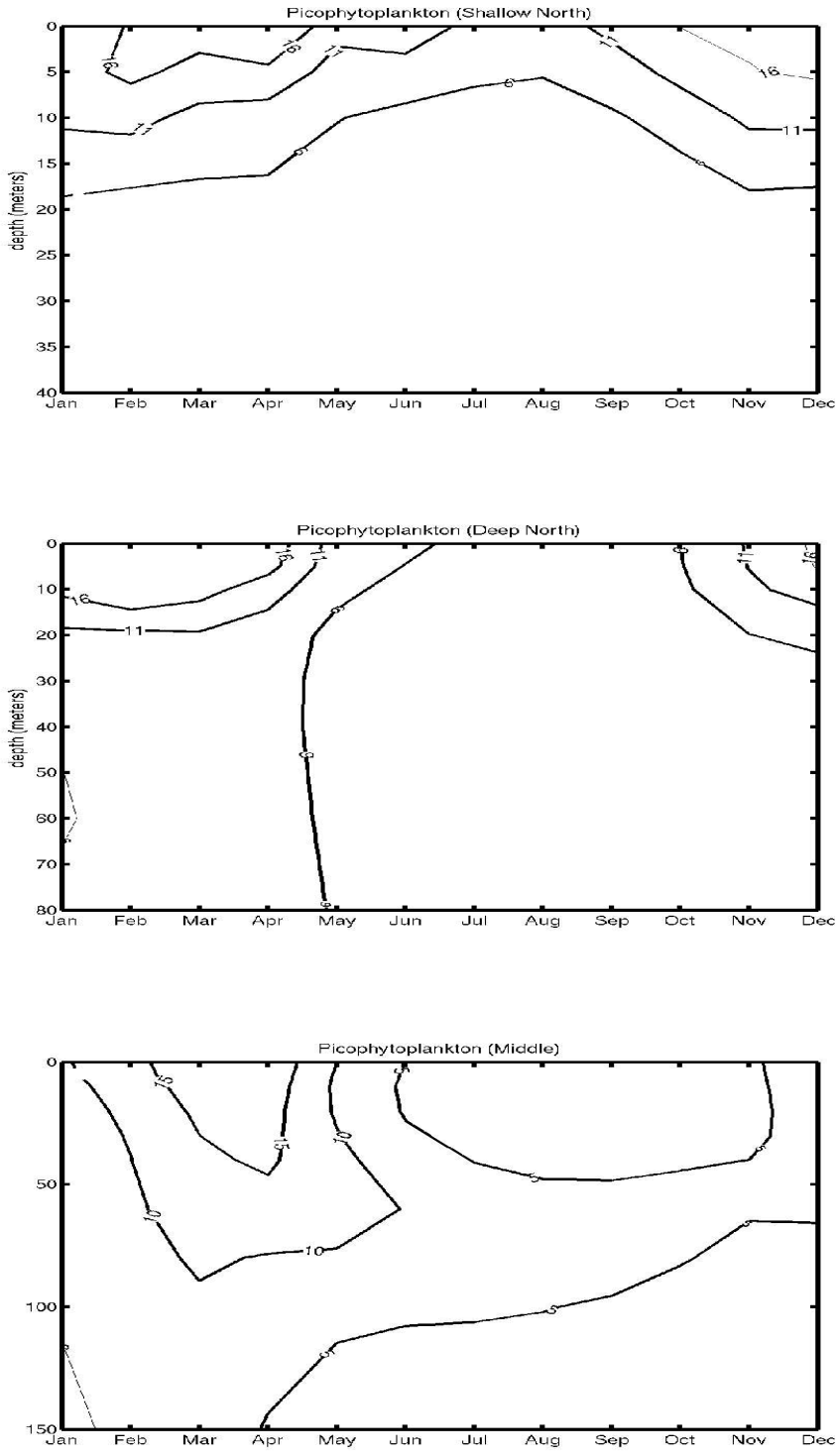

Figure 4.17. Hovmoller diagrams for picophytoplankton functional group annual distribution (mg C/m^3) in the shallow northern, deep northern and middle sub basin.

CHAPTER 5

5 The DOM dynamics and the hypothesis of the DOC accumulation in the northern Adriatic Sea

5.1 Introduction

Although the dynamics of dissolved organic matter in the Adriatic Sea is thought to be involved in important and extreme ecological phenomena such hypoxic and anoxic crises (Pettine *et al*., 1999) and the formation of massive mucillaginous aggregates (Degobbis *et al*., 1999), the observations on the distribution and variability of DOM and its important components are still limited (Pettine *et al*,1999). In the northern Adriatic is clearly observed a seasonal cycle with concentration increase, in summer, related to freshwater DOC input and nutrient discharges (that increase the marine primary production), mainly from Po River (Giani *et al.*, 2004). Pettine *et al*. (1999 and 2001) found that total DOC concentration, in the northern Adriatic basin, varied in the range of 74-281 mmol/m^3, in June, and 53-123 mmol/m^3 in February, while the carbohydrates fraction ranged from 8 to 72 mmol/m^3, in June, and from 6 to 39 mmol/m3 in February. The free amino acids concentration ranged from 0.37 to 2.44 mmol/m^3. The seasonal increase of DOM is, therefore, a factor of approximately 2 (Pettine *et al*., 1999) between February and June. In summer, DOC concentrations show higher values in surface waters with a decrease in the deeper layers; conversely, in February, the vertical profile is almost constant.

The seasonal increase in DOC concentration was also recorded by Fonda Umani *et al*. (1997) and Faganeli and Herndl (1991) who found distinct seasonal variations ranging from 66-154 mmol/m^3 of DOC during the Autumn and Winter to up 500 mmol/m^3 in the summer near the Slovenian part of the Gulf of Trieste. The seasonal pattern in DOC accumulation observed in the northern Adriatic

basin is similar to that observed in other areas such as the Baltic Sea (Zweifel *et al*., 1995), the north western Mediterranean (Copin-Montegut and Avril, 1993) and the Sargasso Sea (Carlson *et al*., 1994). More recently Giani *et al* (2004) recorded a seasonal increase of DOC amount to 70 mmol/m^3 in two section monitored during the Mat project (Mucilage in the Adriatic and Tyrrenian, 1999-2002). The sections were located across the Adriatic Sea, approximately at the Senigallia-Susak connection line (section C in Fig. 5.1) and Cesenatico-Kamenjak connection line (section B in Fig. 5.1). At a northern section connecting Punta della Maestra with Rovigno (section A in Fig. 5.1) the seasonal increase was lower, reaching 47-48 mmol/m^3. The seasonal DOC accumulation could be due to an enrichment in refractory compounds either discharged by rivers or resulting from abiotic chemical interactions or directly produced by biological processes (Azam *et al*, 1993, 1999). The lack of phosphate and the low nutritional quality of organic substrate could be a factor to explain such DOC accumulation. Increases in freshwater residence time, the set up of strong vertical stratification and mesoscales, which characterize the summer period circulation, are all factors which favour the accumulation of riverine organic matter as well as the occurrence of abiotic interactions which may lower the degradation rate of the organic substrate (Keil and Kirchman, 1997;. Pettine *et al*., 1999). Thingstad *et al* (1997) have proposed a theoretical model to explain DOM accumulation according to which bacterial carbon consumption may be limited by bacteria-phytoplankton competition for nutrients and bacterial predators, respectively controlling growth and biomass of bacteria.

In this chapter we test the conceptual model described in the chapter two in a full three dimensional contest. We use the numerical simulation and its comparison with available observation to investigate the DOC dynamics in the Adriatic Sea basin.

5.2 Model design

The simulations presented in this sections are carried out with a coupled biogeochemical-hydrodynamic model implemented in the Adriatic sea. The

biogeochemical model used is based on the European Sea Ecosystem Model (ERSEM) and the hydrodynamic model is the Princeton Ocean Model. For a detailed description of the new dissolved organic matter-bacteria dynamics see chapter 3 and, for the description of the genaral ERSEM assumptions and characteristics, see the chapter 2. For a description of the POM-ERSEM coupling and the model set up see the chapter 4.

The hydrodynamic model was taken at the third year of spin-up with climatological forcing (see chapter 4). After that, the biochemical model was coupled with hydrodynamics and run for four years. All results presented are relative to the fourth year of the simulation with the fully coupled ecosystem model. We make the assumption here that the seasonal cycle simulated by the climatological forcing can reproduce the seasonal dynamics of DOC. This is true if the field statistics is stationary and we will see that this hypothesis is clearly not sufficient to explain all the DOC dynamics in the Adriatic Sea.

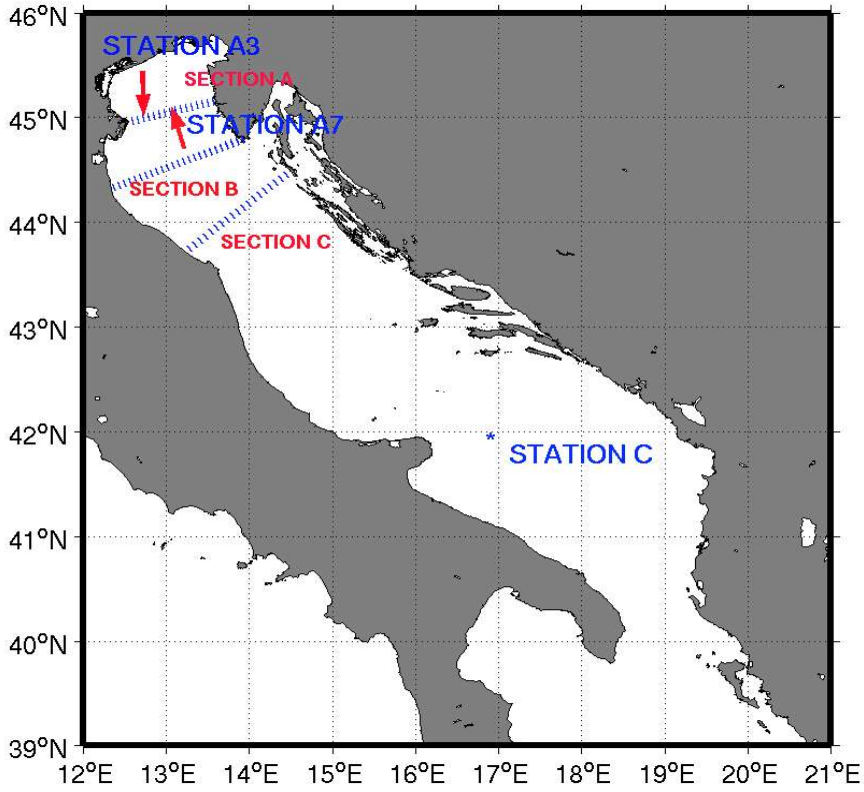

Figure 5.1. The model domain and observational section of the MAT project. Section A is used for the comparison between observations and simulations while section B and C are mentioned in the text. Station C is also used for simulations analysis in order to compare contrasting trofic conditions.

5.3 Analysis of the ecosystem model control simulation

5.3.1 DOC horizontal distributions

In Fig. 5.2 are shown the total DOC surface monthly averaged concentrations in the control experiment (see Table 1). This experiment is meant to be the best fit to the estimates of nutrient inputs from rivers.

The DOC January values are around 50 mmol/m^3 in the northern part of the basin and in the middle basin, along the Italian coasts, while in the southern basin the value of 50 mmol/m^3 is reached only in the Albanian coastal area. In the open waters of the middle and southern basin the DOC concentration is around 25-50

mmol/m^3. During February and March DOC increases along the whole Italian coasts, from the Gulf of Trieste to the Gargano peninsula, where the simulated DOC concentrations reach 100 mmol/m^3. In particular, in March, in a more restricted area of the north-western Adriatic, the DOC reaches 150 mmol/m^3 and, in a little area along the Emilia Romagna region, 200 mmol/m^3.

In the southern basin the DOC concentration is constant and remains at low values with the only exception of the Albanian coasts. In April the DOC concentrations reach the value of 100 mmol/m^3 even in the eastern part of the northern basin. The highest DOC concentrations are achieved in May and June (> 150 mmol/m^3) in the north-western Adriatic coast and, in the southern Adriatic, along the Albanian coast and in the centre of the basin. In particular the model simulation shows a zone with very high DOC levels in the north-western coasts, from the Gulf of Trieste to Ancona, where the DOC reaches the 200 mmol/m^3. The distribution, in July, does not change with exception of a mild decrease of the DOC concentrations in the southern Adriatic. In August DOC decreases in the northern basin, and the high concentrations are limited to a restricted area along the northern Italian coast. Starting from September the DOC concentrations decrease and, in December, the model simulates a DOC concentration of around 50 mmol/m^3 in the southern basin and in the eastern northern basin. Along the Italian coasts, in the northern and middle basin, DOC concentrations are around 100 mmol/m^3.

In order to show the behavior of the new dissolved organic matter model implemented in this thesis, we reproduced in Fig. 5.3, 5.4, and 5.5 the monthly surface concentrations of the 'labile', 'semilabile' and the 'refractory' DOC components.

The 'labile' DOC concentrations (Fig. 5.3) in January, February and March are very low all over the basin and they are negligible in areas such as the central part of the southern basin. 'labile' DOC is present at very low concentration (less then 0.5 mmol C/m^3) in the northern areas, along the Istrian coast. Along the Italian coast, in the middle and southern basin, the model simulation shows some areas with high 'labile' DOC concentrations that in any case do not go over the 4

mmol/m^3. During the Spring period the general level of the 'labile' fraction of DOC increases reaching, in June, the concentration of 1 mmol/m^3 in the southern and middle part of the basin and along the eastern part of the northern basin.

Along the Italian coast and in the northern basin, the 'labile' DOC concentration increase strongly: the area with high concentration (more than 4 mmol/m^3) runs from the Gulf of Trieste to Ancona. From July to September the concentrations decrease to about 1 mmol/m^3 (in August) all over the basin and the area with the highest concentration (4 mmol/m^3) is restricted to the area adjacent to the Po river mouth and along the Emilia Romagna coastal area. In winter the values return to about 1 mmol/m^3, with the exception of the north western coastal area.

The simulated concentrations of the 'semilabile' component of DOC (Fig. 5.4) are, in January, around 50 mmol/m^3 in the north-eastern basin, and less then 25 mmol/m^3 in the middle and southern basin. Only in correspondence to the Italian coast, in the Northern basin, does the model simulate concentration higher than 50 mmol/m^3. This pattern is maintained in February, where just a mild increase of 'semilabile' DOC is present along the northern and middle basin Italian coast. Starting from March the simulated values start to increase and, in May and June, the model simulates concentrations of about 50-70 mmol/m^3 all over the basin and two areas with high semilabile DOC concentration: the northern Italian coast, with concentrations ranging from 100 to 150 mmol/m^3, and the southern basin, both along the Albanian coast and in the centre of the basin (80-100 mmol/m^3).

During the Summer months the northern Italian coastal area still maintains a DOC concentration higher than 100 mmol/m^3 while the southern high concentrations decrease rapidly going back, in September, to a value of 50 mmol/m^3. In October and November the general trend is a strong decrease everywhere in the basin and the 'semilabile' DOC concentrations are more then 50 mmol/m^3 only in in the north-western part of the basin and along the Albanian coast.

In December the concentrations of the 'semilabile' DOC are below the value of 50 mmol/m^3 as a constant value in most of the basin and range between 50 and 70mmol/m^3 along the Italian coast from the Gulf of Trieste to the Gargano

peninsula.

The surface monthly averaged concentrations of the 'refractory' DOC (Fig. 5.5) is almost constant in the winter period with a concentrations less than 30 mmol/m^3 in the middle offshore and southern part of the basin. Concentrations ranging from 30 to 40 mmol/m^3 are reached in the northern part and, in the middle basin, along the Italian coast. During Spring this high concentration area extends southward, covering, in June, the whole middle basin and the eastern part of the southern basin. In the northern basin, along the Italian coast the simulated 'refractory' DOC concentration reaches 50 mmol/m^3. During the summer The simulations show a background value of 30 mmol/m^3 everywhere in the basin and, along the northern Italian coastal area, concentrations ranging from 40 to 60 mmol/m^3. During August and September a patch 'refractory' DOC high concentrations (30 mmol/m^3) is present in the open waters of the northern and middle basin. During Autumn the general trend is a decrease of 'refractory' DOC concentrations and, in December, in the southern basin, the simulations show a value of 20 mmol/m^3 a values ranging from 20 to 40 mmol/m^3 in the middle and northeastern basin, and a value of 50 mmol m^3 only in a restricted area along the Emilia Romagna coastal area.

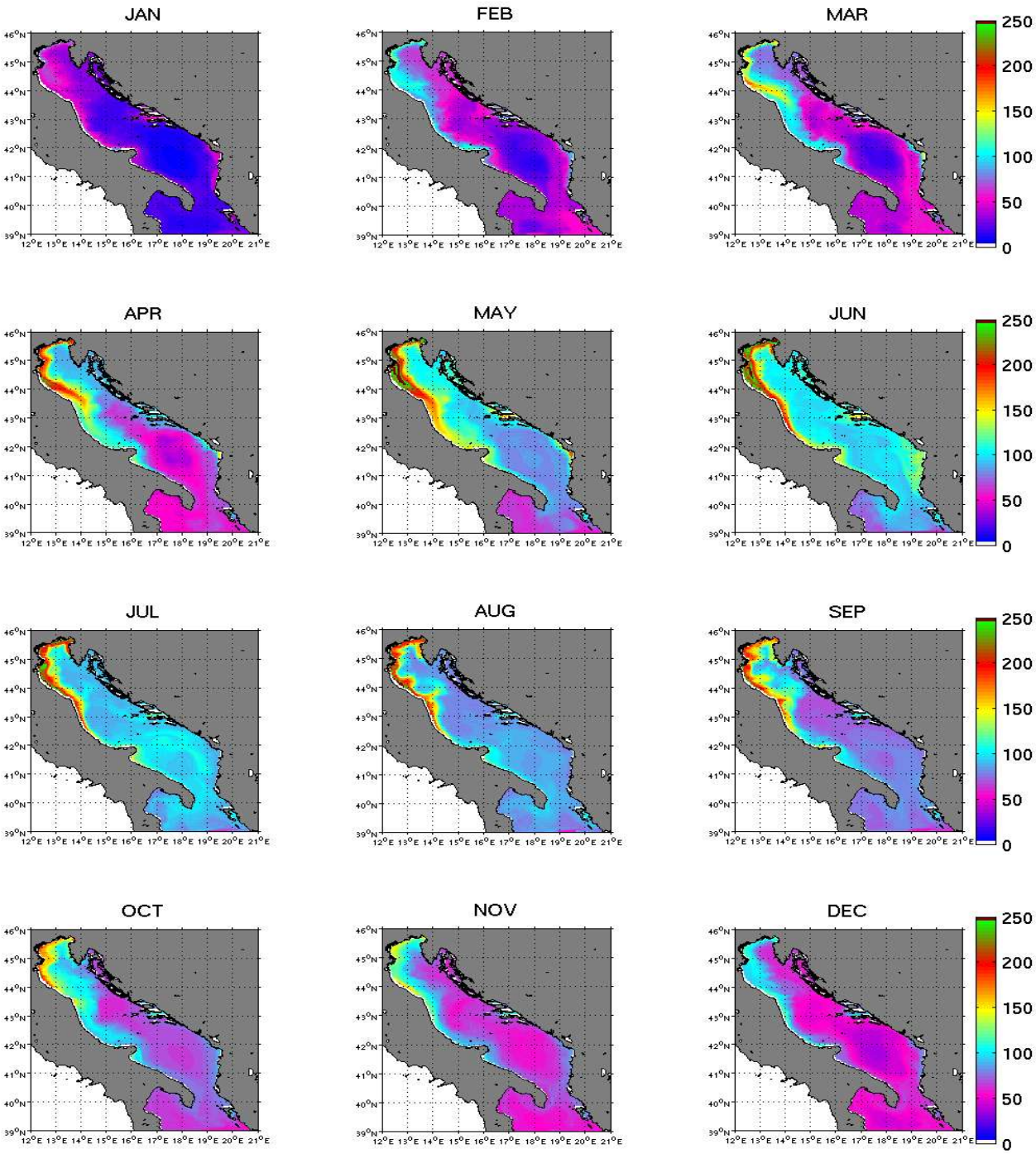

Figure 5.2. Total DOC (mmol/m^3) surface monthly mean distribution.

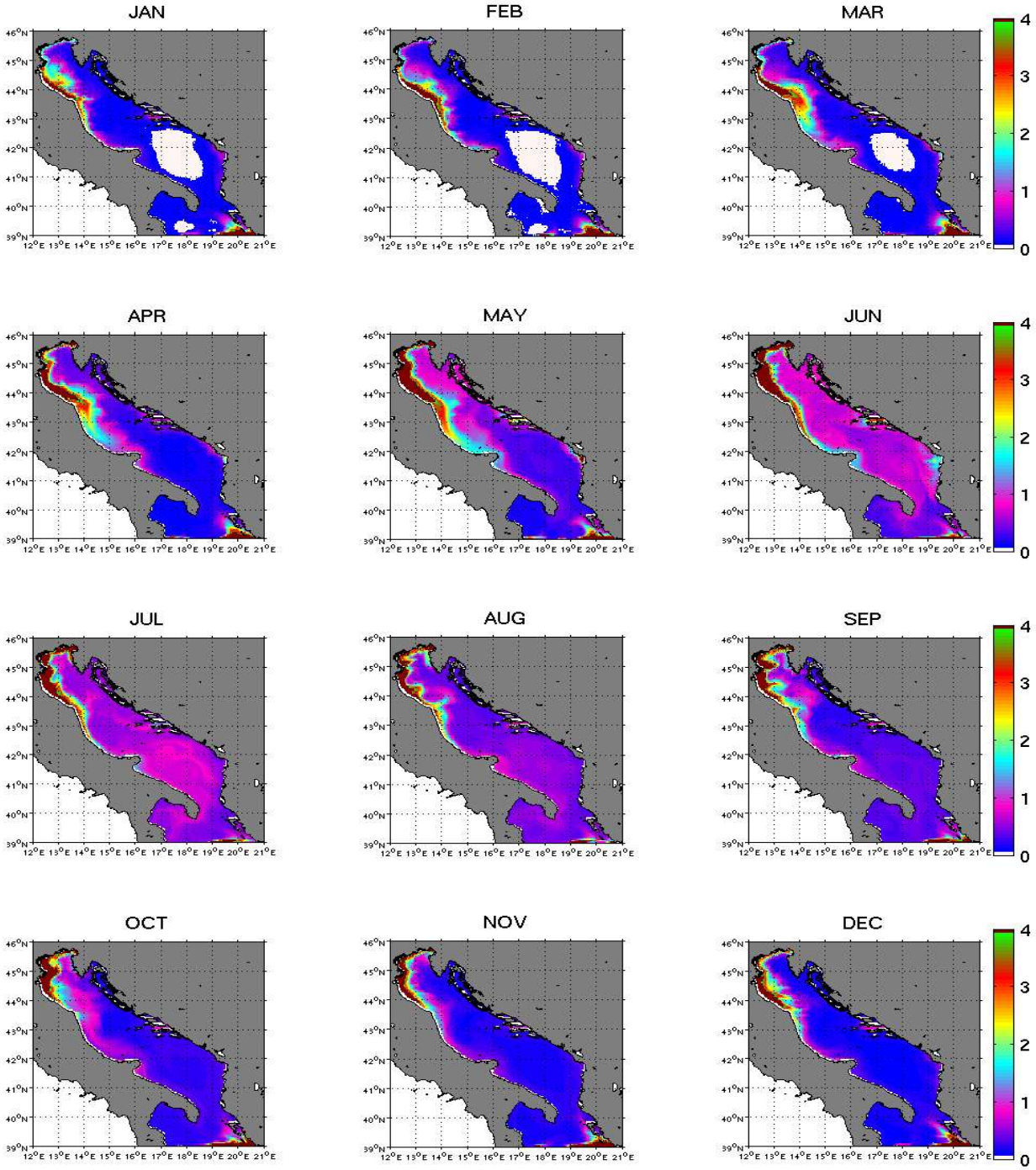

Figure 5.3. 'Labile' DOC (mmol/m^3) surface monthly mean distribution.

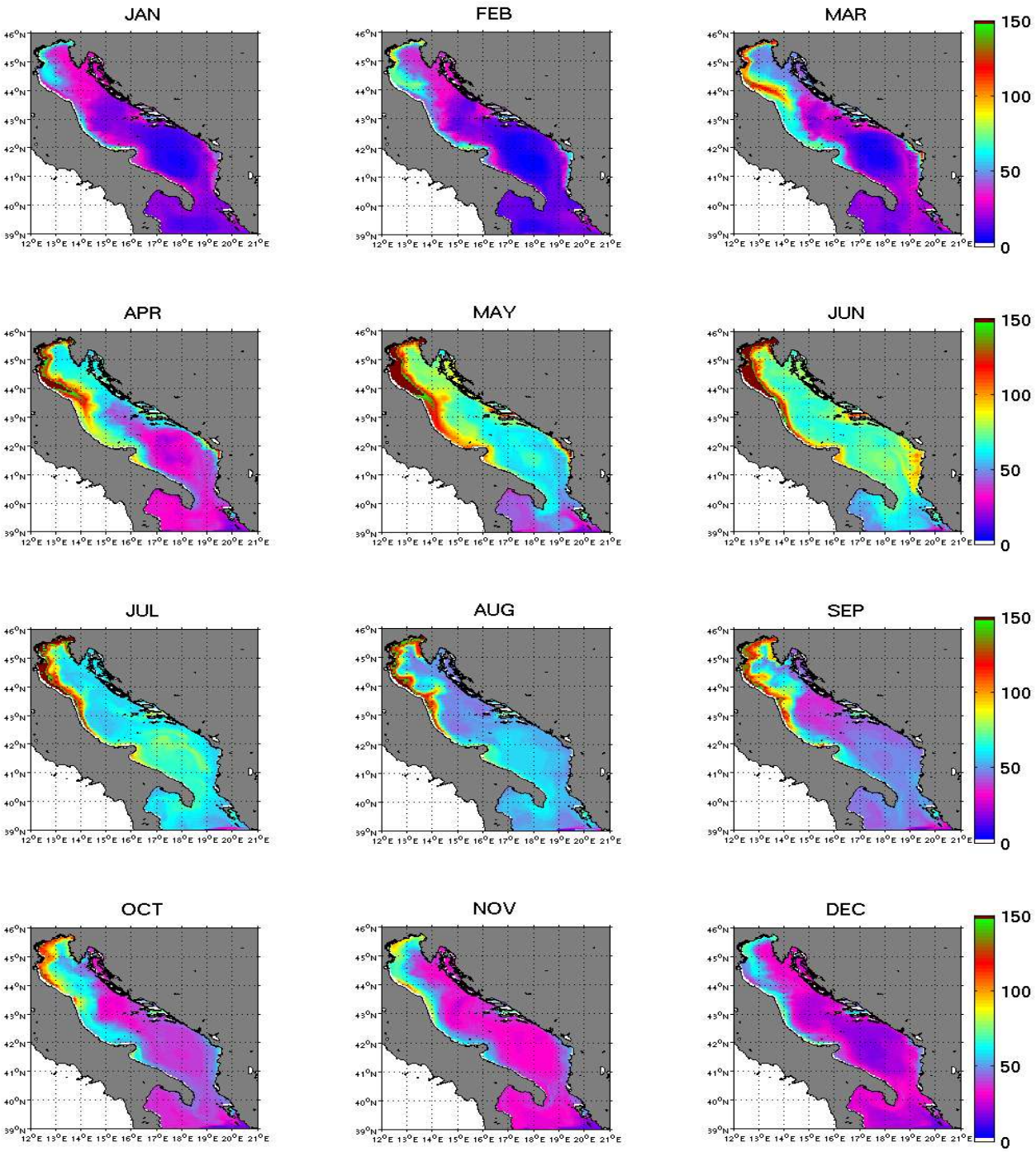

Figure 5.4. 'Semilabile' DOC (mmol/m^3) surface monthly mean distribution.

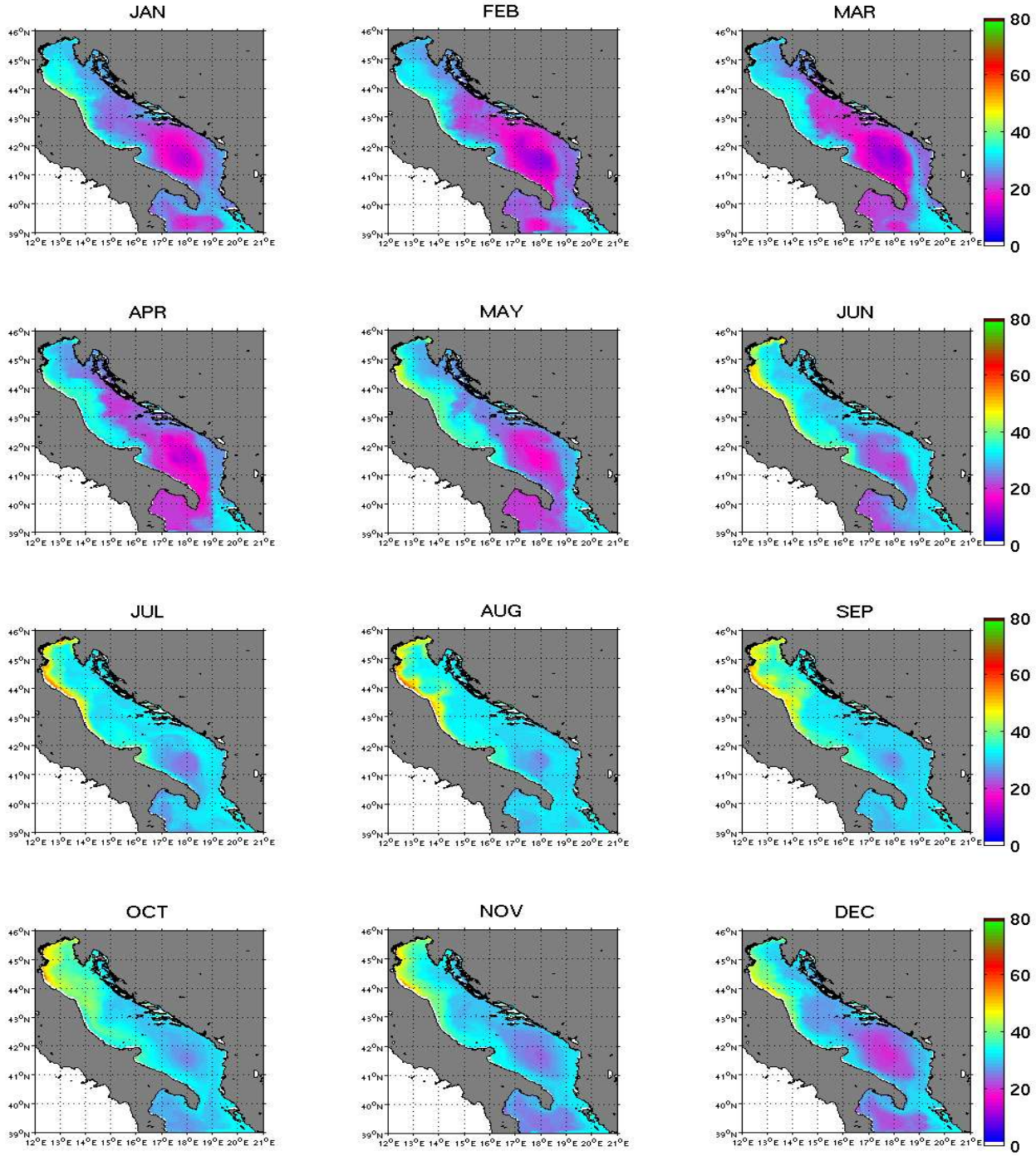

Figure 5.5. 'Refractory' DOC (mmol/m^3) surface monthly mean distribution.

In Fig. 5.6 we show the time series of the 'semilabile' and 'refractory' dissolved organic carbon and the potential primary production, at the surface, in the three stations indicated in Fig. 5.1. Station A3 is very close to the Po river delta area, station A7 is in the centre of the northern basin and station C is in the open waters of the southern basin. In station A3 the potential primary production shows two peaks in spring and autumn clearly related to the Po river runoff. The maximum value in Spring is 200 mg C m^{-3} d^{-1}, while in September-October the maximum value is 400 mg C $m^{-3}d^{-1}$. The distribution of the 'semilabile' DOC is clearly related to the gross primary production with two maxima, one in spring (more than 100 mmol/m^3 in May) and the second one in autumn (90-100 mmol/m^3 in September).

The 'refractory' DOC shows a quite constant value throughout the year (around 40 mmol/m^3) with a presence of a mild increase (around 5 mmol/m^3) from August to October. In station A7 the gross primary production still present two peak in spring and Autumn, but with the values remarkably lower than in the Po delta area (50 mg C m^{-3} d^{-1}, and 65 mg C m^{-3} d^{-1} respectively). The 'semilabile' DOC reflects the gross primary production distribution with two maxima in June and October around 70 mmol/m^3 in both cases. The values are lower with respect to the A3 station. The annual behavior of the gross primary production in the C station shows only one maximum in May with a value of 65 mg C m^{-3} d^{-1}. During the summer and the autumn the surface primary production decrease without any increase during the autumn. The maximum of 'semilabile' DOC is reached in July when the simulated value is 70 mmol C/m^3. The "refractory" DOC concentration are quite constant during the winter with values ranging from 16 to 20 mmol/m^3. Starting from March there is an increase of the 'refractory' DOC reaching 25 mmol/m^3 during the summer and autumn.

5.3.2 DOC vertical distribution

Total DOC vertical profiles are shown in Fig. 5.7. In order to investigate the behavior of the DOC simulated by the model through the water column we averaged the simulated DOC profile in the four sub basins described in chapter 4.

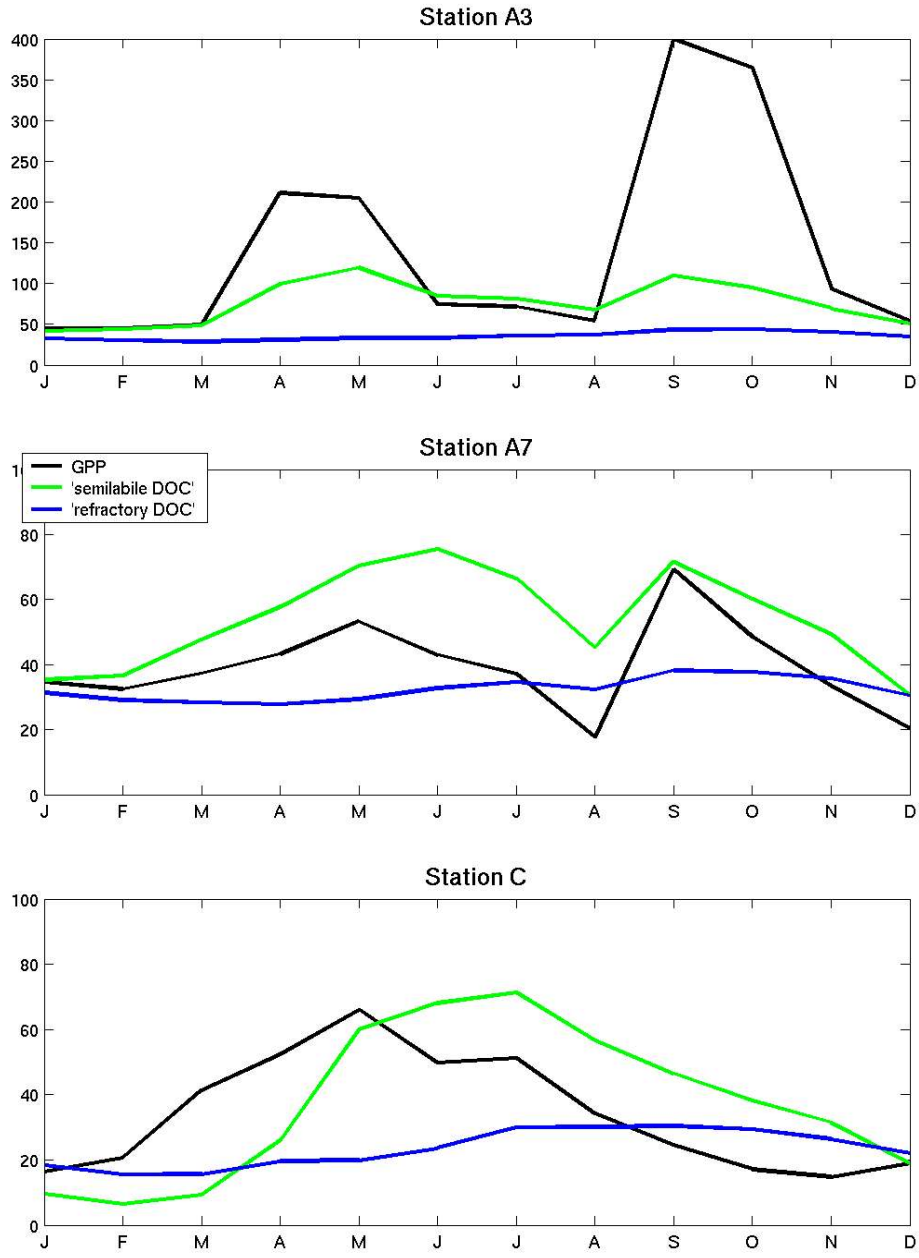

Figure 5.6. Annual surface distribution of gross primary production (mg C m^{-3} d^{-1}), 'semilabile' DOC and 'refractory' DOC (mmol C m^{-3}) in the stations A3, A7 and C.

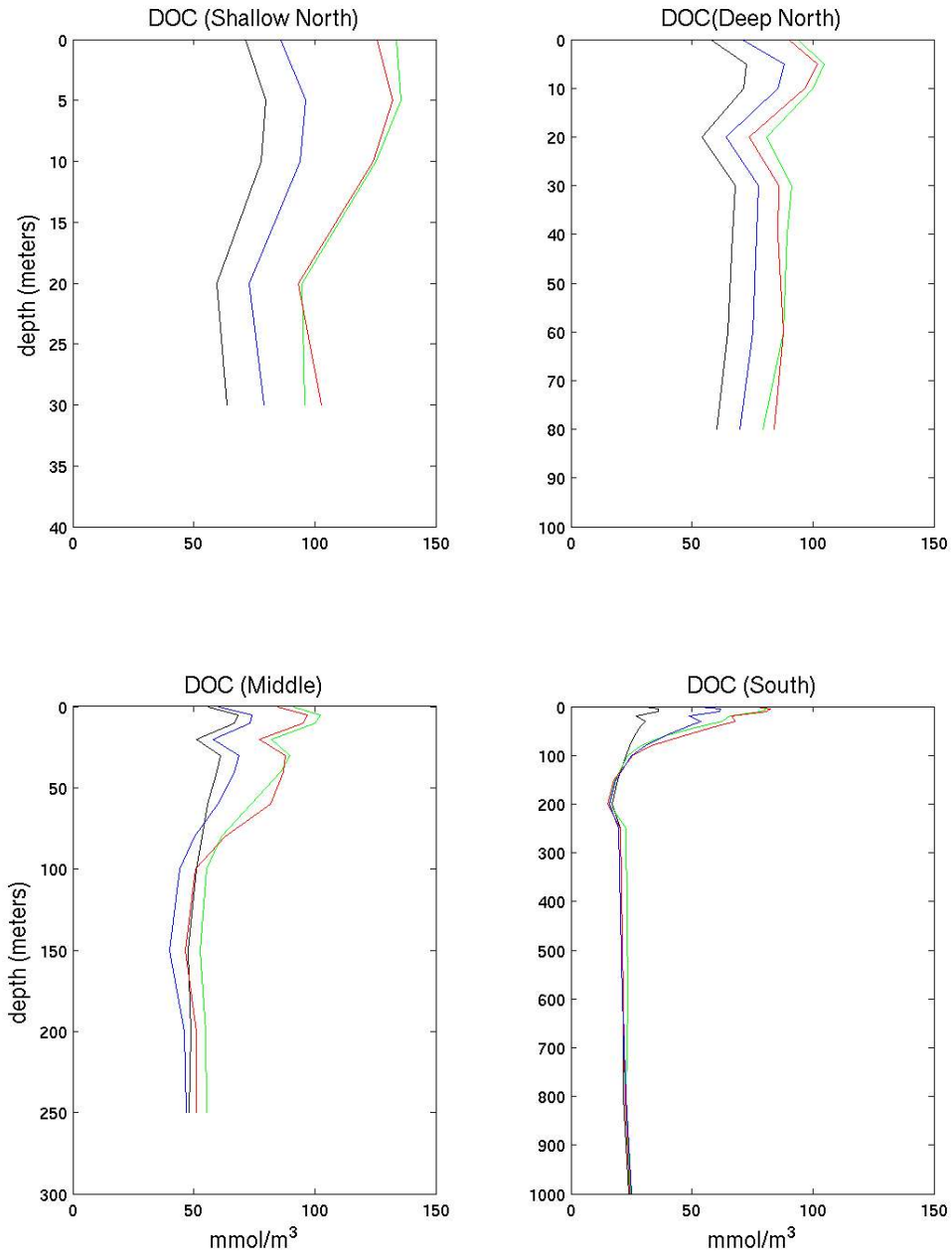

Figure 5.7. Total DOC (mmol/m^3) vertical, seasonal averaged, profiles in the shallow north, deep north, middle and south basin. Black line=winter; green line=spring; red line=summer; blu line=autumn.

In the northern shallow basin the averaged total DOC profiles show a clear seasonality with the highest concentrations in summer and the minimum in winter. The shape of the profile shows a subsurface maximum at 5 meters depth and a minimum at 20 meters in the four seasons. The maximum averaged concentration is, in this sub basin, of 140 mmol/m^3 at 5 meters depth in spring and the minimum is around 60 mmol/m^3 at 20 meters depth in winter.

In the deep northern basin the shape of the profiles are similar to the one of the shallow northern basin but with lower values and with the maximum (110 mmol/m^3) falling in spring rather than in summer.

In the middle Adriatic basin the profile in the first 100 meters of the water column is similar to those of the deep north in terms of both shape and seasonality. From 100 meters to the bottom the values are almost constant (around 50 mmol/m^3)and the intra-seasonal variability very low.

In the southern basin the maximum averaged concentration is attained in summer near the surface, where the value is double than in winter. Below 200 meters the simulated DOC concentration is constant and equal to a value of approximately 30 mmol/m^3 up to 1000 meters

5.3.3 Dissolved organic Nitrogen (DON) and Dissolved organic Phosphorus (DOP) horizontal distribution

Surface monthly averaged DON and DOP concentrations are shown in Fig. 5.8 and 5.9. The DON concentrations (Fig. 5.8) in January February and March are very close to zero in most of the basin with the exception of the northwestern coastal area where the DON concentrations reach the value of 2.5 mmol/m^3. During spring the simulated values show a strong increase in the northwestern coastal area where they reach 4 mmol/m^3. From June the high concentrations start to disappear and, during the summer, the DON concentrations are more than 1 mmol/m^3 only in the northwestern coastal area very close to the Po river mouth and in the Trieste Gulf. During the autumn the DON is depleted even in this zone and in December the distribution of the DON surface concentration appear very similar to that one of January.

The DOP surface concentrations (Fig. 5.9) range from 0.01 to 0.15 mmol/m^3 in

the northern and middle basin along the Italian coast and the DOP is almost totally absent in most of the basin. During Spring the DOP appears almost everywhere in the basin, and increases in the northwestern coastal areas where they reach the value of 0.2 mmol/m^3. The concentrations are quite constant untill July. From August the DOP is rapidly depleted starting from the eastern coastal areas and then in the whole basin with the exception of the Italian coast, from the Gulf of Trieste to the Gargano peninsula, and the DOP simulated maximum values range from 0.01 to 0.15 along the Emilia Romagna coastal area.

5.3.4 Bacterial growth efficiency (BGE) and bacterial production (BCP)

The monthly averaged surface values of BGE are shown in Fig. 5.10. During January, February and March the BGE simulated value range from 0.01 to 0.4. The distribution shows a very low efficiency (from 0.01 to 0.1) in most of the basin and a restricted area with a larger BGE value ranging from 0.1 to 0.4. in the Emilia Romagna coastal area.

Starting from March BGE simulated values starts to increase in the southern basin with values ranging from 0.1 to 0.2; this trend is interrupted in April when the simulations show a BGE decrease in the southern basin and an almost constant value in the others part of the Adriatic. In May the BGE reaches a diffused value of around 0.18 in the the southern and middle basin. In the northern basin we record the highest simulated BGE value (more then 0.35) in the western coast. The remarkable thing is the strong gradient going from the western coastal area toward the Istrian coasts where the BGE is below 0.1. This configuration, in the northern basin, is present for all the year long. In June the area with high BGE levels along the north western coast reaches the middle basin but only in a narrow coastal area. Values around 0.3 are also present in the Gulf of Trieste and, in the south, along the Albanian coasts. During this month is also evident an increase of BGE in the central part in the southern basin where BGE reaches a value of 0.25. During Summer the BGE start to decrease and, starting from August, the values of BGE higher then 0.1 are present only in the northwestern basin in the area surrounding the Po delta river, along the Emilia Romagna coast and along the Albanian coast.

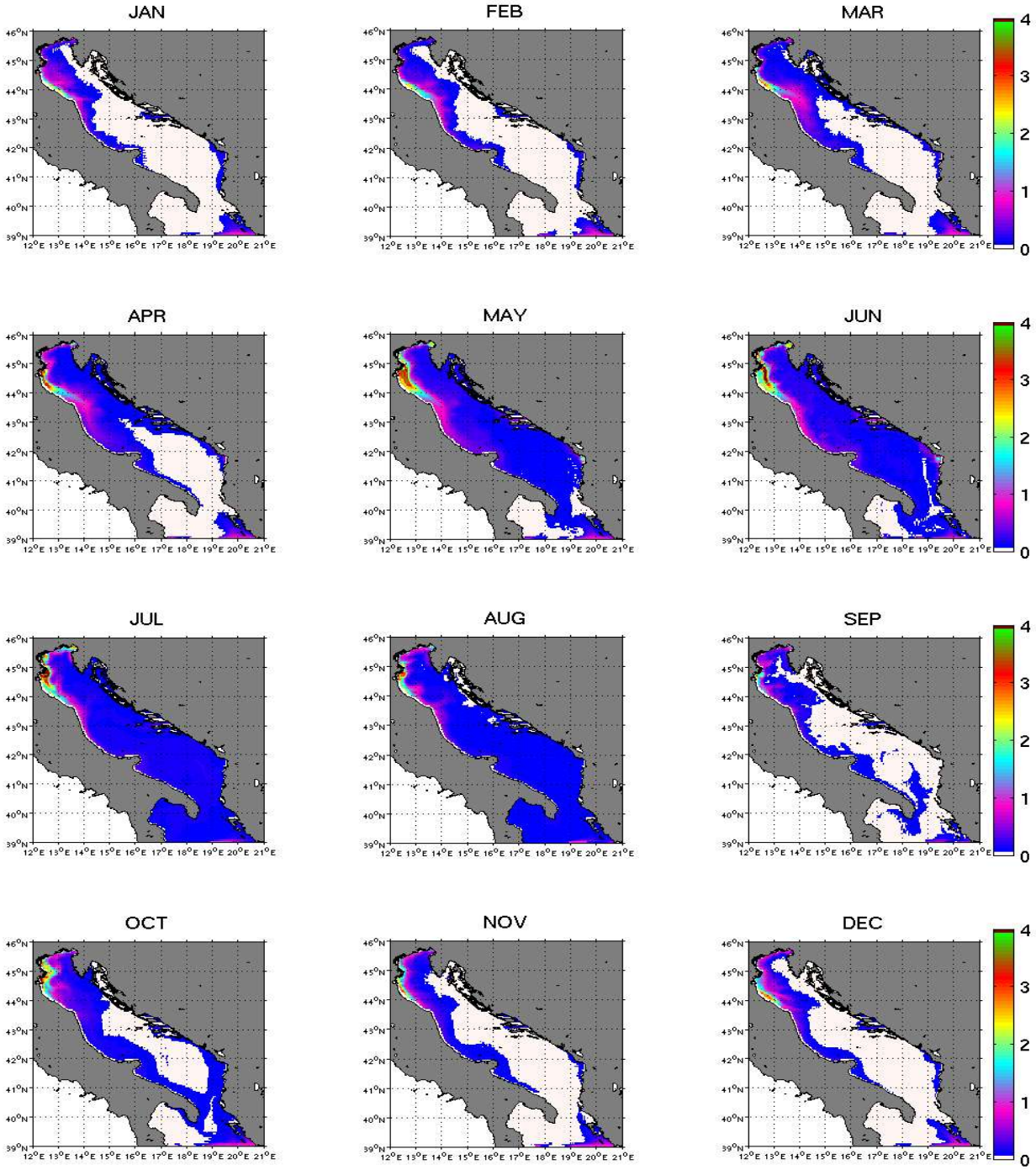

Figure 5.8. DON (mmol/m^3) surface monthly mean distribution.

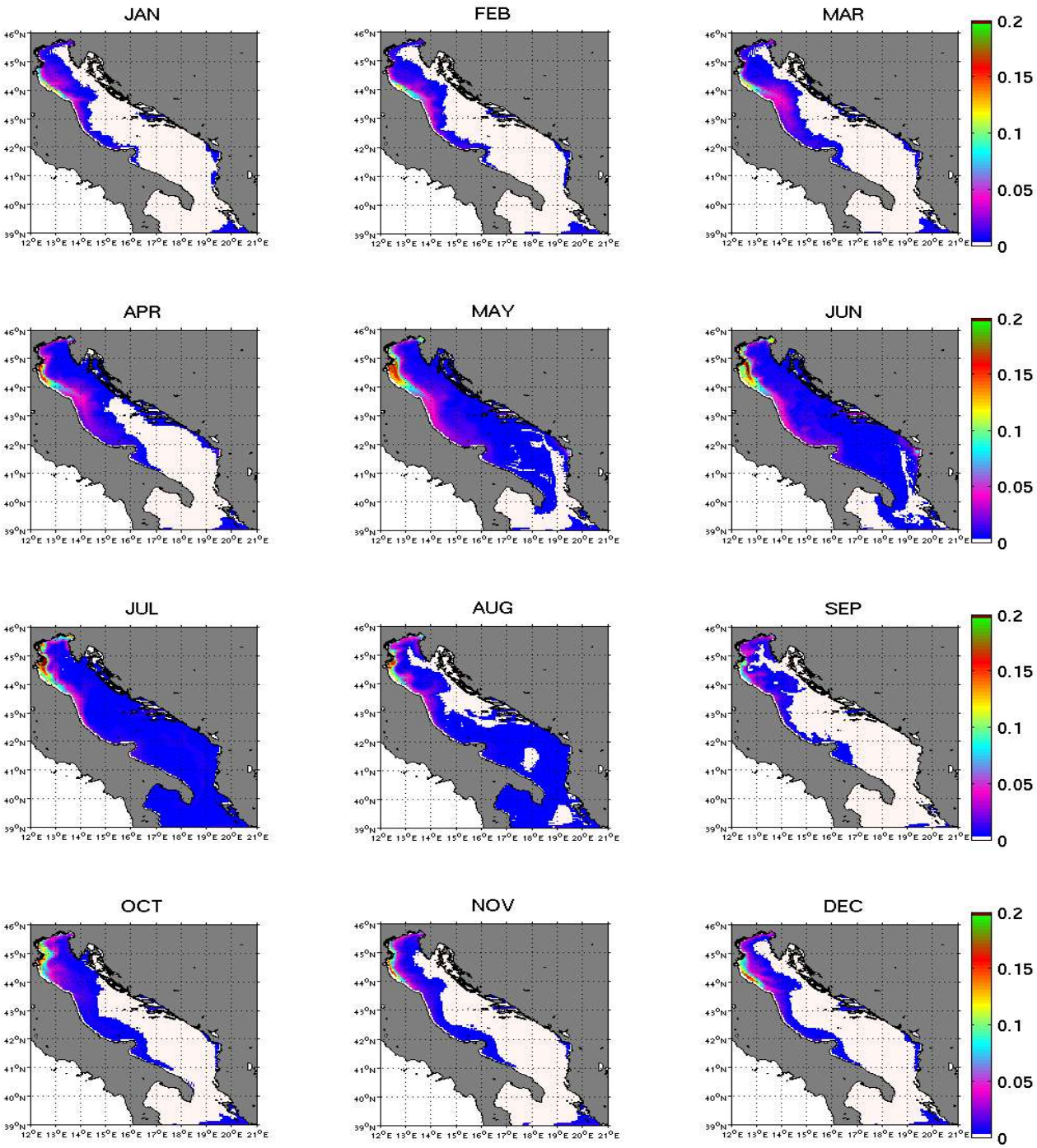

Figure 5.9. DOP (mmol m^{-3}) surface monthly mean distribution.

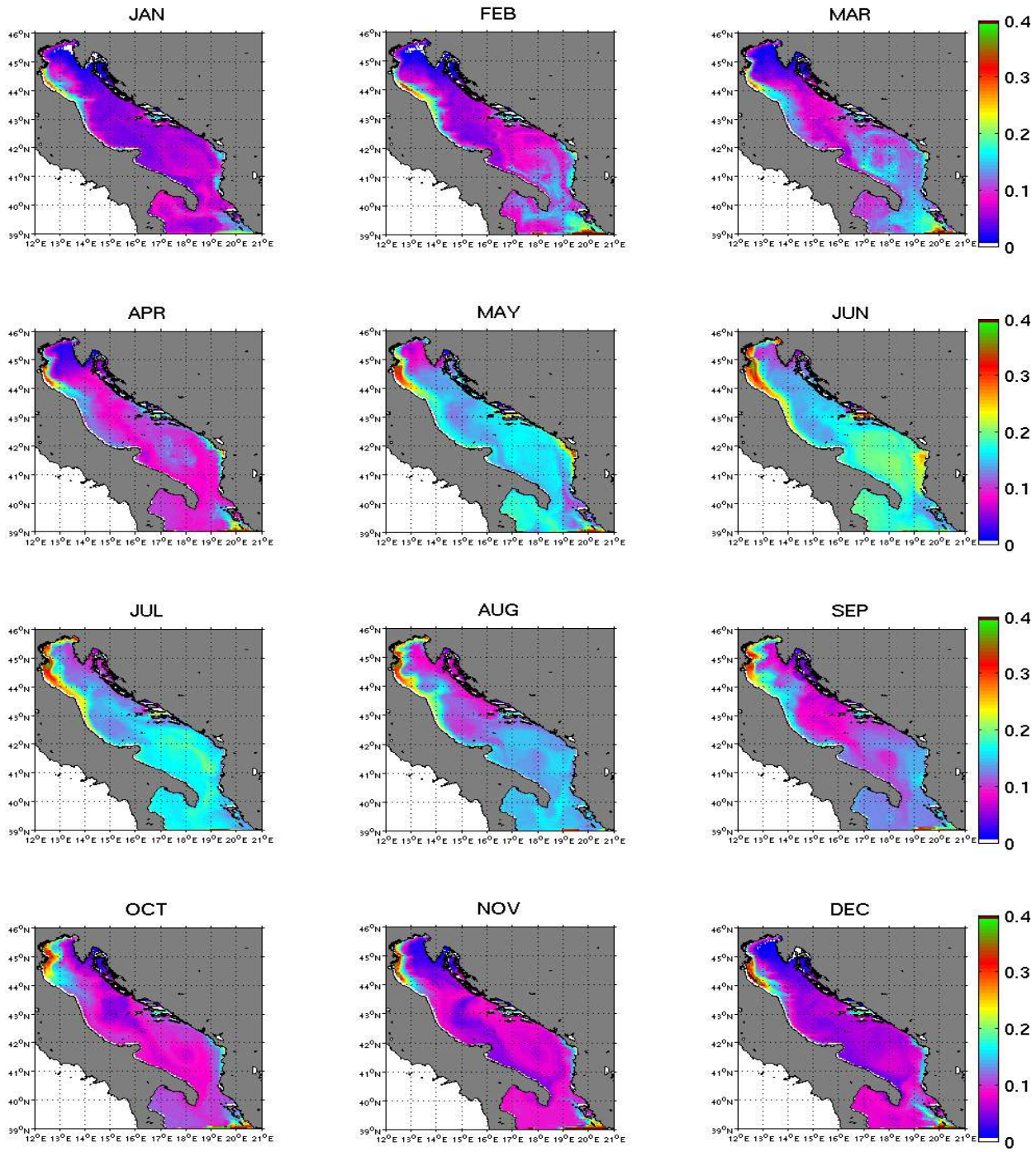

Figure 5.10. Bacterial growth efficiency surface monthly mean distribution.

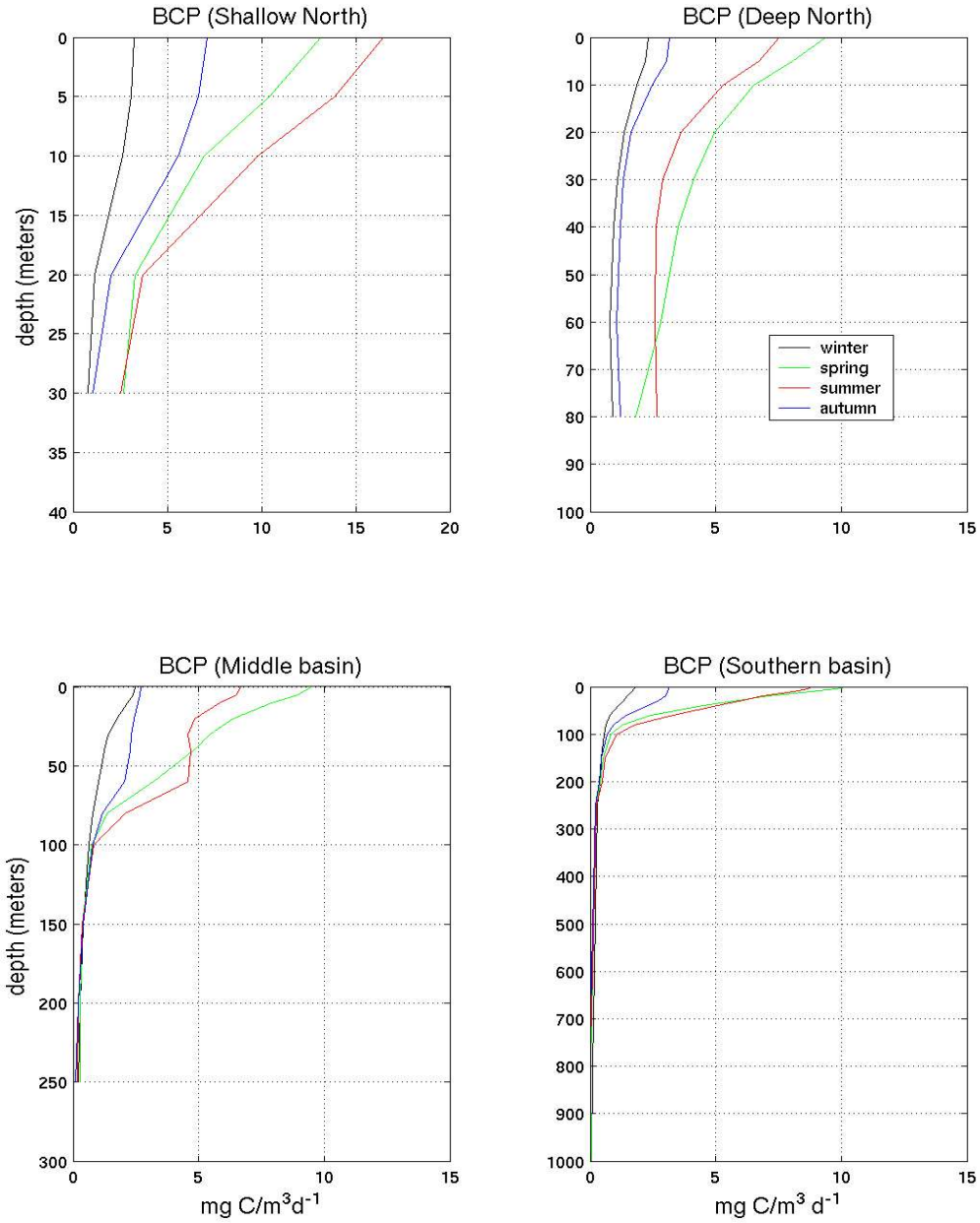

Figure 5.11. Bacterial carbon production (mg C m^{-3} d^{-1}) seasonally averaged profiles in the shallow north, deep north, middle and south basin.

In Fig. 5.11 the vertical mean profiles of bacterial carbon production (BCP) are shown seasonally averaged on the four Adriatic sub basin as described in the chapter 4. In the shallow north the BCP simulated profile show a clear seasonality with maximum in Summer (16 mg C m^{-3} d^{-1} in surface) and minimum in winter (less than 5 mg C m^{-3} d^{-1} through the water column). During summer and spring there is a strong vertical gradient between surface and deeper layer while in winter the value are almost constant. In the middle north basin the maximum simulated value are in spring (9 mg C m^{-3} d^{-1} near the surface and the minimum are in winter (less the 2 mg C m^{-3} d^{-1} below 20 meters depth). During summer and spring there is still a strong vertical gradient while in winter and autumn the simulated BCP values are more constant throughout the water column. Below 20 meters depth the BCP is in the four seasons below 5 mg C m^{-3} d^{-1}.

In the middle basin the BCP simulated values show two distinct gradients depending on the water column depth. In the upper 100 meters maximum values show a clear seasonality with maximum in Spring (9 mg C m^{-3} d^{-1} near the surface) and minima in winter (lass than two mg C m^{-3} d^{-1}) below 50 meters depth. From 100 meters depth to the bottom, on the contrary, the values are almost constant in the four seasons and very close to zero starting from 150 meters depth. The summer simulated profiles showing a maximum value near the surface (6 mg C m^{-3} d^{-1}) and a relative maximum around 60-70 meters depth.

Even in the southern basin the seasonal variability is present only in the upper 100 meters of the water column. The simulated profiles show the maximum in spring near the surface when the BCP reach 10 mg C m^{-3} d^{-1} The summer simulated profile is very similar to the one simulated in spring, while the values in winter and autumn are remarkably lower (less than 4 mg C m^{-3} d^{-1}) in the upper part of the water column. From 100 meters depth two 200 the simulated values are very similar in the four seasons and are around 1 mg C m^{-3} d^{-1}. From 200 meters depth the BCP decrease slowly going to zero from 300 meters to the bottom.

5.3.5 Sensitivity Analysis

In order to understand the the model response and to different environmental conditions, a set of sensitivity experiments was performed. The system is clearly controlled by the river inputs and our knowledge of runoff and nutrients loading is very inadequate. Thus we varied the runoff and the N/P ratio of the discharged nutrients, trying to account for the different biochemical processes occurring in the Po delta with respect to the other rivers. Our decrease of runoff has only an impact on the nutrient loading and not on the physics. This will be changed in the future model development. In addition we varied the availability rate of 'refractory' DOC. The different model assumptions for each experiment are described in Table 1

The Control experiment uses, to the best of our knowledge, the observed river runoff loading and 'refractory' DOC availability estimate from literature (Stoderegger and Herndl, 1998). In the experiments SENS1 we increase the phosphate discharge in correspondence of the Po river mouth grid points in order to reach a N/P ratio equal to the Redfield ratio (N/P=16). In the experiment SENS2 we reduce the riverine nutrients discharge of all the rivers with the exception of the Po river to 1/10 of the Po river discharge. In the experiment SENS3, on the same implementation of the experiments SENS2, the parameter controlling the degree of availability of the 'refractory' organic carbon (variable R7 in the model of chapter 2) was augmented by one order of magnitude

5.3.6 The DOC distribution for the sensitivity experiments

In this section we compare the model simulations with observational data from the MAT project Database. The data were collected with monthly periodicity starting from the summer 1999 to the summer 2002; in order to have the same number of data in each season only the years 2000 and 2001 are considered. The comparison was performed on the section crossing the northern basin (A section, see Fig. 5.1) and in two stations A3 and A7 (see again Fig. 5.1). For the section analysis the MAT data were interpolated on a regular grid along the section A using the objective analysis technique (Carter and Robinson, 1987). Model simulations were interpolated on the same grid. Both observations and simulations were seasonally averaged and then compared and analyzed.

In Fig. 5.12 it is shown the seasonally averaged total DOC, simulated and observed, distribution along the section A. In winter the simulated DOC concentrations range from 90 to100 mmol/m^3, in the area close to the Italian coast till 20 km from the Po river mouth, and they reach a constant value of 70 mmol/m^3 in the eastern part of the section. The simulations are in good agreement with the observations in the Italian coastal area, while, on the eastern side, the model tend to underestimate the observations. No vertical structure are present in the simulated DOC distribution, while the observations present a minimum (about 80 mmol/m^3) in the central part of the section between 10 and 15 meters depth and a relative maximum (110 mmol/m^3) in the upper 5 meters of the water column in the eastern part. During the spring simulated values show a stratified condition all along the section with maximum values in the upper layer. The west-east gradient is still present with highest values (120 mmol/m^3) on the western part of the section in the area 10-15 km from the Italian coast. A surface value of 100 mmol/m^3 is also present in the off shore zone till 50 km far from the Italian coast.

The observations show a maximum value in the upper water column layers between 20 and 40 km from the Italian coast. Quite high DOC concentration are present, in the upper layer, even in the eastern part and DOC concentration of 115 mmol/m^3 are present even along the Istrian coast. In this season the general agreement between model and observations appears satisfactory even if, some observed vertical structure, as a subsurface maximum (115 mmol/m^3) present at 20 meters depth, are not captured by the model.

The summer simulated value range from 160 mmol/m^3 in the western coastal area and 100 mmol/m^3 in the central part of the section where is present an area with low concentrations from the surface to 25 meters depth. The increase in the western part is strong with respect to the spring and is evident the appearance of a maximum (130 mmol/m^3) in the eastern coastal area that was not present in the previous season. The comparison with the observations shows a good agreement in the west and eastern part while the main discrepancy is that the minimum simulated value(100 mmol/m^3) is not present in the observations.

During the autumn the simulated value range from 120 mmol/m^3 in the western coastal area in the upper 10 meters to 80 mmol/m^3 as constant value in the eastern

part of the section, starting from 40 km from the Italian coast. The agreement with the observations appear to be very good in the western part while in the eastern side of the section the model produce a little underestimation.

SIMULATIONS			
	River nutrient discharge	N/P ratio in nutrients discharge	"refractory"DOC availability (d^{-1})
CONTROL	full	37	0,01
SENS1	full	16	0,01
SENS2	All except Po reduced	37	0,01
SENS3	All except Po reduced	37	0,1

Table 5.1. Sensitivity experiments description.

In Fig. 5.13 are shown the DOC simulated concentrations along the section A in the SENS1 and SENS2 experiments. In winter the SENS1 simulations does not show significant differences with respect to the control simulations. On the contrary the SENS2 simulations produce lower DOC (about 70 mmol/m^3) concentrations without any accumulation in the western part of the section. In spring the SENS1 simulations show a net increase along the Italian coast where the DOC concentration reaches the value of 150 mmol/m^3 This value is higher than the control experiment and closer to the observations. In the central and eastern part of the section, on the contrary, the simulation SENS1 produce lower values (80 mmol/m^3) with respect to the control experiment and underestimate the observations. SENS2 spring simulations show a mild increase along the Italian coast in the upper 10 meters (90-100 mmol/m^3) In the central-eastern part there is the appearance of a maximum (105 mmol/m^3) near the surface. The concentration in the eastern part is higher with respect both to the SENS1 experiment and the control, and are closer to the observations. During the summer the SENS1 simulation is again very close to the control one. On the contrary the SENS 2 simulation show a totally different behavior with high values along the Italian coast in the center of the section. This maximum is present in the observed field

and the SENS2 experiment is, in summer, the experiment that better reproduce the observations, even if the values in the eastern part near the Istrian coast and in the deeper layer are lower with respect to the observations. In Autumn the SENS1 simulations are very similar to the control while the SENS2 simulated value are lower in the western part (90 mmol/m^3) and very similar in the eastern side of the section (80 mmol/m^3).

In Fig. 5.14 we show the SENS3 experiment simulation along the section A. As expected the DOC concentration decrease with respect to the control experiment and the other sensitivity experiments because the enhanced availability of the 'refractory' component of the dissolved detritus. During the winter the simulated concentrations are less than 50 mmol/m^3 over the whole section. In spring there is a general DOC increase with the formation of a maximum in the central part of the basin where in the upper layer the DOC reaches the value of 90 mmol/m^3. The DOC distribution is very similar to the one of the experiment SENS2 but with lower concentrations. During summer the values range from 90 mmol/m^3 in the deepest layer of the section to 140 mmol/m^3 in the upper 5 meters between 30 and 40 Km far from the italian coast. In autumn the simulated values range from 80 mmol/m^3 in the area close to the Italian coast to 65 in the eastern part of the section as constant value through the water column. As expected the strongest decrease in the SENS3 simulations is during winter and autumn, when the contribution of the 'refractory' dissolved organic carbon to the total DOC pool is higher.

These experiments already suggest a conclusion: the total runoff of the basin (not only the Po) is a major controlling factor to simulate correctly the DOC distribution in the Northern Adriatic. In particular, lower basin runoff gives the largest values of DOC accumulation in the central part of the northern basin. The N-P ratio of the riverine input do not have such a large influence on the structure of the DOC distribution.of the basin

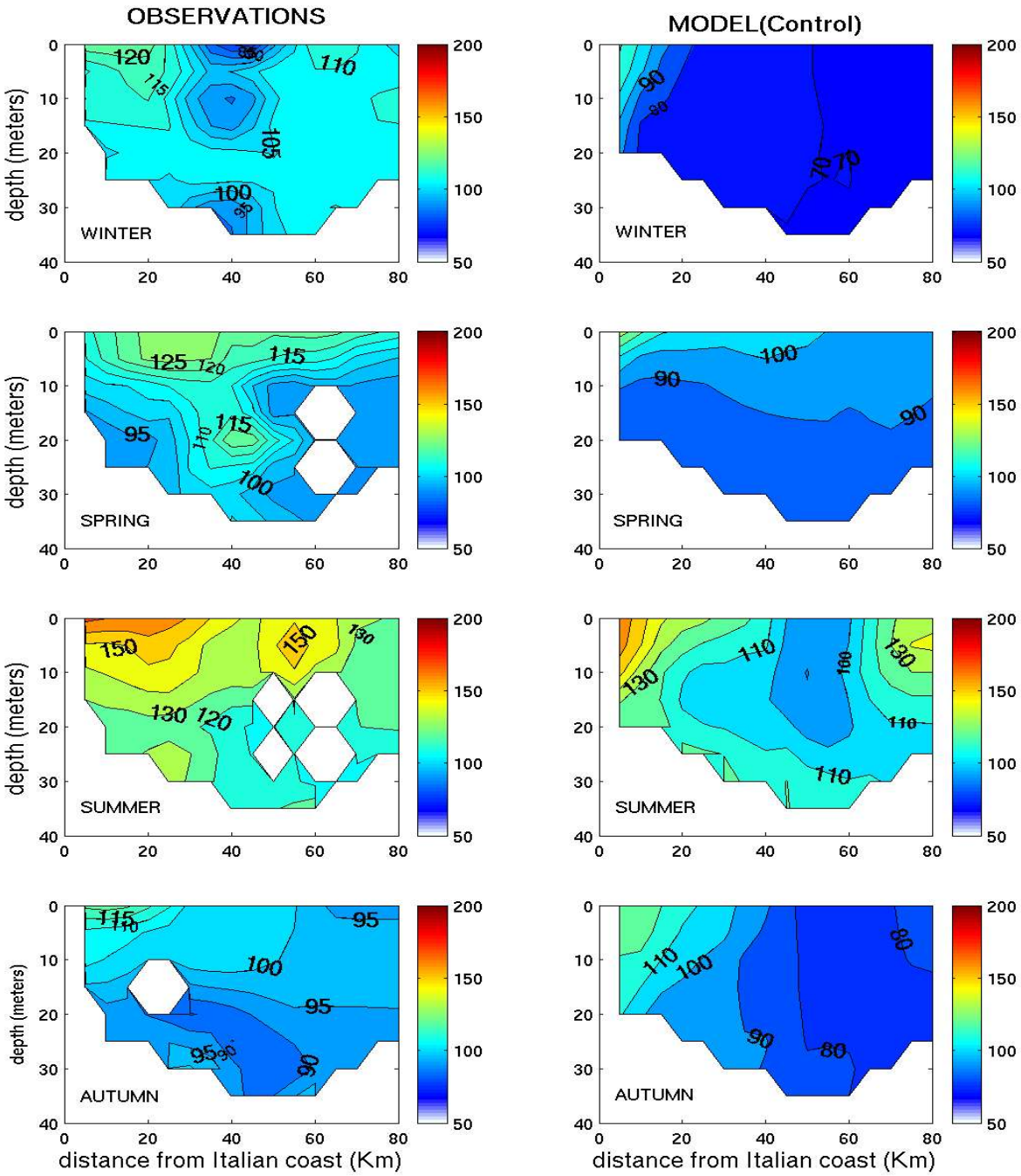

Figure 5.12. DOC (mmol/m^3) seasonally averaged distribution of data (left side) and model control simulations (right side) along the section A.

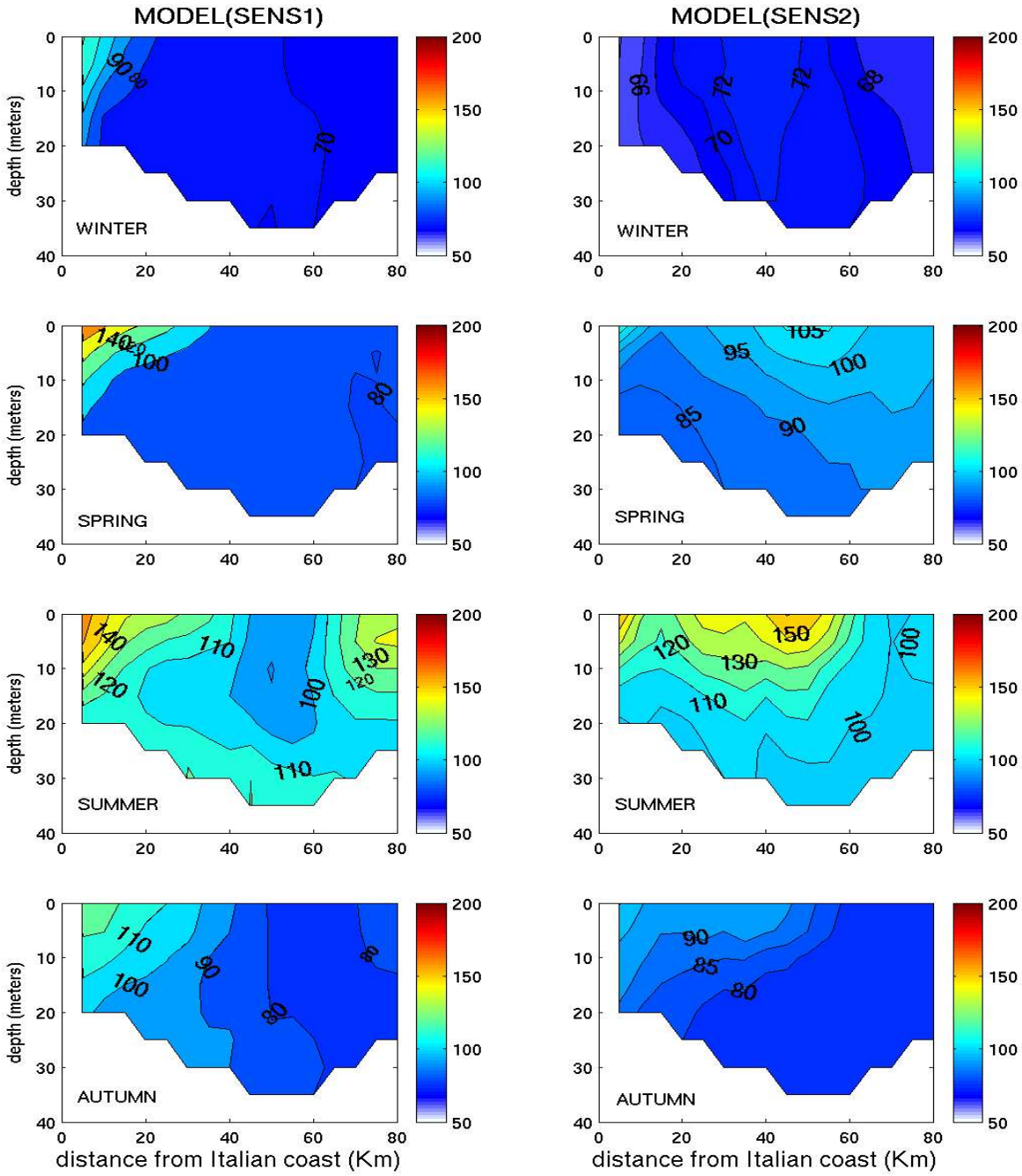

Figure 5.13. DOC (mmol/m^3) seasonally distribution of model SENS1 simulation (left side) and model SENS2 simulation (right side).

The comparison between surface DOC simulated concentrations and observations at the station A3 and A7 is shown in Fig. 5.14. The comparison was carried out for the control experiment (dark line) and for the SENS2 experiment (green line). In the A3 station in the first part of the year, from January to March, both the control experiment and the SENS2 are below the observed values that never go under 100 mmol/m^3, while the control simulations are about 90 mmol/m^3 and the SENS2 simulated concentrations are below 80 mmol/m^3. Starting from April the control simulation increases rapidly reaching in May the 180 mmol/m^3. In this part of the year the agreement with the observations is good. The SENS2 simulation, on the contrary, shows a strong underestimation with respect to the observations: values increase slightly from April, reaching the maximum value (140 mmol/m^3) in August. In the last part of the year, from August to December, the control simulation shows a second peak reaching 220 mmol/m^3 in September. This high values is not present in the observational data that, during the Autumn do not go over the 140 mmol/m^3. Starting from August the agreement between the observations and the SENS2 simulations is very good both in terms of amount and distribution.

In the A7 station both the control and the SENS2 simulation reflect the observations distribution with a maximum in summer (July for the observation and the SENS2 simulation and June for the control simulation) and one in September (control) and October (observations and SENS2). During the first four months of the year simulations both control and SENS2 produce DOC concentrations quite close and remarkably lower with respect to the data. The spring increase, present in the observations, is well captured by both the experiments simulations but, while the control experiment values reach only 120 mmol/m^3 in June, the SENS2 simulation peaks in the same month of the observations (July) reaching a value of 160 mmol/m^3. The agreement with the observation is, from September to December, good for both model experiments.

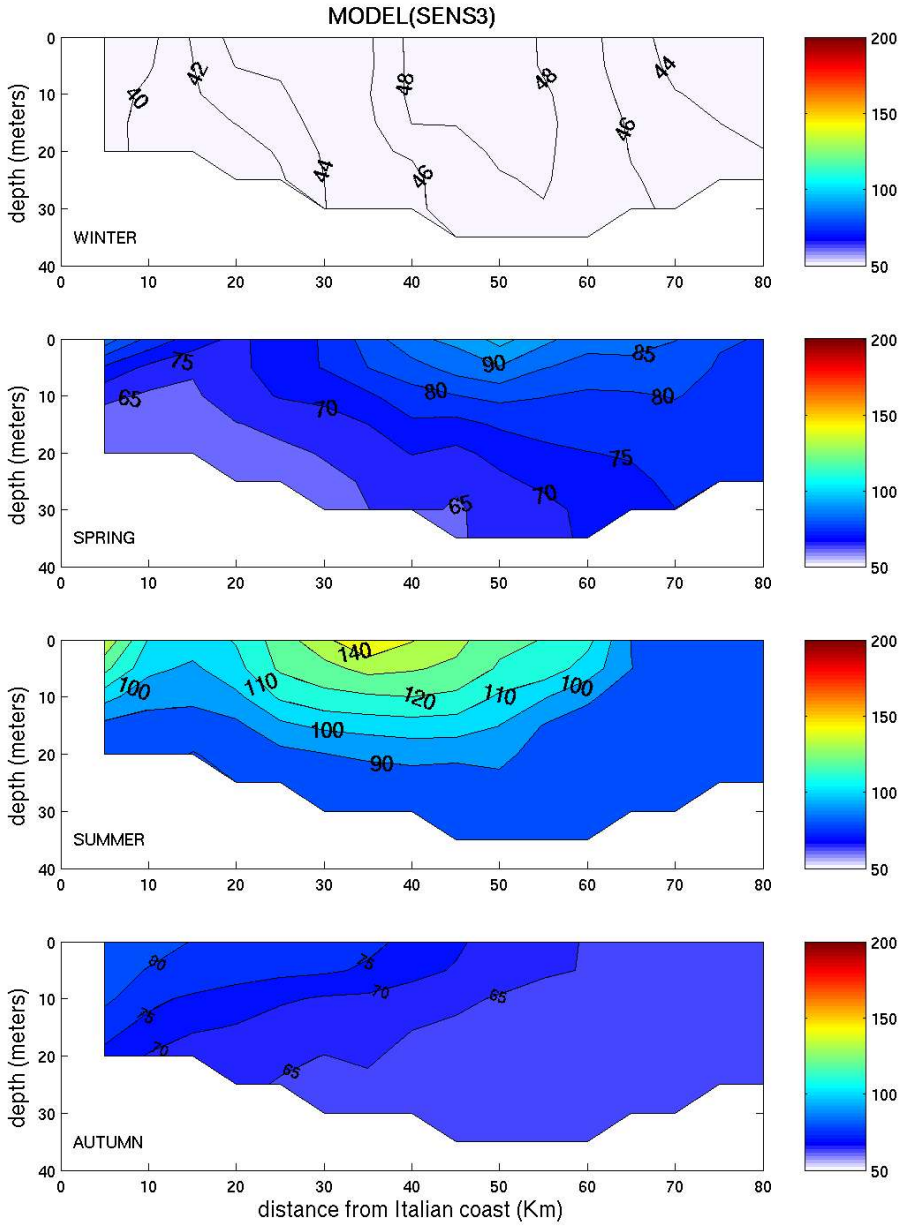

Figure 5.14. DOC (mmol/m^3) seasonally averaged distribution of the model SENS3 simulation along the section A.

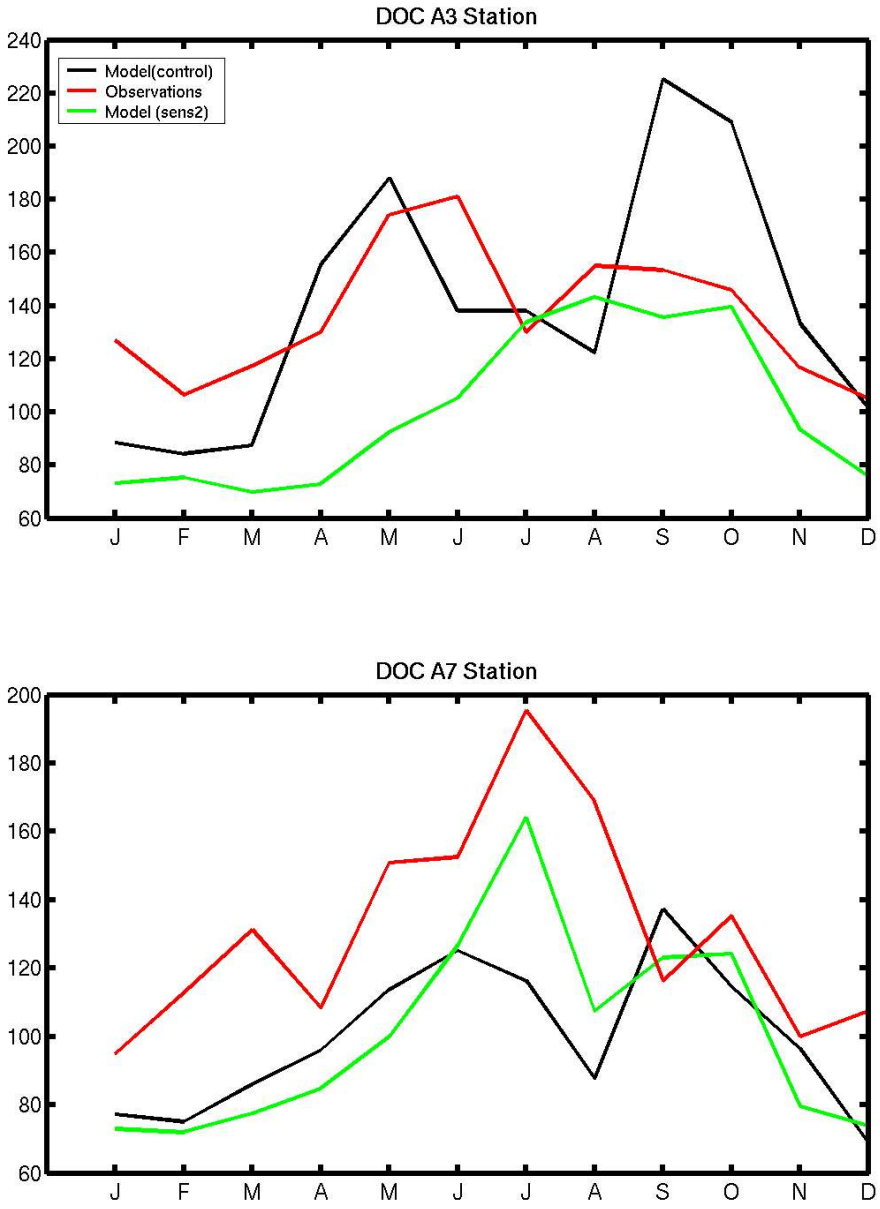

Figure 5.15. DOC (mmol/m^3) surface monthly mean distribution for observation (red line) control model simulation (dark line) and SENS2 model simulation (green line) at stations A3 and A7.

Figure 5.16. Observed (red line) and simulated (control experiment=dark line, SENS2 experiment=green line) BCP (mg C m^{-3} h^{-1}) at the station A3. (A=surface, B=10 meters depth and C=bottom).

5.3.7 Comparison between simulated and observed Bacterial carbon production (BCP)

In Fig. 5.16 a comparison is shown between simulated bacterial carbon production in the control and SENS2 experiment and and observations at stations t A3 and A7 at surface, at 10 meters depth and at the bottom. In the surface layer the control model simulations seems to overestimate the bacterial production at the A3 station. The general distribution of the bacterial production, with two peaks in spring and autumn, is, however, well reproduced The SENS2 simulations, on the contrary underestimate the observations in winter-spring where the simulated peak is about 0.3 mg C m^{-3} h^{-1}. During the second part of the year the control experiment overestimate the observations while the SENS2 simulations is more consistent with the data.

At 10 meters depth the discrepancy between the control experiment value and the observations become higher with exception of the winter months when the agreement is good both at 10 meters depth and at the bottom. The SENS2 simulation, on the contrary, tends to underestimate the observations in winter, while the agreement is very good in summer and autumn. At the bottom the SENS2 values are always below the observations but the trend of the distribution is good.

At station A7 the control simulation is again higher than the observation. The overestimation is more consistent at the bottom of the water column. The general shape of the BCP distribution during the year is, however, well captured. The SENS2 simulated values are in very good agreement with the observation with the exception of the autumn, at the surface, where is present a remarkable overestimation with respect to the observations.

5.4 Discussion and conclusions

The simulated DOC concentrations are in good agreement with the value reported in literature for some area of the Adriatic Sea (Pettine *et al*., 1999 and 2001; Giani *et al*., 2004.). The distribution, with the maximum located in the high production area, is also reasonable and in agreement with the actual knowledge of the DOC dynamics. A clear seasonal cycle is also well captured by the model and the spring-summer simulated increase, that can double the winter concentration, is consistent with that one reported in literature (Pettine *et al*., 1999; Giani *et al*., 2004).

The analysis of the different DOC components proposed in our implementation, offers a possibility to explain some of the feature of the DOC dynamics in the Adriatic basin. The 'labile' fraction is a small percentage of the total DOC during the whole year. A seasonal cycle is present and it is clearly related to the primary producers cycle (see the surface chlorophyll distribution in chapter 4). This fraction of DOC range from 0 to 4 mmol/m^3 and is about 1-2 % of the total DOC amount that is a fraction consistent with the fraction reported in literature for the proteins (Pettine *et al*.,1999). Although the dissolved organic carbon in the model is classified only on the basis of its functionality with respect to the bacterial activity (see chapter 3), this fraction of DOC is the only related to the organic nitrogen and phosphorus, so we can speculate that well represent the dissolved proteins.

The 'semilabile' fraction of the DOC, that is the main products of phytoplankton and bacteria exudation, is the most abundant in the areas characterized by high productivity, while, in the more oligotrophic zone, as the open water of the southern Adriatic basin, its concentration is equal or less to that one of the 'refractory' DOC (Fig. 5.4 and 5.5). This is clear from the analysis of the DOC and gross primary production distribution trough the year (Fig. 5.6). That analysis also show a clear link between the 'semilabile' DOC and the primary production. The 'refractory' DOC surface distribution show a seasonal cycle less pronounced with respect to the others DOC components and the surface distribution is almost constant through the year in the sampled station (Fig. 5.6) suggesting that this

fraction of DOC is responsible of the background DOC level. The value of the 'refractory' DOC range from 20 to 50 mmol /m^3 that is a value consistent with those one reported in the literature for the open ocean high turnover time DOC. In the northern coastal area 'refractory' DOC concentrations are higher with respect to the southern basin, but in the south, during winter, the 'refractory' DOC is the main fraction of the total DOC pool. This means that bacteria, in a nutrients depleted regime, are not able to convert detritus in biomass and they transform organic carbon onto 'refractory' organic carbon. Vertical DOC profiles with maximum in the upper layer and a quite constant value in the deeper layers below the euphotic zone are also consistent with the DOC vertical profile shape described in literature (Pettine *et al*., 1999).

Dissolved organic nitrogen and phosphorus concentrations show a distribution very similar to that one of the 'labile' DOC with maxima in May and June. The DON simulated concentrations are consistent with the value reported in literature for free amino acids (Pettine *et al*., 1999 and 2001). Moreover the DON and DOP simulated concentrations could be affected by the assumptions that link the lability/refractivity concept only to the carbon allowing bacteria to use very easily all the organic dissolved nitrogen and phosphorus available. Probably the inclusion of a small fraction of 'refractory' DON and DOP will be present in a future model development.

No climatological data were available for DOM and bacterial activity parameters, but the comparison with the MAT data showed a general good agreement with the control model simulation; in particular, the good agreement between modeled and observed bacterial carbon production (BCP) allow us to think that the bacterial sub model here proposed and implemented is based on correct assumptions.

All the sensitivity experiments performed simulate a reasonable DOC concentration, and the model is capable to reproduce a realistic seasonal cycle. The analysis of the different sensitivity experiments gave a clear indication on the DOC dynamics in different environmental conditions. The experiments with a larger nutrients discharge (control and SENS1) show a better agreement with the observation in the coastal area where the primary production is high and,

consequently, even the DOC production is high (mainly in its 'semilabile' components). The DOC concentrations, as described by the zero dimensional experiments (see Chapter 2) are, therefore, related to the primary production (see Fig. 5.6). On the other hand in an eutrophic contest even the bacterial degradation activity is enhanced as shown by the BGE surface distribution that results to be strongly related to DOC distributions (Fig. 5.2, 5.3, 5.4, 5.5 and 5.10).

The experiment with a reduced nutrients inputs (SENS2) tends to underestimate the DOC in the high productivity level coastal area, while reproducing the accumulation in the central part of the section present in the observations very well. This suggests a relationship between DOC accumulation and nutrients depletion conditions. The SENS 1 experiments show that the nutrients N/P ratio in the Po river discharge do not affect significantly the DOC distribution in the northern Adriatic basin, as the simulated concentrations on the section A are, with the exception of an increase in Spring in the Italian coastal area, very close to the control experiment. The SENS3 experiment shows that, changing the degree of refractivity of the 'refractory' DOC component, the total DOC simulated amount decreases, mainly during the non accumulation period (winter and autumn) when the 'refractory' component is higher, but there is not a remarkable change in the general DOC cycle and distribution.

A recent study (Engel *et al*., 2004) demonstrated that polysaccharide aggregation is one of the main mechanisms causing sinking of dissolved organic carbon in the ocean; we can speculate that the aggregation processes is a function of the amount of carbon and of the residence DOC time so the accumulation concept could be a key point in order to understand the aggregation mechanism. By means of the model simulation, in the next section, we try to explain the northern Adriatic Sea DOC accumulation

5.4.1 The DOC accumulation conundrum

In Fig. 5.17 we show the total DOC concentration, the BGE, the DOC 'utilization time' (defined below) and the ratio between the 'semilabile' and the 'refractory' DOC. In all the pictures the velocity field is overlaid on the biochemical field. The figure is referred to a surface snapshot of the second half of

June, that is the month in which, usually, there is the strongest DOC increase and when mucilage phenomena starts to be observed .

The analysis of the control model simulation highlight the large gradients in terms of trophic structure of the Adriatic Sea (mainly in the northern part). Some important ecological parameters, such as the bacterial growth efficiency, are strongly related to these different trophic conditions. Observed BGE values range from 0.5 in coastal and estuarine area to 0.1 or even less in ultraoligotrophic systems such as the eastern part of the Mediterranean sea (Del Giorgio and Cole, 1998).

The simulated value of the BGE are very close to 0.5 in the prodelta area of the Po river where the high nutrients discharge allows the phytoplankton growth and then the DOM production but even enhance the bacterial capacity to convert dissolved detritus in biomass. The DOC present in this area, both concerning model simulations and observations, is produced and used rapidly because the system is highly energetic. So, the DOM dynamics in this zone, is characterized by high production but not accumulation. In order to clarify this concept we define a theoretical DOC utilization time (DUT) by dividing the total DOC amount for the bacterial carbon demand (BCD) that is the bacterial production plus the bacterial respiration:

$$DUT = DOC / BCD$$

This parameters (Fig. 5.17) range from less than 15 days along the western coastal area to 40 days in the central part of the basin.

In the central part of the basin, Fig. 5.17 shows a DOC maximum in correspondence of a large DOC utilization time. This maximum is not present in the experiments with high nutrients discharge (control and SENS1). Since the BGE decreases in the central part of the northern basin, this means that the transfer of organic carbon to the high trophic level is low and that the DOC accumulates. This suggests, in turn, that the fraction of 'refractory' organic pool is higher with respect to the coastal areas and this is very well reproduced in the simulation (Fig. 5.17).

On the other hand the low primary production level in the central northern Adriatic areas (see chlorophyll distribution in chapter 4) does not allow a significant accumulation of freshly produced DOC.

Following this idea we need two different (contrasting) conditions to trigger DOC accumulation: the first is a region with high primary production, such as the western Adriatic coastal areas, and the second is a context characterized by an ecological regime of very low BGE that normally is connected to the open ocean. Our idea is that, when these two different systems are close in space and/or in time and linked by means of a circulation structures, an "anomalous" DOC accumulation may occur.

As shown in Fig. 5.17 seasonal mesoscale circulation processes link the western part of the northern Adriatic basin with the central part: the cyclonic current breaks down into jets and offshore currents that manage to transport DOC produced by phyto, bacterio and zooplankton in the central part of the northern basin where the system has low BGE and long DUT. The simulated DUT shows a very steep gradient starting from the Po delta area (less than 10 days) toward the off shore region (even more than 35 days).

Further exploring this idea it could be more important, in order to trigger DOC accumulation, the amount of nutrients in the oligotrophic part of the northern basin, since they determine the local BGE values, with respect to the amount of nutrients discharged by the Po river. The latter in fact allows an high primary production but, on the same time, enable bacteria to work efficiently recycling the organic matter produced and thus not accumulating DOC. This idea is confirmed by the simulations with a reduced nutrients inputs from all the others Adriatic rivers except the Po (SENS2) that reproduces the presence of a maximum of DOC concentration in the center of the basin which is seen in the observations. This maximum disappears when we increase the nutrients input from the same rivers. Nutrients discharge "fertilize" the central part of the basin enhancing the BGE and reducing the (BGE) gradient with respect to the coastal areas.

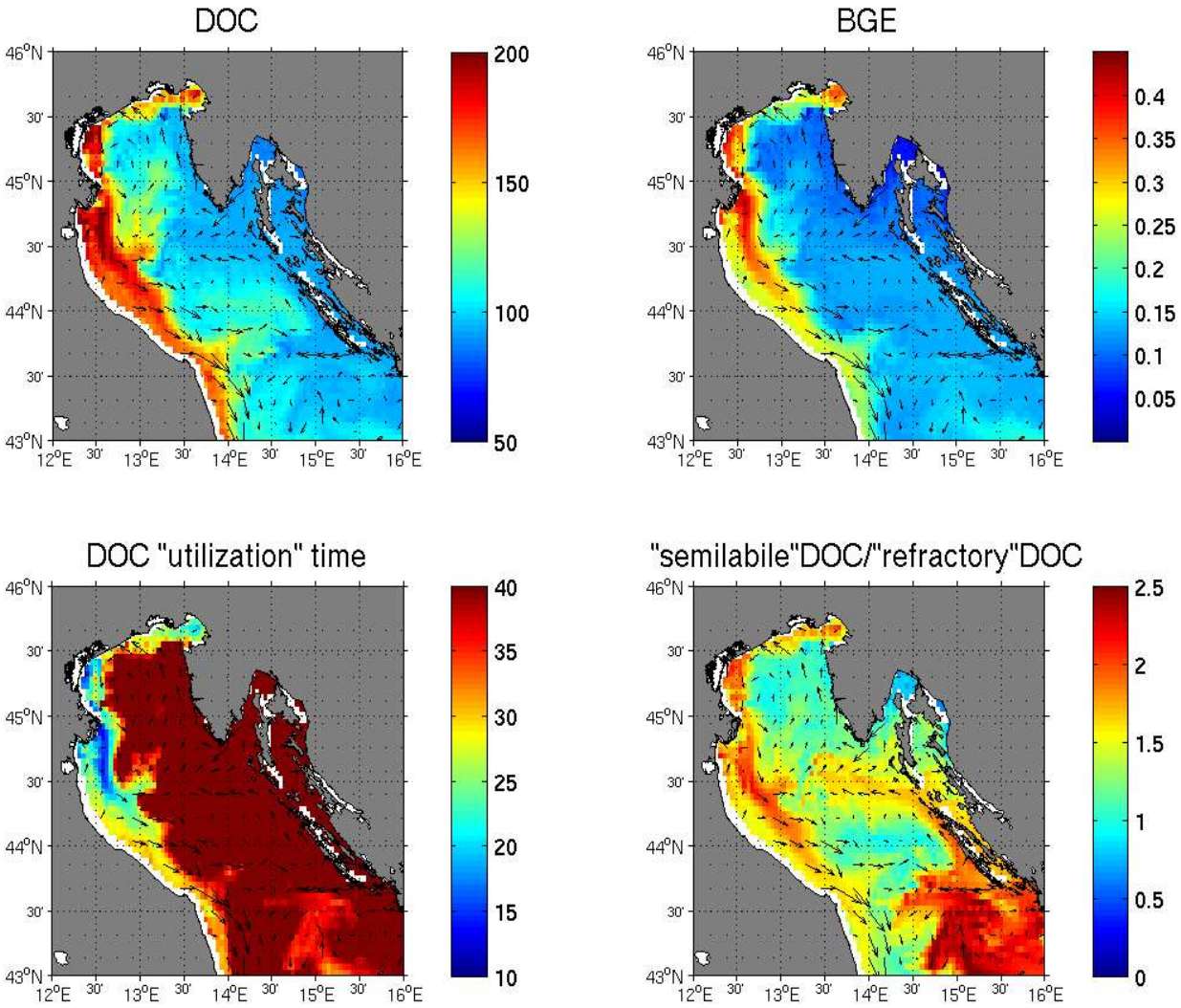

Figure 5.17. Total DOC (mmol/m3) distribution, BGE (%), DOC "utilization" time (d), 'labile' to 'refractory' DOC ratio and velocity fields in the northern Adriatic derived from a surface snapshot of June in the SENS2 simulation.

References

Allen J.I., Somerfield P.J., Siddorn J., 2002. Primary and bacterial production in the Mediterranean Sea: a modelling study. *Journal of Marine System, 33-34: 473-495.*

Artegiani A., Bregant D., Paschini E., Pinardi N., Raicich F., Russo A., 1997 a. The Adriatic sea general circulation. Part I: air sea interactions and water mass structure. *Journal of Physical Oceanography, 27: 1492-1514.*

Artegiani A., Bregant D., Paschini E., Pinardi N., Raicich F., Russo A., 1997 b. The Adriatic sea general circulation. Part II: baroclinic circulation structure. *Journal of Physical Oceanography, 27: 1515-1532.*

Azam F., Fenchel T., Field J.G., Gray JS., Meyerreil LA, Thingstad F 1983. The ecological role of water column microbes in the sea. *Marine Ecology Progress Series, 10(3): 257-263.*

Azam F., Smith D.C, Steward G.F., Hagstrom A., 1993. Bacteria-Organic Matter Coupling and Its Significance for Oceanic Carbon Cycling. *Microbial Ecology, 28: 167-179.*

Azam F., Fonda Umani S., Funari E., 1999. Significance of bacteria in the mucilage phenomena in the northern Adriatic Sea. *Annali Istituto Superiore Sanità, 35(3): 411-419.*

Barale V., Schiller., Tacchi R., and Marechal C., 2004. Trends and Interactions of physical and Bio-geo-chemical features in the Adriatic Sea as derived from satellite observations. *Science of the Total environment, MAT special issue, in press.*

Baretta J.W., Ebenhoh W., Ruardij P., 1995. The European Regional Seas Ecosystem Model, a complex marine ecosystem model. *Netherland Journal of Sea Research, 33: 233-246.*

Baretta-Bekker J.G., Baretta J.W., Hansen AS., Reimann B., 1998. An improved model of carbon and nutrient dynamcis in the microbial foodweb in marine enclosures. *Aquatic Microbial Ecology,. 14: 91-108.*

Baretta-Bekker J.G., Baretta J.W., Rasmussen E.K., 1995. The microbial food web in the European Regional Seas Ecosystem Model. *Netherland Journal of Sea Research, 33: 363-379.*

Bignami F., Marullo S., Santoleri R., Schiano M.E., 1995. Long-wave radiation budget in the Mediterranean Sea. *Journal Goephysics Research, 100: 2501-2514.*

Blackford J.C., Allen J.I., Gilbert F.J., 2004. Ecosystem dynamics at six contrasting sites: a generic modelling study. *Journal of Marine Systems, 52: 191-215.*

Blumberg A.F., Mellor G.L., 1987. A description of a three dimensional coastal ocean circulation model. *In: N. S. Heaps, (Ed.), Three dimensional coastal ocean model, AGU, pp 1-16.*

Brankart J.M., Pinardi N., 2001. Abrupt cooling of the Mediterranean Levantine Intermediate Water at the beginning of the 1980`s: Observational evidence and model simulation. *Journal of Physical Oceanography, 31: 2307-2320.*

Broekhuizen N., Heath N.R., Hay S.J., and Gurnay W.S.C., 1995. Modelling *t*he dynamics of the North sea's mesozooplankton. *Netherland Journal of Sea research, 33:381-406, 1995.*

Carlson C.A., Ducklow H.W., Michaels A.F., 1994. Annual flux of dissolved organic carbon from the euphotic zone in the northwestern Sargasso sea. *Nature, 371: 405-408.*

Carter E.F., Robinson A.R., 1987. Analysis models for the estimation of oceanic fields. *Journal of Atmospheric and Oceanic Technology, 4: 49-74.*

Castellari S., Pinardi N., Leaman K., 1998. A model study of air sea interactions in the Mediterranean Sea. *Journal of Marine Systems, 18: 89-114.*

Cavalieri L., Bertotti L., 1997. In search of the correct wind and waves fields in a minor basin. *Monthly Weather Review, 125: 1964-1975.*

Church J.M., Hutchins D.A., Ducklow H.W., 2000. Limitation of Bacterial Growth by Dissolved Organic Matter and Iron in the Southern Ocean. *Applied and Environmental Microbiology, pp. 455-466.*

Copin-Montegut G., 2000. Consumption and production on scales of few days of inorganic carbon, nitrogen and oxygen by the planktonic community: results of continuous measurements at the Dyfamed Station in the northwestern Mediterranean Sea (May 1995). *Deep Sea Research, I 47:447-477.*

Copin-Montegut G., & Avril B., **1993.** Vertical distribution and temporal variation of dissolved organic carbon in the North-Western Mediterranean Sea. *Deep sea Research, 40:1963-1972.*

Da Silva A.M., Young C.C., Levitus S., 1995. Atlas of surface marine data. *NOAA Atlas NESDIS 7, pp. 78.*

Degobbis D., Gilmartin M., Relevante N., 1986. An annotated nitrogen budget calculation for the northern Adriatic Sea. *Marine Chemistry, 20: 159-177.*

Degobbis D., Gilmartin M., 1990. Nitrogen, Phosphorus and biogenic Silicon budgets for the Northern Adriatic Sea. *Oceanologica Acta, 13: 31-45.*

Degobbis D., Malej A., & Fonda Umani S., 1999. The mucilage phenomenon in the northern Adriatic Sea. Acritical review of the present ascientific hypotheses. *Annali Istituto Superiore di Sanità, 35:373-381.*

Del Giorgio P.A., Cole J.J., 1998. Bacterial Growth efficiency in natural aquatic systems. *Annales Review Ecological Systems, 29: 503-41.*

Demirov E., Pinardi N., 2002. Simulation of the Mediterranean Sea circulation from 1979 to 1993: Part I. The interannual variability. *Journal of Marine Systems, 33/34: 23-50.*

Droop M.R., 1973. Some thoughts on nutrient limitation in algae. *Journal of. Phycolgy, 9: 264-272.*

Ducklow H.W., Carlson C.A., 1992. Oceanic bacterial production. *Advances Microbiology Ecology, 12: 113-181.*

Ebenhoh W., Baretta J.G., and Baretta J.W., 1997. The primary production module in the marine ecosystem model ERSEM II with emphasis on the ligth forcing. *Journal of Sea Research, 38: 173-193.*

Eiler A., Langenheder S., Bertilsson S., Tranvik L.J., 2003. Heterotrophic Bacterial Growth Efficiency and Community Structure at Different Natural Organic Carbon Concentrations. *Applied and Environmental Microbiology, pp. 3701-3709.*

Engel A., Thoms S., Riebesell U., Rochelle-Newall E., Zondervan I., 2004. Polysaccharide aggregation as a potential sink of marine dissolved organic carbon.

Nature, 428: 929-932.

Faganeli J., and Herndl G., 1991. Dissolved organic matter in the waters of the gulf of Trieste (Northern Adriatic). *Thalassia Jugoslavica, 23:51-63.*

Fajon C., Cauwet G., Lebaron P., Terzic S., Marijan A., Malej A., Mozetic P., Turk V., (1999). The accumulation and release of polysaccharides by planktonic celles and the subsequent bacterial response during a controlled experiment. *FEMS Microbiology Ecology, 29: 351-363.*

Fonda Umani S., Cauwet G., Cok S., Martecchine E., & Predonzani S., 1997. Chemical and biological seasonal patterns of the gulf of Trieste: the exemple of early and late summer. *In PALOMA-Production and Accumulation of Labile Organic Matter in Adriatic (Cauwet G., ed) contract no. EV5V-CT94-0420.*

Franco P., 1984. Fattori influenti sulla produttività primaria dell´Adriatico settentrionale. *Bollettino di Oceanologia Teorica Applicata, 2: 125-140.*

Giani M., Savelli F., Berto D., Zangrando V., Ćosović B., Vojvodić V., 2004. Temporal dynamic of dissolved and particulate organic carbon in the northern Adriatic Sea in relation to the mucilage events. *Science of the Total Environment, MAT special issue, In press.*

Gibson J.K., Kallberg P.K., Uppala S., Hernandez A., Nomura A., Serrano E., 1997. ERA description. *ECMWF Reanalysis Project Report Series 1, pp. 72.*

Gilmartin M., Degobbis D., Relevante N., Smodlaka N., 1990. The mechanisms controlling plant nutrient concentration in the northern Adriatic Sea. *Internationale Revue der Gesamten Hydrobiologie, 75: 425-445.*

Goldman J.C., Caron A., Dennet M.R., 1987. Regulation of gross growth

efficiency and ammonium regeneration in bacteria by substrate C:N ratio. *Limnology and Oceanography, 32: 1239-1252.*

Hagstrom A., Azam F., Kuparinen J., Zweifel U.L., 2001. Pelagic Plankton Growth and Resource Limitations in the Baltic Sea. *Ecological studies, Vol 148 F. Wulf et al. (eds) A Systems Analysis of the Baltic Sea.*

Hellerman S., Rosestein M., 1983. Normal monthly wind stress over the world ocean with error estimates. *Journal of Physical Oceanography, 13 1093-1104.*

Jerlov N.G., 1976. Marine Optics. *Elsevier Science, Amsterdam.*

Jurgens K., Gasol J.M., Vaquè D., 2000. Bacteria-flagellate coupling in microcosm experiments in the Central Atlantic Ocean. *Journal of Experimental Marine Biology and Ecology, 245: 127-147.*

Keil R., Kirchman D.L., 1994. Abiotic transformation of labile protein to refractory protein in sea water. *Marine Chemistry, 45: 187-196.*

Killworht P.D., 1996. Time interpolation of forcing fields in ocean models. *Journal of Physical Oceanography, 26: 136-143.*

Kondo J., 1975. Air-Sea bulk transfer coefficients in diabatic conditions. *Boundary Layer Meteorology, 9: 91-112.*

Korres G., Lascaratos A., 2003. A one way nested eddy resolving model of the Aegean and Levantine basins: Implementation and climatological runs. *Annales Geophysicae, 21: 205 220.*

Legates D.R., Wimott C.J., 1990. Mean seasonal and spatial variability in a gauge corrected global precipitation. *International Journal of Climatology, 10: 121-127.*

Legendre L., Rassoulzadegan F., 1996. Food-web mediated export of biogenic carbon in oceans. *Marine Ecology Progress Series, 145: 179-193.*

Maranon E., Cermeno P., Fernandez E., 2004. Signifiance and mechanisms of photosynthetic production of dissolved organic carbon in a costal eutrophic ecosystem. *Limnology and Oceanography, 49(5): 1652-1666.*

Mellor G.L., Yamada T., 1982. Development of a turbulence closure model for geophysical fluids problems. *Review of Geophysics and Space Physics, 20: 851-875.*

Moran M.A., Hodson R. E., 1990. Bacterial production on humic and nonhumic composition of dissolved organic carbon. *Limnology and Oceanography, 35(8): 1744-1756.*

Nyholm n., 1977. kinetics of nitrogen-limited algal growth. *Progress in Water Technology, 8:347-358, 1977.*

Ogura N., 1976 Further studies on decomposition and dissolved organic carbon matter in coastal sea water, *Marine Biology, 13: 89-93*.

Osterroth C., and Thomas H., 2000. New production enhanced by nutrient supply from non-Redfield remineralisation of freshly produced organic material. *Journal of Marine System, 25:33-46.*

Payne R.E., 1972. Albedo at the sea surface. *Journal of Atmospheric Science, 29: 959-970.*

Pettine M., Patrolecco L., Manganelli M., Capri S., Farrace M.G., 1999. Seasonal variations of dissolved organic matter in the northern Adriatic Sea. *Marine Chemistry, 64: 153-169.*

Pettine M., Capri S., Manganelli M., Patrolecco L., Puddu A., Zoppini A., 2001. The Dynamics of DOM in the Northern Adriatic Sea. *Estuarine Coastal and Shelf Science, 52: 471-489.*

Provini A., Crosa G., Marchetti R., 1992. Nutrient export from the Po and Adige river basin over the last 20 years. *Science of the Total Environment supplement, 291-313.*

Raicich F., 1994. Note on the flow rates of the Adriatic Rivers. *CNR, Istituto Sperimentale Talassografico, Technical Report, RF-02/94, Trieste, 8 pp.*

Raicich F., 1996. A study of the freshwater balance of the Adriatic Sea. *Journal of Marine Systems, 9: 305-319.*

Redfield A.C., Ketchum B., and Richards F., 1963. The influence of organisms on the composition of sea water. In M. hill, editor, *The sea, pages 26-77. Interscience, New York, 1963.*

Reed R.K., 1975. An evaluation of formulas for estimating clear sky insolation over the ocean. *NOAA-ERL 352-PMEL Technical Report, 26 pp. 25.*

Reed R.K., 1977. On estimating insolation over the ocean. *Journal of Physical Oceanography, 7: 482-485.*

Revelante N., Gilmartin M., 1992. The lateral advection of particulate organic matter from the Po delta region durino summer stratification and its implication for the northern Adriatic. *Estuarine and Coastal Shelf Science, 35: 191-212.*

Reynolds R.W., Smith T.M., 1994. Improved global sea surface temperature analyses using optimum interpolation. *Journal of Climate, 7: 929-948.*

Robinson A., R., 1999. Forecasting and Simulating Coastal Ocean Processes and Variabilites with the Harvard Ocean Prediction System. Coastal Ocean Prediction *(C. N. K. Mooers, ed.), AGU Coastal and Estuarine Studies Series, 77-100. American Geophysical Union.*

Rosati A., Miyakoda K., 1988. A general circulation model for upper ocean simulation. *Journal of Physical Oceanography, 18: 1601-1626.*

Sambrotto R.N., Savidge G., Robinson C., Boyd P., Takahashi T., Karl D.M., Langdon C., Chipman D., Marra J., and Codispoti L., 1993. Elevated consumption of carbon relative to nitrogen in the surfaec ocean. *Nature, 363: 248-250.*

Smagorinsky J., 1993. Some historical remarks on the use of nonlinear viscosities. *In: Galperin, B., Orszag, S.A. (Ed.), Large simulation of complex engineering and geophysical flows. Cambridge University Press, pp. 3-36.*

Smodlaka N., 1986. Primary production of organic matter as an indicator of the eutrophication in the Northern Adriatic Sea. *Science of the Total Environment, 56: 211-220.*

Sommer U., 1994. Planktologie. *Springer-Verlag, Berlin.*

Stoderegger K., Herndl G.J., 1998. Production and release of bacterial capsular material and its subsequent utilization by marine bacterioplankton. *Limnology and Oceanography, 43(5): 877-884.*

Thingstad T.F., Hagstrom A., Rassoulzadegan F., 1997.Accumulation of degradable DOC in surface waters: is it caused by a malfunctioning microbial loop?. *Limnology and Oceanography*, 42*: 3*98-404.

Thomas H., Ittekkot V., Osterroht C., and Schneider B., 1999. Preferential

recycling of nutrients – the ocwans's way to increase new production and to pass nutrient limitation? *Limnology and Oceanography*, 44 (8)*:*1999-2004.

Varela R.A., Cruzado A., and Gabaldon J.E., 1995. Modelling primary production in the North Sea using the European Regional Seas Ecosystem Model. *Netherland Journal of Sea Research*, 33: 337-361.

Vichi M., 2002. Predicability studies of coastal marine ecosystem behavior, Ph D. Thesis, University of Oldemburg, Oldemburg, Germany, http//docserver.bis.unioldemburg.de/publikationen/dissertation/2002/vicpre02/vicpre02html.

Vichi M., Oddo P., Zavatarelli M., Colluccelli A., Coppini G., Celio M., Fonda Umani S., Pinardi N., 2003. Calibration and validation of one dimensional complex marine biogeochemical fluxes model in differents areas of the northern Adriatic shelf. *Annales Geophysicae, 21: 413-436.*

Vichi M., Zavatarelli M., Pinardi N., 1998. Seasonal modulation of microbial mediated carbon fluxes in the northern Adriatic Sea : a model study. *Fishery Oceanography, 7: 182-190.*

Vichi M., Ruardij P., and Baretta J.W., 2004. Link or sink: a modelling interpretation of the open Baltic biogeochemistry. *Biogeosciences, 1: 79-100.*

Vilicic D., Vucak Z., Skrivanic A., Grzetic Z., 1989. Phytoplankton blooms in the oligotrophic open South Adriatic waters. *Marine Chemistry, 28: 89-107.*

Whitman W.B., Coleman D.C., Wiebe W.J., 1998. Prokaryotes: The unseen majority. *Proceedings of the National Academy of Science, USA 95: 6578-6583.*

Williams P.J.leB., 1995. Evidence for seasonal accumulation of carbon-rich dissolved organic material, its scale in comparison with changes in particulate

material and the consequential effect on net C/N assimilation ratios. *Marine Chemstry, 51: 17-29.*

Zavatarelli M., Baretta J.W., Baretta-Bekker J.G., Pinardi N., 2000. The dynamics of the Adriatic Sea ecosystem. An idealized model study. *Deep Sea Research, 47: 937-970.*

Zavatarelli M., Pinardi N., 2003. The Adriatic Sea modelling system: a nested approach. *Annales Geophysicae, 21: 345-364.*

Zavatarelli M., Pinardi N., Kourafalou V.H., Maggiore A., 2002. Diagnostic and prognostic model studies of the Adriatic Sea circulation. Seasonal variability. *Journal of Geophysics Research 107, Ant. No. 3004.*

Zavatarelli M., Raicich F., Artegiani A., Bregant D., Russo A., 1998. Climatological biogeochemical characteristics of the Adriatic Sea. *Journal of Marine Systems, 18: 227-263.*

Zoppini A., Pettine M., Totti C., Puddu A., Artegiani A., Pagnotta R., 1995. Nutrients, Standing crop and Primary Production in western coastal waters of the Adriatic Sea. *Estuarine and Coastal Shelf Science, 41: 493-513.*

Zweifel U., Wikner J., Hagstrom A., 1995. Dynamics of dissolved organic carbon in a coastal ecosystem. *Limnology and Oceanography, 40:299-305.*